Strål säkerhets myndigheten
Swedish Radiation Safety Authority

Author: Ali R. Massih
Lars Olof Jernkvist

Research

2015:46

Assessment of data and criteria for cladding burst in loss-of-coolant accidents

Report number: 2015:46 ISSN: 2000-0456
Available at www.stralsakerhetsmyndigheten.se

SSM perspective

Background

In accident conditions in nuclear power plants it is plausible that the fuel rods are damaged due to high temperatures and pressure difference over the cladding. In analytical tools used for predicting fuel behavior in accident conditions there are empirically-based criteria for determining when the fuel rods get so weakened that they would burst. Burst characteristics are dependent on several physical phenomena and the most crucial of these are implemented as models in computational programs. Tests in test reactors and materials testing facilities are continuously being performed to test new materials and examine the effects of expanded operating conditions. With new tests the need arises to review and update the models in the computational programs.

Objective

A Loss of Coolant Accident (LOCA) safety evaluation method must include a model for cladding ballooning and burst in order to calculate and evaluate the impact on the coolable geometry of the reactor core and to estimate the release of activity during accident conditions. For SSM it is important to know about available options and models for LOCA analysis, what they imply and how they should be used in best estimate and conservative (bounding) analysis.

Results

This report presents a detailed and focused overview of burst-criteria for cladding materials in LOCA conditions and is a continuation of the work reported in SKI Report 2007:14.

In this report, the latest publically available data from tests of burst characteristics are compiled and compared with burst criteria in QT/SSM-FRAPTRAN. The report continues with comparisons between calculated and experimentally measured burst characteristics and a statistical analysis of the differences. The stress-based, best-estimate, burst criterion as formulated by Rosinger in 1984 is suggested as being suitable for applications to Zircaloy and ZIRLO claddings since it shows a relatively small deviation in comparison with test data.

Need for further research

Continued improvement of calculation tools are needed to accurately describe the performance of the nuclear fuel in the reactor under transient and accident conditions. In the concluding section of this report some suggestions on how to proceed with further improvements of cladding burst criteria are discussed.

Project information

Contact person SSM: Anna Alvestav
Reference: SSM2014-2355

Strål
säkerhets
myndigheten
Swedish Radiation Safety Authority

Author: Ali R. Massih, Lars Olof Jernkvist
Quantum Technologies AB, Uppsala

2015:46

Assessment of data and criteria for cladding burst in loss-of-coolant accidents

Date: November 2015
Report number: 2015:46 **ISSN:** 2000-0456
Available at www.stralsakerhetsmyndigheten.se

This report concerns a study which has been conducted for the Swedish Radiation Safety Authority, SSM. The conclusions and viewpoints presented in the report are those of the author/authors and do not necessarily coincide with those of the SSM.

SSM 2015:46

RESEARCH

Assessment of data and criteria for cladding burst in loss-of-coolant accidents

Ali R. Massih and Lars Olof Jernkvist

17 November 2015

Quantum Technologies AB
Uppsala Science Park
SE-751 83 Uppsala, Sweden

Assessment of data and criteria for cladding burst in loss-of-coolant accidents

Ali R. Massih and Lars Olof Jernkvist

Quantum Technologies AB
Uppsala Science Park
SE-751 83 Uppsala, Sweden

Quantum Technologies Report: TR14-001v1
Project # - SSM2014-2355-6

Contents

Abstract

We attempt to systematize the zirconium-base fuel cladding burst data obtained under loss-of-coolant accident (LOCA) conditions that have been reported from various experimental programs since the late 1970's. Our objective is to assess the usable data and evaluate them with the various burst criteria that are available in the QT/SSM version of the FRAPTRAN computer program. The FRAPTRAN program computes the transient behavior of light-water reactor fuel rods during reactor transients and hypothetical accidents, such as LOCAs. The cladding materials in the data base include Zircaloy-4, ZIRLO and Zr-1wt%Nb type alloys. The report summarizes the data base, the method of computation, the expressions for the various burst criteria, and the outcome of our assessment in the form of measured versus calculated plots: cladding time-to-burst, cladding burst temperature and cladding burst stress/strain. A summary of the uncertainties in the computations is also provided. We have found that the stress-based Rosinger best-estimate burst criterion, originally developed for Zircaloy-4 cladding, is suitable for applications to Zircaloy and ZIRLO claddings on a best-estimate basis. For the ZIRLO cladding, additional improvements of this burst criterion can be made, provided sufficient amount of measured data on burst properties and material characteristics would be available.

Sammanfattning

Vi söker i rapporten systematisera data avseende zirkoniumbaserade bränslekapslingsrörs brottbeteende under haverifall med kylmedelsförlust (LOCA), som rapporterats från experimentella studier sedan slutet av 1970-talet. Vårt mål är att fastställa användbara data och utvärdera dessa gentemot de brottkriterier som är tillgängliga i QT/SSM:s version av beräkningsprogrammet FRAPTRAN. Detta program beräknar transientbeteendet hos kärnbränslestavar i lättvattenreaktorer under reaktortransienter och hypotetiska olyckor, såsom LOCA. Databasen omfattar kapslingsmaterialen Zircaloy-4, ZIRLO och legeringar med sammansättningen Zr-1wt%Nb. Rapporten sammanfattar databasen, beräkningsmetodiken och uttrycken för de olika brottkriterierna, samt presenterar resultaten av vår utvärdering genom att jämföra beräkningsresultat med mätdata i diagram över tid till kapslingsbrott, brottemperatur, och kapslingens brottspänning och brottöjning. Dessutom ges en kort översikt av osäkerheterna i beräkningarna. Vi har funnit att Rosingers spänningsbaserade brottkriterium, vilket ursprungligen utvecklades för “best-estimate”-prediktering av kapslingsbrott i Zircaloy-4, är tillämpbart för såväl Zircaloy-4 som ZIRLO-kapsling, om en bästa skattning av kapslingsbrott erfordras. Vad gäller ZIRLO-kapsling, kan nämnda brottkriterium förbättras ytterligare, under förutsättning att en tillräcklig mängd mätdata avseende brott- och materialegenskaper är tillgänglig.

1 Introduction

In a postulated loss-of-coolant accident (LOCA) in light-water reactors (LWRs), zirconium alloy fuel cladding tubes are subjected to high temperatures (> 700 K) and internal over pressures. The condition can cause excessive outward expansion (ballooning) of the cladding tube, primarily by creep mechanisms, which may lead to rupture of cladding upon the temperature transient. Cladding ballooning will also reduce the subchannel area available for flow of the coolant water, or may cause coolant blockage in the refilling and flooding stages of LOCA [1–3].

In the LOCA safety analysis, a cladding failure or burst criterion is needed to predict the temperature and time at which cladding ruptures, and also the hoop stress or strain at, or close to, the location of rupture. The behavior of cladding during the accident is governed by phase transformation, Zr-H_2O reaction (oxidation), creep deformation, and rupture of zirconium alloy all within a time span of a few minutes [4]. Cladding burst criterion is not an item of the widely practiced LOCA acceptance criteria [5, 6], however, a LOCA safety evaluation method must include a model for predicting cladding ballooning and burst by considering the temperature of the cladding and the difference in pressure between the inside and outside of the cladding, both as functions of time. Moreover, for the model to be acceptable the ballooning and burst computations must be based on pertinent data in a manner that the degree of ballooning and incidence of burst are not underestimated [5].

In this report, zirconium-base fuel cladding burst data obtained under loss-of-coolant accident conditions from various experimental programs since the late 1970's are summarized and assessed. Our objective is to identify a suitable burst criterion for application in the computer program `FRAPTRAN` [7] used for fuel rod safety analysis. The cladding materials in the assessed data base comprise Zircaloy-2/4, Zr-1wt%NbO alloys M5 and E110, and ZIRLO. The chemical compositions of these alloys are listed in Table 1.

Zirconium alloys in solid state undergo a phase transformation from the low temperature hexagonal closed-packed (hcp) α-phase to body-centred cubic (bcc) β-phase [8]. Solid state phase equilibria of Zircaloy-4 have been investigated experimentally by Miquet et al. [9], who reported a prevalence of four phase domains, namely, $(\alpha + \chi)$ up to 1081 K, $(\alpha + \beta + \chi)$ from 1081 to 1118 K, $(\alpha + \beta)$ between 1118 and 1281 K, and β-phase above 1281 K. Here, χ refers to the intermetallic hexagonal Laves phase $Zr(Fe,Cr)_2$, see e.g. [10]. For the sake of illustration, we have depicted an *isopethal* (constant composition) section of Zircaloy-4 with only the oxygen concentration as a variable in Fig. 1. The phase equilibria of the Zr-Nb-O system have recently been evaluated in [11]. Kaddour et al. [12] report that the starting temperature of the $\alpha \rightarrow (\alpha + \beta)$ transition, determined by a resistivity technique, for Zircaloy-4 is about 1093 K and for Zr1%Nb alloy is around 1043 K. Similarly, the start of the $(\alpha + \beta) \rightarrow \beta$ transition is about 1250 K for Zircaloy-4 and 1210 K for Zr1%Nb. A LOCA will presumably involve $\alpha \leftrightarrow (\alpha + \beta) \leftrightarrow \beta$ transitions.

Oxidation of Zr-alloy cladding involves both oxygen and hydrogen atoms pickup by the cladding. Oxygen is an α-stabilizer, meaning that it expands the α-domain in the phase diagram, while hydrogen is a β-stabilizer. Furthermore, hydrogen elevates the solubility of oxygen in the β-phase and it also raises the rate of diffusion of oxygen into the β-domain. The high-temperature β-phase is known to be "softer" than the low-temperature α-phase

in zirconium alloys, meaning that it has a higher creep rate at a given stress than the latter. It is worth mentioning that because of the low solubility of niobium in zirconium at low temperature, the Zr1%Nb alloy contains a few percent of β phase even at low temperature. It is believed that this small amount of β phase dispersed as metastable particles in a sea of α phase does not affect the deformation behavior of Zr1%Nb [12].

This report is organized as follows. Section 2 presents the cladding burst data obtained from various test programs. Models for cladding oxidation, deformation, phase transformation and burst under LOCA conditions, implemented in the QT/SSM version of the FRAP-TRAN computer program (`QT/SSM-FRAPTRAN`), are briefly described in section 3. In section 4, we evaluate and assess the measured data with the aid of the models presented in section 3. Section 5 is devoted to discussion on cladding burst criteria. Finally, section 6 summarizes and concludes the report plus gives a view for further considerations.

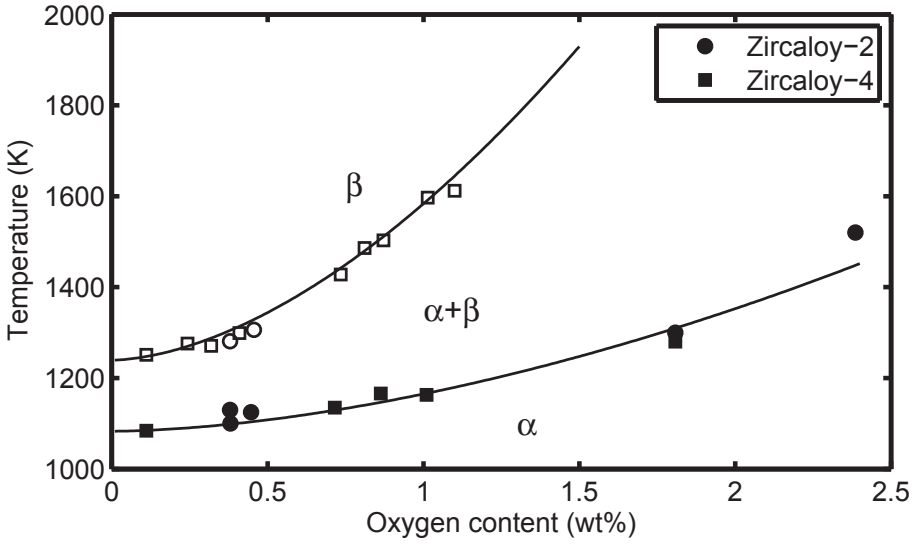

Figure 1: An isopethal section of Zircaloy phase diagram versus oxygen concentration [13]. The data were obtained from resistivity measurements.

Table 1: Nominal chemical composition of Zr-base cladding materials.

Alloy	Sn wt%	Nb wt%	Fe wt%	Cr wt%	Ni wt%	O wppm
Zircaloy-2	1.5	...	0.2	0.1	0.05	1200
Zircaloy-4	1.3-1.5	...	0.2	0.1	...	1200
M5	...	1.0	...	...	...	1200
E110	...	1.0	...	0.01	...	600
Std. ZIRLO	1.0	1.0	0.1	...	...	1000
Opt. ZIRLO	0.7	1.0	0.12	...	...	1000

2 Burst test data

In this section, we summarize cladding burst or rupture data obtained under LOCA conditions from various experimental programs over the past few decades, from ca 1980 to present. Our summary comprise a brief description of each test program and the resulting data generated from it. The burst data of interest include the heating rate that the sample cladding is subjected to, cladding burst temperature, hoop (circumferential) stress, hoop strain and time-to-burst plus the initial conditions for the specimen prior to the transient.

The experimental data are from the burst tests performed in the former *Kernforschungszentrum Karlsruhe* or KfK [14–16] in Germany and those made available by Oak Ridge National Laboratory or ORNL [17, 18] in the USA, and the creep rupture tests made in the former Central Electricity Generating Board (CEGB) of UK. More recent data include those produced at CEA (*Commissariat á l'ènergie atomique et aux ènergies alternatives*) of France, AEKI Institute Hungary, Argonne National Laboratory (ANL) USA, Studsvik Nuclear Sweden, and the Halden reactor IFA-650 LOCA experiments in Norway. Table 2 outlines the main features of these tests. These tests were primarily made in steam environments except the creep rupture tests of CEGB, which were done in vacuum and some AEKI tests made in argon gas. The database also comprise irradiated rods (KfK-83, Studsvik-12 and Haldein IFA-650). Previous reviews of cladding burst data include refs. [19, 20] up to ca 1980 and [21].

Table 2: Database on fuel cladding burst experiments performed in LOCA conditions.

Data set …	Test series	Heating method	Heating rate °C/s (K/s)	CTD* °C (K)	Source …
Zircaloy-4					
I	ORNL-79	Internal	5-31	0-100	[17–19]
II	KfK-79	Internal	0.8-31	Low	Data set J [19]
III	KfK-82	Induction	1-35	< 15	[14]
IV	KfK-83	Internal/Nucl.	7-19	6-20	[15, 22]
V	KfK-85	Internal	7	20-70	[16, 23]
VI	KfK-87	Induction	0, 5, 80	Low	[24]
VII	KfK-88	Internal	1.0	Low	[25]
VIII†	CEGB-84/5	Induction	0	0	[26, 27]
IX	CEA-02	Induction	0+transient	0	[28]
Zr1%Nb					
X	CEA-00 (M5)	Induction	0-100	0	[29]
XI	AEKI-00 (E110)	Furnace	6.4-13.5	0	[30, 31]
ZIRLO					
XII	W-EDF-09	NA	2.8-28	NA	[32]
XIII	ANL-10	Furnace	5	NA	[33, 34]
XIV	Studsvik-12	Furnace	5	NA	[35, 36]
Halden IFA-650 integral LOCA tests					
XV	Tests 2-7	Electric/Nucl.	2-9	Low	[37], refs therin
XVI	Tests 9-14	Electric/Nucl.	…	…	…

*Circumferential temperature difference.†Biaxial creep deformation rupture tests in vacuum. Nucl.(Nuclear).

2.1 ORNL tests: Zircaloy-4 cladding

Chapman and co-workers at ORNL have in a series of experiments studied the deformation and burst behaviour of unirradiated Zircaloy-4 cladding in steam using fuel rod simulators

with internal heaters [17–19]. The cladding samples were tested one at a time, i.e. by single-rod tests. Moreover, the single-rod tests reported by Chapman et al. can be divided into two types, namely, (i) transient burst tests and (ii) creep-rupture tests, depending on the way they were performed. In the former, the cladding was heated at a constant rate until burst, whereas in the latter, the temperature increase was stopped at a predefined temperature level and then held at that level until rupture occurred. The cladding used in the tests had an outer diameter and wall thickness of 10.92 and 0.635 mm, respectively. The heated length of the samples was 915 mm. In what follows, we briefly describe the transient burst tests and summarize pertinent data from the aforementioned references.

The ORNL fuel rod simulator consisted of a heater rod surrounded by the Zircaloy-4 cladding [17]. The heater rod was separated from the cladding radially by a narrow gas gap filled with helium. The fuel rod simulator was placed freely suspended at its ends in a test vessel. An unheated flow shroud surrounds the simulator to give well-defined boundary conditions. A schematic of the single-rod burst test assembly is shown in Fig. 2. The inner diameters of the flow shroud and the test vessel were 34.8 and 102 mm, respectively. Before transient testing, the entire assembly was equilibrated at an initial temperature of about 613 K (340°C), using external electric heaters (outside the test vessel) and a concurrent small downward flow of superheated steam at atmospheric pressure [17]. The power to the fuel rod simulator was off during this phase of the operation.

In these tests [17], twelve type S (Pt/Pt-10Rh) 0.25 mm diameter, bare-wire thermocouples were spot-welded to the outer cladding surface for monitoring the temperature during the test. In some samples, these were equally spaced in a spiral pattern along the heated length to determine axial temperature distributions. In other samples, four thermocouples were equally spaced around the cladding at three axial positions to measure circumferential temperature gradients. Some simulators comprised four sheathed thermocouples spot-welded to the inner surface.

Directly before the transient, the helium pressure in the fuel rod simulator was adjusted to the desired initial value (p_0) and the simulator was disconnected from the gas supply system. A constant direct-current voltage was then applied to the simulator to initiate the thermal and pressure transients. Typical time evolutions of the internal rod pressure (p) and cladding temperature (T) responses from the transient burst tests are illustrated in Fig. 3. Commonly, the initial rod pressure p_0 (at time t_0) increases during the transient and attains a maximum value designated by p_{max} before excessive cladding deformation (ballooning) commences. Cladding burst usually occurs upon ballooning at a pressure denoted by p_B. The initial and rupture temperatures indicated in figure 3 are denoted by T_0 and T_B, respectively. The fuel rod simulators in these transient burst tests were pressurized with initial values ranging from $p_0 = 1$ to 20 MPa. The cladding samples were subjected to heating rates from $\dot{T} = 1$ Ks^{-1} to about 30 Ks^{-1}. However, most of the tests were performed at a nominal heating rate of around 28 Ks^{-1}.

As noted in [17], because the cladding deformation is sensitive to small temperature differences, and the local temperature changes are, consecutively, affected by the local deformation, the definition of burst temperature is rather imprecise. Therefore, Chapman et el. [17] defined burst temperature as the maximum temperature measured by any external thermocouple, without regard to its location, at the time of burst. This definition is based on

the premise that the temperature at the burst is at least as high as the maximum measured but does not exclude the possibility of being higher.

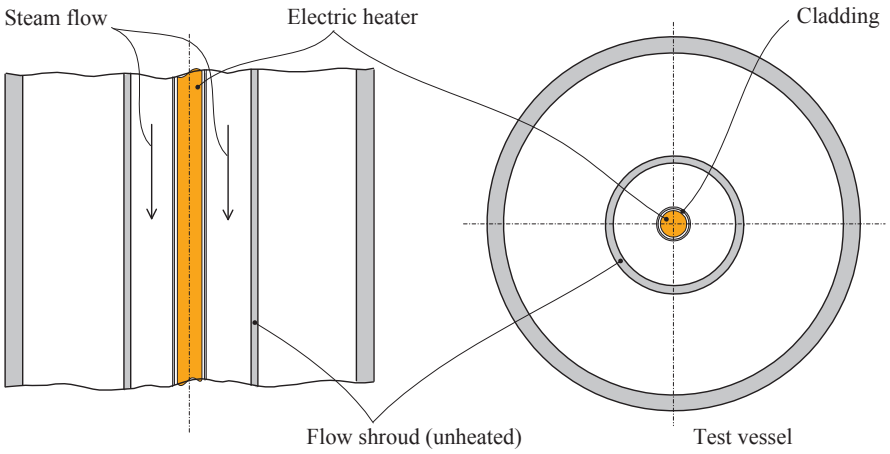

Figure 2: Schematic cross-sections of heated zone of single-rod test vessel used at ORNL-79. The fuel rod simulator consists of electric heater and the surrounding cladding.

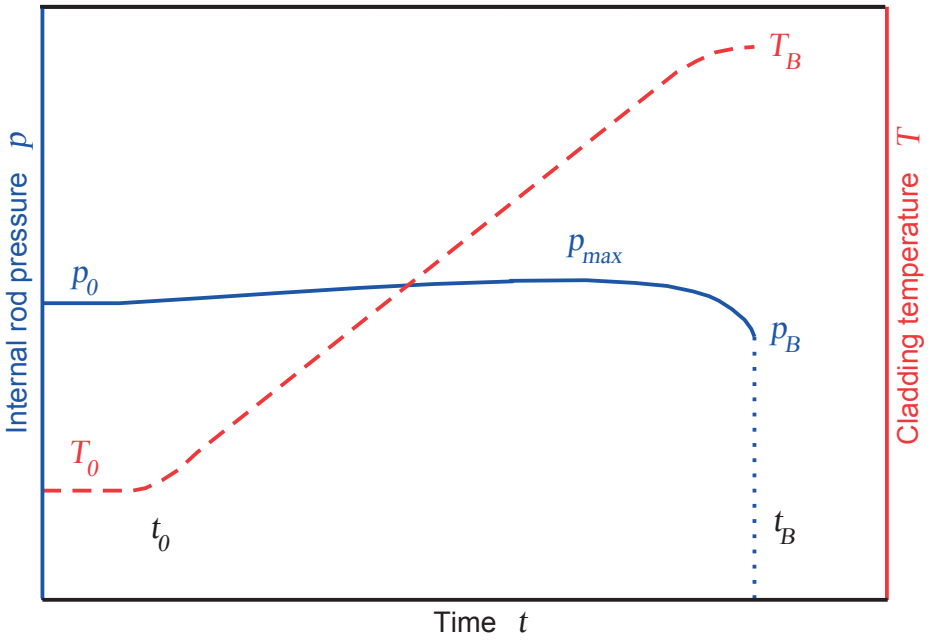

Figure 3: Schematic time evolution of cladding temperature (T) and internal rod gas pressure (p) of transient single-rod burst tests performed by Chapman et al. [17–19].

The test conditions and the obtained cladding burst data are summarized in Tables 3-5. These data are: the initial temperature (T_0), the heating rate ($\dot{T}$), the initial rod pressure (p_0), the maximum attained rod pressure (p_{max}), time to burst (t_B), burst temperature (T_B), burst pressure (p_B), burst strain (ϵ_B) and burst stress (σ_B).

The burst (hoop) stress values given in these tables are calculated according to [38]

$$\sigma_B = (p_B - p_a)\Big(\frac{R_m}{w} - \frac{1}{2}\Big), \tag{1}$$

where p_B is the rod pressure at burst, $p_a \approx 0.1$ MPa is the external pressure, R_m is the instantaneous mean radius of the cladding tube, and w is the instantaneous thickness of the cladding wall, which are related to their initial values through

$$w = w_0/(1+\epsilon_\theta), \tag{2}$$
$$R_m = R_0(1+\epsilon_\theta), \tag{3}$$

where ϵ_θ denotes the engineering hoop strain and the subscript "0" indicates the initial undeformed state. At time of cladding burst $\epsilon_\theta = \epsilon_B$. Heating rate values listed in Tables 3 and 4 are obtained by using the relation $\dot{T} = (T_B - T_0)/t_B$, where t_B is the time to burst. We should note that the t_B values given in [18] are slightly larger than the ones calculated here. The heating rate and the internal rod pressure were roughly constant during each test. The experimental data on rod pressure indicate that the maximum pressure increase, calculated as $(p_{max} - p_0)/p_0$, in Chapman et al.'s tests is less than 10% [17, 18], see Tables 3 and 4. We should mention that the post-test measurements of the total circumferential elongation (TCE) were taken in ≈ 15 mm intervals with a device that comprised the vernier wheel of a planimeter. According to Chapman et al. [17, 18], the resolution of the measurements is 0.075 mm. Chapman et al. reduced their data as plots of TCE versus axial position, which also indicate the position of the burst.

Chapman et al. [18] also compared their results with earlier published data for uniformly heated tubes conducted in inert environments. They observed that their steam-test data (28 K/s) exhibited much smaller TCE for burst temperatures below 875°C and above 975°C. The difference was attributed to localization of deformation in certain parts of the tube circumference. They noted that the test environment have no important effect in the low temperature region ($T < 875$°C). Moreover, they noticed from their tests that in the α-Zircaloy range of temperature the tubes were slightly crooked with several short axial bows with different circumferential orientations. The bows had occurred in regions of relatively large TCE, and the burst openings were generally found on the concave side of the bow. As the test temperature increased into ($\alpha + \beta$)-domain, the short axial bows became less prominent and disappeared in the β-domain.

In α-Zircaloy, with a strong radially oriented texture, circumferential orientation is accommodated to certain degree by axial contraction instead of merely by wall thinning [18]. The oriented texture causes the deforming tube to bow toward rather than away from the hot side of the rod simulator. This increases the azimuthal (circumferential) temperature variation on the tube by reducing the gas gap on the hot side while increasing the gap on the cold side of the tube, thereby enhancing the nonuniformity in cladding temperature distribution, thus augmenting localized deformation and rod bowing. On the other hand, β-Zircaloy, being essentially isotropic, accommodates deformation primarily by wall thinning [18].

In the high-temperature range, $T > 975$°C, the lower TCE values were explained by the effect of Zircaloy oxidation. Since the duration of a high-temperature transient was quite

long, it led to substantial formation of ZrO_2 layer on the tube surface. Cracks developed in the oxide layer and extended with simultaneous necking of the tube wall on the inner surface under the oxide crack according to Chapman et al. [18]. Consequently, TCE can be relatively small compared to uniformly heated tubes in an inert milieu despite that the local strain in the necked region can be quite large [18].

Table 3: ORNL-79 single-rod burst tests (data set I) in steam on unirradiated Zircaloy-4 cladding using fuel rod simulators [17].

Test ID	T_0 °C (K)	$\dot{T}$ K/s	p_0 MPa	p_{max} MPa	t_B s	T_B °C (K)	p_B MPa	ϵ_B %	σ_B MPa
PS-1	351 (624)	27.1	6.45	7.04	20.0	893 (1166)	6.36	18	68.5
PS-3	334 (607)	26.9	6.52	6.86	20.0	873 (1146)	5.58	29	72.4
PS-4	343 (616)	25.1	6.44	6.78	21.0	871 (1144)	5.86	21	66.6
PS-5	343 (616)	25.1	6.41	6.76	21.5	882 (1155)	5.72	26	70.7
PS-8	349 (622)	23.0	6.47	6.81	21.5	843 (1116)	6.00	20	67.0
PS-9	346 (619)	22.6	6.48	6.89	23.0	866 (1139)	5.65	25	68.7
PS-10	352 (625)	25.9	6.44	6.83	21.2	901 (1174)	6.00	20	67.0
PS-12	340 (613)	25.7	6.52	6.90	21.75	898 (1171)	6.14	18	66.2
PS-14	337 (610)	24.1	6.45	6.83	22.65	883 (1156)	5.82	25	70.7
PS-15	352 (625)	25.4	6.49	6.78	20.95	885 (1158)	6.16	17	65.2
PS-17	340 (613)	27.2	13.27	13.88	16.1	778 (1051)	12.13	25	147.4
PS-18	350 (623)	19.5	0.80	0.862	42.0	1171 (1444)	0.772	24	9.2
PS-19	348 (621)	22.3	2.59	2.82	27.45	959 (1232)	2.59	28	33.1
SR-1	347 (620)	25.9	0.85	0.91	31.6	1166 (1439)	0.80	26	9.9
SR-2	344 (617)	28.7	1.13	1.22	25.7	1082 (1355)	1.01	44	16.5
SR-3	346 (619)	29.7	1.77	1.90	22.4	1011 (1284)	1.72	43	27.6
SR-4	337 (610)	28.3	4.40	4.70	20.65	921 (1194)	4.48	17	47.4
SR-5	345 (618)	25.8	10.12	10.48	18.0	810 (1083)	9.52	26	117.7
SR-7	338 (611)	25.6	15.11	15.53	15.55	736 (1009)	14.44	20	161.2
SR-8	336 (609)	27.2	1.42	1.52	25.15	1020 (1293)	1.23	43	19.8
SR-13	325 (598)	30.6	1.31	1.43	24.65	1079 (1352)	1.07	79	27.2
SR-15	342 (615)	25.7	20.35	21.28	14.5	714 (987)	19.15	14	192.0
SR-17	344 (617)	27.9	1.31	1.41	25.25	1049 (1322)	1.06	53	19.6
SR-19	335 (608)	24.2	19.97	20.83	14.6	688 (961)	19.04	16	198.0
SR-20	332 (605)	28.6	1.29	1.41	25.1	1049 (1322)	1.06	55	20.1
SR-21	340 (613)	27.9	1.31	1.43	24.5	1023 (1296)	1.12	48	19.3
SR-22	332 (605)	27.5	1.13	1.23	27.2	1081 (1354)	0.89	50	15.8
SR-23	336 (609)	28.8	1.12	1.23	25.7	1077 (1350)	0.96	35	13.7
SR-24	332 (605)	27.0	1.20	1.30	26.9	1057 (1330)	0.99	67	21.9
SR-25	345 (618)	28.2	1.13	1.24	26.5	1092 (1365)	0.96	78	24.2
SR-26	340 (613)	26.4	1.00	1.06	29.9	1130 (1403)	0.83	34	11.7
SR-27	340 (613)	27.7	1.13	1.19	26.9	1084 (1357)	0.92	41	14.4
SR-28	335 (608)	25.9	8.93	9.40	19.3	835 (1108)	8.40	27	105.5
SR-29	340 (613)	25.1	8.68	9.05	20.0	843 (1116)	8.04	27	101.0
Average	341 (614)	26.2	...	...	...	...	...	...	...

Table 4: ORNL-79 single-rod burst tests (data set I) in steam on unirradiated Zircaloy-4 cladding using fuel rod simulators [18].

Test ID	T_0 °C (K)	$\dot{T}$ K/s	p_0 MPa	p_{max} MPa	t_B s	T_B °C (K)	p_B MPa	ϵ_B %	σ_B MPa
SR-37	305 (578)	26.1	14.410	14.965	17.4	760 (1033)	13.560	23	159.4
SR-38	340 (613)	27.7	14.660	15.265	15.5	770 (1043)	13.775	20	153.8
SR-41	340 (613)	8.9	10.510	10.915	46.9	757 (1030)	9.765	27	122.7
SR-42	344 (617)	8.9	10.495	10.900	47.1	761 (1034)	9.465	28	120.9
SR-43	340 (613)	4.9	8.465	8.800	89.1	773 (1046)	7.620	29	98.9
SR-44	382 (655)	4.8	7.935	8.250	82.5	777 (1050)	7.310	30	96.4
Average	342 (615)	...	...	...	...	...	...	...	...

Table 5: ORNL-79 single-rod burst tests (data set I) in steam on unirradiated Zircaloy-4 cladding using fuel rod simulators; data set I in [19].

Test ID	T_0 °C (K)	$\dot{T}$ K/s	p_0 MPa	p_{max} MPa	t_B s	T_B °C (K)	p_B MPa	ϵ_B %	σ_B MPa
SR-47	... (...)	10	...	...	...	775 (1048)	9.901	78	249.1
SR-49	... (...)	5	...	...	...	783 (1056)	7.632	95	231.2
SR-50	... (...)	10	...	...	...	897 (1170)	4.592	56	88.2
SR-52	... (...)	10	...	...	...	761 (1034)	9.908	49	173.2
SR-60	... (...)	28	...	...	...	879 (1152)	7.143	24	85.4
SR-61	... (...)	28	...	...	...	762 (1035)	14.293	31	191.5
SR-62	... (...)	28	...	...	...	937 (1210)	4.192	31	56.2
SR-64	... (...)	5	...	...	...	766 (1039)	8.487	110	298.9
SR-65	... (...)	5	...	...	...	748 (1021)	9.011	74	216.4
SR-67	... (...)	1	...	...	...	824 (1097)	4.447	107	152.1
SR-69	... (...)	1	...	...	...	854 (1127)	3.992	116	148.8

2.2 KfK tests: Zircaloy-4 cladding

2.2.1 KfK-79

The KfK-79 burst data (data set II in Table 2) are tabulated in [19] as Data Reference J. Its source is given as a letter from F. J. Erbacher (KfK) to R. H. Chapman (ORNL), dated 16 October 1979. No description of test procedure is provided in [19]. Briefly, the tests were conducted on 38 unirradiated Zircaloy-4 clad (single) rods, with heated shrouds, in steam atmosphere in laboratory. Data provided are the heating rate, rod pressure at burst, burst temperature, burst strain and stress. The initial cladding temperature and rod pressure data are not given. The provided data are reproduced in Table 6 in SI units.

Table 6: KfK-79 Zircaloy-4 clad single rod burst tests (data set II) in steam [19].

Rod ID	$\dot{T}$ K/s	p_B MPa	T_B K	σ_B MPa	ϵ_B -
100	10.4	13.62	1038	94.94	0.72
101	10.1	13.24	1028	92.26	0.73
102	10.5	11.57	1068	80.60	0.82
103	10.6	9.60	1098	66.95	0.93
104	10.4	7.80	1128	54.33	0.75
105	9.5	5.92	1167	41.23	0.46
106	9.7	4.01	1111	27.92	0.51
107	10.7	7.74	1137	53.92	0.86
108	10.1	7.75	1125	53.99	0.85
109	1.4	13.62	996	95.01	0.76
110	1.9	11.78	1021	82.12	0.82
111	1.9	9.85	1052	68.61	0.81
112	1.7	7.84	1092	54.61	1.04
113	1.7	5.89	1139	41.03	0.73
114	28.9	13.59	1067	94.67	0.37
115	29.3	13.40	1066	93.43	0.63
116	27.8	11.87	1075	82.74	0.44
117	29.2	9.79	1117	68.19	0.60
118	33.7	7.63	1189	53.16	0.37
119	35.0	7.93	1177	55.23	0.37
120	37.9	9.84	1156	68.54	0.50
121	8.9	11.84	1054	82.53	0.72
122	9.6	9.89	1083	68.95	0.57
123	9.0	7.93	1107	55.23	0.72
124	9.0	7.92	1110	55.16	0.66
125	8.9	6.04	1158	42.06	0.73
126	9.9	4.45	1036	100.67	0.57
127	31.5	13.73	1100	95.70	0.45
128	25.2	11.78	1076	82.12	0.48
129	29.5	11.80	1090	82.26	0.57
130	31.5	9.90	1171	69.02	0.54
131	24.1	7.91	1143	55.09	0.52
132	25.4	9.84	1120	68.54	0.60
133	0.8	9.92	1010	69.16	0.75
134	1.6	11.89	1019	82.88	0.86
135	0.8	13.80	974	96.19	0.79
136	0.9	7.94	1059	55.30	1.16
137	0.9	5.98	1097	41.71	1.13
138	0.8	4.00	1143	27.86	0.78

2.2.2 KfK-82

Single rod burst tests were conducted within the REBEKA program of KfK using fuel rod simulators with electric heating and 325 mm heated length in steam environment [14, 39].

To attain well-defined test boundary conditions, the internal rod overpressure and heating rate were kept constant during the deformation process. A heated shroud surrounding the test rod minimized the temperature gradient on the cladding circumference (< 15 K). Figure 4 schematically displays the test procedure. The test parameters, rod overpressure and heating rates, were in the range 1.0 to 14.0 MPa and 1 to 30 K/s, respectively. the cladding tubes were made of Zircaloy-4 with inner and outer diameters of 9.30 and 10.75 mm, respectively [14].

The resulting measured data include cladding temperature (T_B), rod pressure (p_B), and cladding hoop strain (ϵ_B) at burst. The cladding hoop stress was calculated from the formula [14]:

$$\sigma_B = \frac{p_B}{p_0}\sigma_0(1+\epsilon_B)^2, \tag{4}$$

where σ_0 is the initial hoop stress and the other variables were defined earlier. We have digitalized the burst stress and strain versus burst temperature data from figures 1 and 5 in [14] and displayed them here in Fig. 5. As can be seen from the figures, the data cover heating rates from 0.8 to 35 K/s not 1 to 30 K/s as stated earlier and in [14].

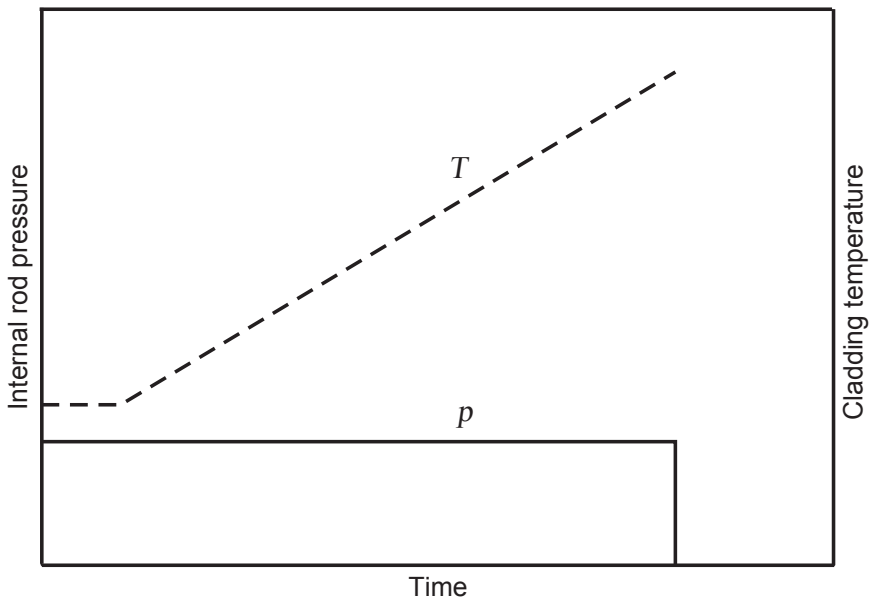

Figure 4: Schematic description of single-rod burst test procedure conducted in steam in the KfK-82 test series [14]. The heating rate and internal overpressure were in the range: $\dot{T} = 1 \rightarrow 30$ K/s and $p = 1 \rightarrow 14$ MPa.

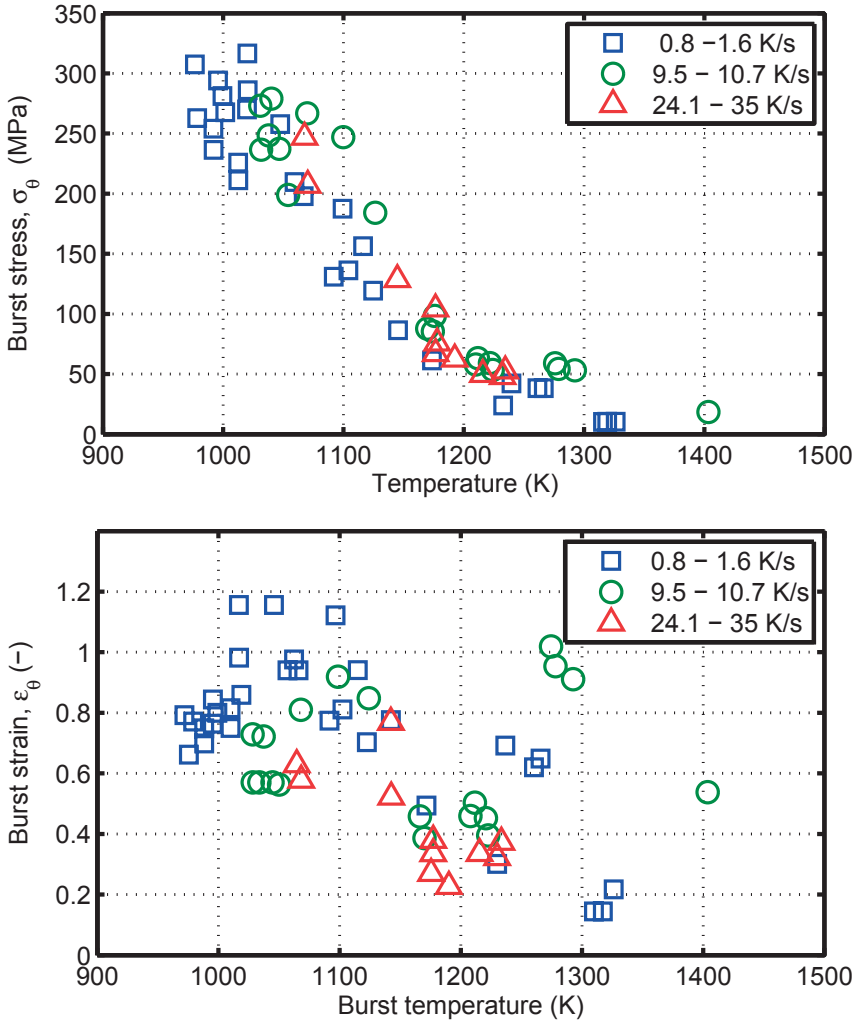

Figure 5: Measured Zircaloy-4 cladding burst hoop stress (upper panel) and burst hoop strain (lower panel) versus burst temperature in REBEKA (KfK-82) test series, performed in steam at various heating rates; from Erbacher et al. [14].

2.2.3 KfK-83

In-pile tests were carried out in the FR2 research reactor to examine the effect of neutron flux environment on fuel failure [15, 22].[1] Consequently, fuel burnup was chosen as the main parameter of the test program. In a test loop of FR2 both unirradiated and irradiated single fuel rod specimens, with rod burnup ranging from 2.5 to 35 MWd/kgU, and some electrically heated fuel rod simulators were exposed to transients simulating a postulated second heatup phase of LOCA in a PWR after a double ended break of a main coolant inlet line. During this kind of accident, the second heatup phase has the highest probability of fuel failure because of the relatively long time the cladding is at high temperature while the rod internal overpressure causes elevated cladding stresses. Besides the variations in fuel burnup, the rod internal pressure was varied from 2.5 to 12.5 MPa at a steady state temperature. The test rod was then subjected to a prototypical temperature history for a

[1] Neutron flux environment is characterized here by the heat generation in UO_2 fuel and the heat transfer from the fuel to the cladding depending on the state of the fuel.

PWR during a postulated LOCA. Heating rates varied between 6 and 20 K/s.

The design of a UO_2 fueled test rod is shown in Fig. 6. The test rod radial dimensions (Table 7) were typical of a German 1300 MWe PWR fuel rod. The active fuel length was 500 mm, roughly equal to the axial distance between spacer grids of fue1 elements in a reactor. Two different pellet-cladding gap sizes were used for the tests with nuclear active rods [15]. In the test series G3 (35 MWd/kgU) and for comparison with the B3 series (0 MWd/kgU), the cold diametric gap size of the rods was reduced from 190 to 150 μm to compensate for the low coolant pressure environment of the FR2 reactor, relative to that of commercial PWRs [15]. Detailed characterizations of each fuel rod, i.e. cladding and fuel pellet, and rod instrumentation are provided in [15].

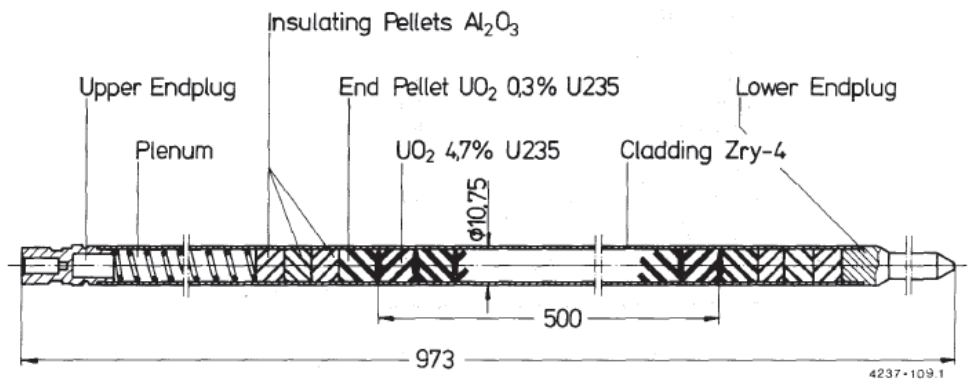

Figure 6: KfK-83 test rod design with numerical values in mm; from Karb et al. [15].

Each test started with a steady state phase, during which the rod was pressurized to a prescribed level at a steady state temperature ($\approx$ 623 K) by addition of helium to the fission product gas generated during preirradiation [15]. The test rod was then exposed to a prototypical temperature history obtained by computer simulation of a PWR fuel rod during a LOCA (a double-ended break of the cold leg pipe). The transient in the test loop was started by interruption of the loop coolant flow and system depressurization. The coolant flow rate past the test rod was reduced to zero and the system pressure to atmospheric pressure. During the subsequent heatup phase, the test rod power was kept constant until the target cladding temperature of about 1200 K was attained. At that temperature, the rod power was rapidly reduced by a reactor scram. A schematic illustration of the test procedure is given in Fig. 7, see [15].

Cladding deformation and burst were monitored during each test per traces of cladding temperature and internal rod pressure. When the fuel-cladding gap distended considerably by radial expansion close to or at the instant of burst, all thermocouples showed a temperature drop. Heatup continued until the power was reduced, e.g. at about 80 s. Then, say at about 160 s, quenching was initiated causing the cladding temperature to fall rapidly to coolant temperature.

Table 7: KfK-83 nominal fuel rod data [15].

Fuel cladding		
Material		Zircaloy-4
Outer diameter	mm	10.75
Inner diameter	mm	9.3
Wall thickness	mm	0.725
Fuel pellets		
Material		UO_2
Diameter	mm	9.11/9.15
Length	mm	11
^{235}U (active zone)	wt%	4.7
^{235}U (end pellets)	wt%	0.3
Active length	mm	500
Density	g/cm^3	10.35
Theoretical density	%	94.4
Insulating pellets		
Material		Al_2O_3
Diameter	mm	9.15
Length	mm	8.0
Void volumes		
Dishing per pellet	mm^3	16
Gap volume	cm^3	1.57
Total plenum volume	cm^3	28.12
Fill gas composition		100% Helium

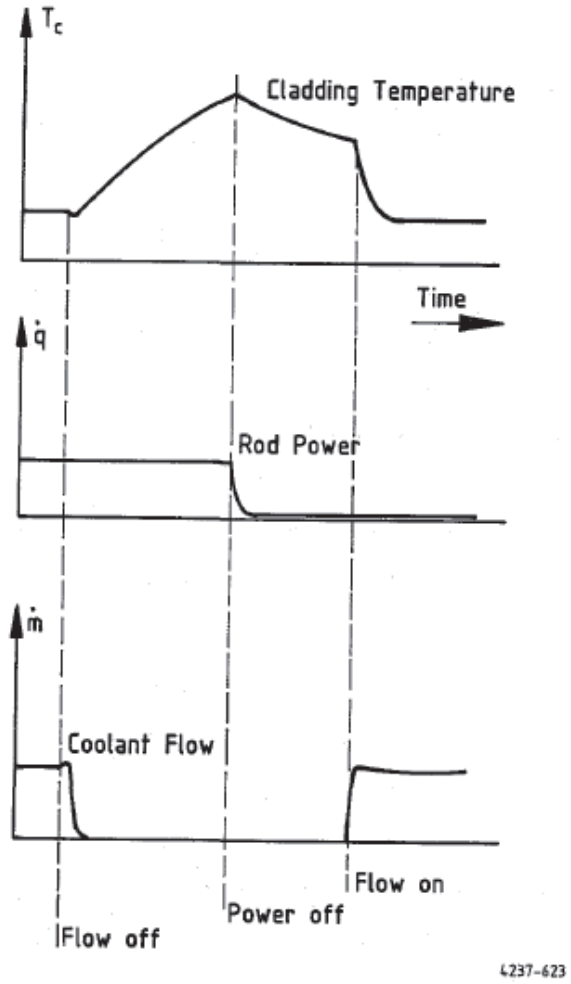

Figure 7: KfK-83 test procedure schemata; from Karb et al. [15].

Cladding burst data, i.e., burst temperature, burst pressure and maximum circumferential strain at the rupture location for KfK-83 tests are listed in Table 8. The main conclusions from these tests are as follows:

- Post-test analysis of Zircaloy-4 cladding microstructure indicated coarse-grained structures for the temperature region around the $\alpha \rightarrow (\alpha + \beta)$ phase boundary and within the single-phase β-region, whereas grain growth was rather limited for the two-phase microstructures. Microstructura1 analysis of the maximum cladding temperature revealed azimuthal (circumferential) temperature differences from 0 to about 100 K. Microstructure basically confirmed the temperature measurements. Figure 8 shows cladding burst strain versus maximum azimuthal temperature difference at the burst elevation for the FR2 in-reactor tests and compared with the REBEKA burst criterion based on laboratory tests (KfK-82 series).

- The burst data of the tests with nuclear active fue1 rods (burst temperature, burst pressure, and burst strain) were similar to the results obtained in laboratory tests using electrically heated simulators and those from other out-of-reactor experiments.

- Fuel pellets in unirradiated tests rods usually remained intact during transient test, whereas pellets in irradiated rods, already cracked during preirradiation, were found fragmented after the transient test in sections of the tube with major deformation. Significant axial fuel relocation was observed for the preirradiated rods with appreciable ballooning.

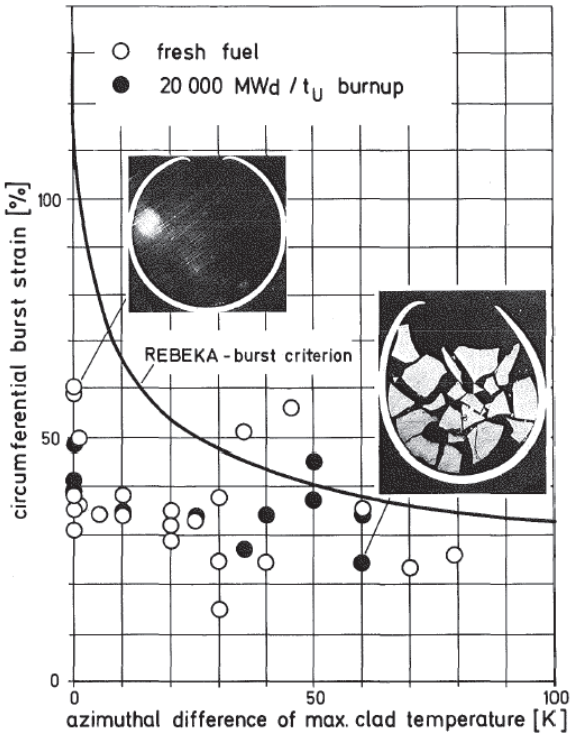

Figure 8: Circumferential burst strain of Zircaloy-4 tubes versus azimuthal temperature difference at maximum cladding temperature [23].

Table 8: KfK-83 single-rod burst tests (data set IV) in steam [15, 22].

Rod No	Burnup MWd/kgU	$\dot{T}$ K/s	p_0 MPa	p_B MPa	$p_{\max}$ MPa	T_B K	$\epsilon_{\theta,\max}$ %	t_B s
A1.1	0	7.0	5.2	5.0	5.4	1083	64	79
A2.1	0	19.0	9.4	8.8	10.0	1093	36	20
A2.2	0	12.1	6.7	5.8	7.5	1133	56	38
A2.3	0	13.0	2.6	2.5	2.7	1288	35	55
B1.1	0	17.5	5.6	5.2	5.9	1173	29	40
B1.2	0	8.7	5.0	4.5	5.5	1188	26	72
B1.3	0	12.5	6.6	6.1	7.1	1118	34	37
B1.5	0	9.2	5.2	4.5	5.8	1183	60	72
B1.6	0	8.2	8.5	8.0	9.0	1098	38	56
B1.7	0	11.5	6.6	6.1	7.1	1113	34	41
B3.1	0	10.0	8.5	7.9	9.1	1098	37	46
B3.2	0	12.1	5.6	5.0	6.1	1188	50	55
C1	2.5	14.0	5.1	5.6	5.6	1173	51	47
C2	2.5	12.6	3.2	3.4	3.4	1218	39	58
C3	2.5	13.2	10.5	11.2	11.2	1022	37	32
C4	2.5	12.1	7.3	8.1	8.1	1088	44	41
C5	2.5	9.3	2.4	2.5	2.5	1189	62	78
E1	8	12.5	2.5	2.6	2.6	1183	30	59
E2	8	11.7	12.1	12.9	12.9	981	46	29
E3	8	11.2	5.3	5.6	5.6	1133	31	47
E4	8	11.6	7.9	8.6	8.6	1054	55	35
E5	8	11.5	2.3	2.6	2.6	1129	67	63
F1	20	10.6	6.4	7.2	7.2	1163	59	43
F2	20	8.7	5.8	6.2	6.2	1166	38	57
F3	20	10.1	4.4	4.6	4.6	1205	27	57
F4	20	11.1	7.8	8.4	8.4	1108	34	37
F5	20	10.1	6.6	7.2	7.2	1153	41	49
G1.2	35	6.9†	7.2	7.5	7.5	1003	30	55
G1.3	35	9.0	4.6	5.1	5.1	1163	62	70
G1.4	35	6.1	8.7	9.1	9.1	1058	33	58
G1.5	35	12.0	5.6	6.0	6.0	1053	41	60
G2.1	35	13.6	3.7	…	…	1142	32	38
G2.2	35	13.0	7.1	7.5	7.5	1119	28	31
G3.1	35	12.3	3.3	…	…	1173	46	55
G3.2	35	15.4	6.5	7.4	7.4	1111	41	33
G3.3	35	9.8	12.0	12.8	12.8	1023	32	29
BSS12*	…	12.2	6.3	7.2	7.2	1115	35	47
BSS22*	…	12.9	5.1	5.9	5.9	1135	64	54
BSS23*	…	12.0	8.8	9.5	9.5	1088	40	37
BSS24*	…	12.6	2.6	2.6	2.6	1231	30	51
BSS25*	…	12.3	11.2	12.0	12.0	1020	29	31
BSS26*	…	12.1	9.9	10.9	10.9	1068	42	34
BSS28*	…	12.6	2.1	2.2	2.2	1240	34	61

†Abnormal heatup, burst during temperature plateau; *Electrically heated fuel rod simulators.

We should note that the burst quantities obtained from the FR2 in-pile tests were defined by Karb et al. [15] as follows:

Burst temperature was the temperature of the cladding at the burst location at the time of burst, which was determined by interpolation between two thermocouples or extrapolation from the thermocouple closest to the burst location. Using this method, azimuthal temperature variations could not be taken into account. However, with the microstructural evaluation of the cladding temperature, it was possible to determine the temperature at any given angular position. But this method could not be directly applied to the burst temperature because the results were only available for the maximum cladding temperature.

Burst pressure was the rod internal pressure at the beginning of the fast pressure drop, i.e., when the pressure decrease rate $\Delta p/\Delta t$ exceeded 1 MPa/s. The time after initiation of the transient was called the *burst time*.

Burst strain was defined as the largest circumferential strain within the ruptured section. More precisely, $\epsilon_{\theta,\max} = \Delta\ell/\ell_0$, where $\Delta\ell = \ell_f - \ell_0$ is the increase in cladding circumference, $\ell_0 = \pi d_0$ the initial circumference with d_0 the initial cladding outer diameter. In computations (Sec. 4.1), we assume $\epsilon_B = \epsilon_{\theta,\max}$.

Burst stress σ_B was defined as "engineering hoop stress", given as

$$\sigma_B = p_B \frac{d_{i,0}}{2w_0}, \tag{5}$$

where p_B is the burst pressure, $d_{i,0}$ the initial cladding inner diameter, and w_0 the initial cladding wall thickness. Note the difference between this formula and that in equation (1).

Burst uncertainties Karb et al. [15] also evaluated the uncertainties in the burst data which are summarized in Table 9; a detailed description of the uncertainties of the burst parameters is provided in appendix C of [15].

Table 9: Uncertainties in burst data of KfK-83 tests [15].

Parameter	Maximum uncertainty	Remark
Burst temperature		
a) Nuclear active rods	± 70 K	Thermocouple A
	± 45 K	Thermocouple B
b) Rod simulators	± 80 K	Thermocouple B
Burst pressure	± 0.15 MPa	
Burst strain	$\pm 4\%$	% of measured strain

2.2.4 KfK-85

Erbacher and Leistikow have presented [16, 23] data on Zircaloy-4 cladding burst obtained from multirod (bundle) tests carried out within the REBEKA program on electrically heated rod simulators. The Zircaloy-4 cladding tubes had an outer diameter of 10.75 mm and an

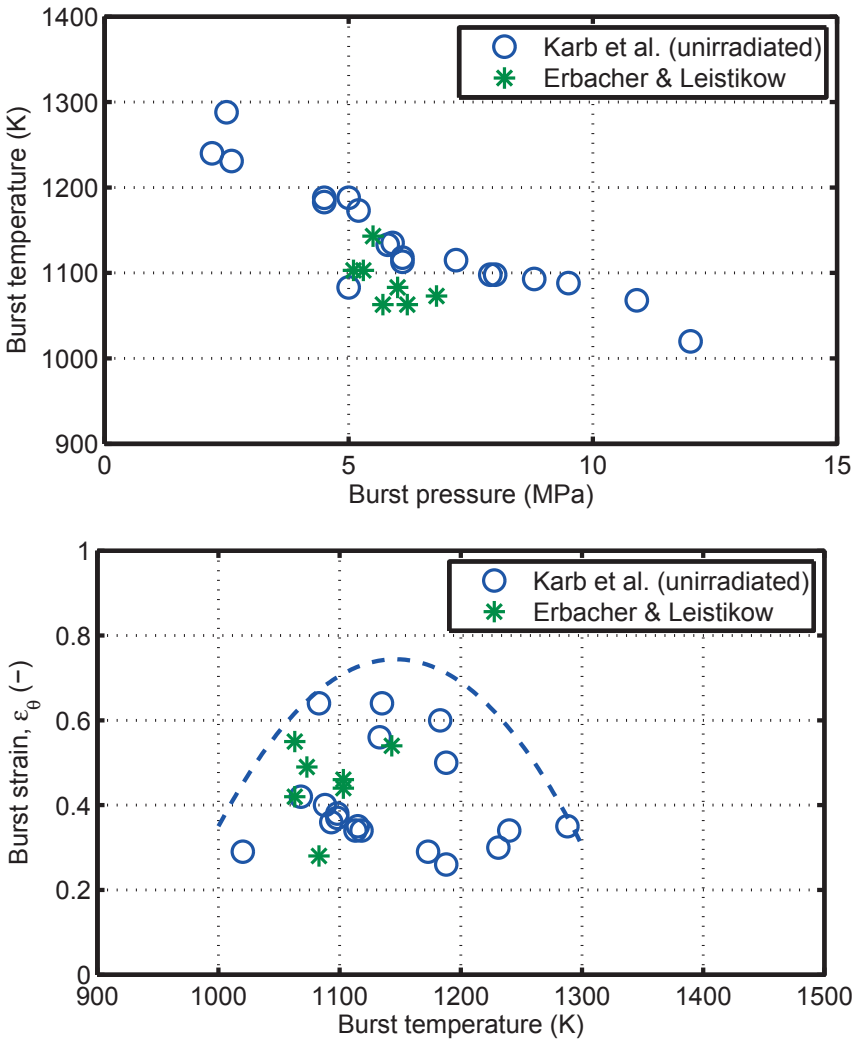

Figure 9: Measured Zircaloy-4 cladding burst data from KfK-83 (Karb et al. [15]), ∘) and KfK-85 (Erbacher & Leistikow [23], ∗). The dome over the burst strain vs. temperature data is a trend line.

inner diameter of 9.3 mm; and they were cold-worked and stress-relieved. The rod internal pressure in these tests was produced by pressurizing the rods with helium, adjusted to 7 MPa, at the beginning of the heat-up phase [40]. The KfK-85 data represent tests that had the potential for maximal ballooning, meaning that cladding burst occurred in the high α-phase of Zircaloy, which is around 1073 K (800°C). The heating rate during heatup in the tests was 7 K/s or less. The burst pressures were between 5 and 7 MPa and the measured hoop strain ranged from 0.28 to 0.55. In addition, the azimuthal temperature difference of cladding tubes varied between 20 and 70 K. Figure 9 depicts the KfK-85 data (asterisks) on burst temperature vs. burst pressure and burst hoop strain vs. burst temperature. Moreover, for the sake of comparison, we have also plotted in the same diagrams the corresponding KfK-83 data (circles), namely the unirradiated rods in Table 8. The top panel in Fig. 9 shows a steady decline of burst temperature with increasing pressure, while in the bottom panel, it is seen that the burst strain data exhibit a heap-like scatter peaked around 1150 K.

2.2.5 KfK-87

Creep and rupture behavior of pressurized Zircaloy-4 were investigated in steam and other gas mixtures in a KfK laboratory under LOCA conditions of PWRs [24]. The tests were performed in atmospheric pressure. The cladding material's main chemical composition was specified as Zr-base, 1.6Sn-0.23Fe-0.11Cr-0.12O-0.0015H by wt% [24]. The tube specimens tested were 50 mm long with an outer diameter of 10.75 mm and a wall thickness of 0.725 mm. They were pressurized with argon gas up to 15 MPa in the temperature range of 873 to 1573 K; see figure 16 in [24].

Leistikow and Schanz [24] performed a series of isothermal and temperature varying tests under isobaric and pressure-transient conditions in steam and other gas mixtures. After the tests, the cladding specimens were examined mainly at the location of rupture, where the extent of hoop strain was measured and the crack morphology was identified. In particular, the formation of oxygen-rich layers, their cracking during deformation plus microstructural changes of the matrix were investigated [24].

Here, we consider both isothermal-isobaric creep rupture testing data in steam (3.2-7.1 MPa, 1073 K) and temperature-transient/isobaric testing data conducted in steam (0.7-1.9 MPa, 1223-1573 K). The former burst test data are listed in Table 10, while the latter in Table 11. The burst data consist of tube internal pressure, the engineering hoop stress [cf. Eq. (5)] at burst, burst temperature and time to burst. Figure 10 depicts the cladding temperature versus time for the transient tests.

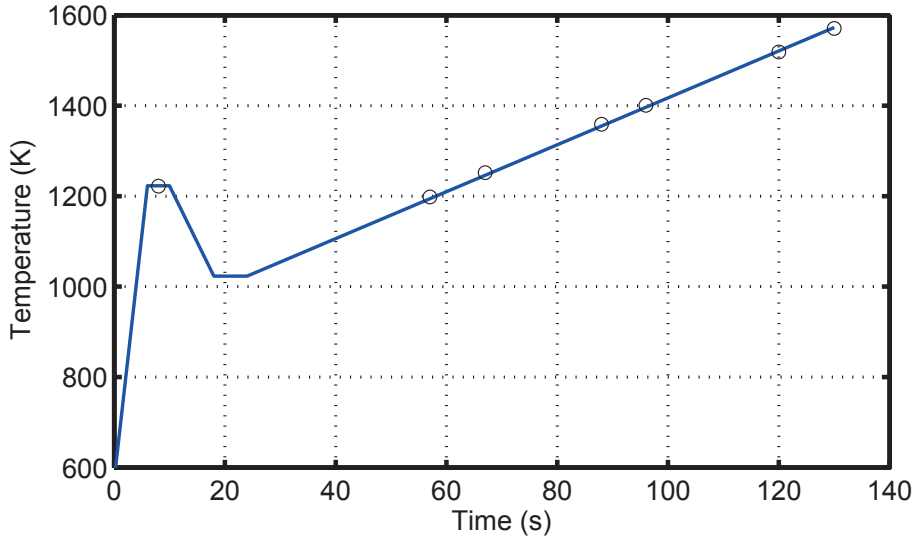

Figure 10: Temperature-transient history of isobaric creep-rupture testing of Zircaloy-4 tube specimens in steam. The circles indicate the points at which rupture occurred in the seven tubes tested with different internal pressures; see figure 20 in [23].

Table 10: Measured data obtained from isothermal-isobaric creep-rupture testing of Zircaloy-4 tubes in steam at 1073 K [24], KfK-87 data set VI.

Test # -	Tube pressure MPa	Burst hoop stress MPa	Burst hoop strain -	Burst time s
1	3.2	20.6	0.723	2223
2	4.12	26.5	0.780	574
3	5.13	33.1	0.977	180
4	6.0	38.6	0.901	55
5	7.06	45.7	0.931	42

Table 11: Measured data obtained from transient-temperature isobaric creep-rupture testing of Zircaloy-4 tubes in steam [24], KfK-87 data set VI.

Test # -	Tube pressure MPa	Burst hoop stress MPa	Burst hoop strain -	Burst temperature K	Burst time s
1	1.88	11.9	0.812	1222	8
2	1.7	10.8	0.377	1206	57
3	1.49	9.6	0.578	1252	67
4	0.9	5.8	0.701	1359	88
5	0.8	5.2	0.569	1401	96
6	0.72	4.6	0.371	1519	120
7	0.7	4.4	0.296	1571	130

2.2.6 KfK-88

Single rod burst tests on pressurized heavy-water reactor (PHWR) Zircaloy-4 cladding specimens conducted in the KfK REBEKA test facility have been reported in [25, 40]. Transient tests were done at a variety of internal pressures and temperatures to establish data under LOCA conditions and examine the influence of material parameters. The main objectives of these tests were: (i) to obtain data on the ballooning behavior of the Argentine Zircaloy-4 cladding under specified internal pressures, temperatures and temperature gradients. (ii) to establish a quantitative difference with the cladding tubes manufactured by CONVAR (Argentina) and NRG (Germany); (iii) to include the mechanical properties information into fuel modeling codes for evaluating cladding deformation over a range of LOCA scenarios.

The nominal cladding outer diameter (COD) was 11.9 mm with a wall thickness of 0.55 mm. All the specimens were 500 mm long with an internal heated length of about 325 mm. A stack of alumina ($A1_2O_3$) annular pellets was used to simulate the fuel column in a fuel rod. The diametral gap between the cladding inner diameter (CID) and OD of the pellets was 0.15 mm. The axial gap distance between the end plugs and alumina pellets stack was 15 mm. Hence, one may suppose that these tests were carried out under axially unconstrained conditions.

The cladding was heated indirectly by conduction heating from inside using an electrically insulated heater rod installed at the center. The Zircaloy cladding, the aluminium oxide pellets and the heater rod were assembled into the complete fuel rod simulator, Fig. 11. The test device consisted mainly of a fuel rod simulator, a gas-handling equipment to pressurize the sample, a steam generator and a DC power supply for indirect electrical heating of the tube. In the REBEKA test facility, the test environment was almost stagnant steam at atmospheric pressure at 473 K [40]. Figure 12 shows the equipment schematically [25].

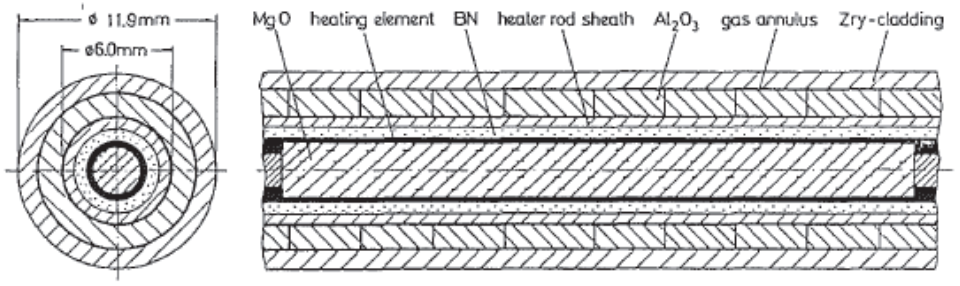

Figure 11: Schematic design of the fuel rod simulator in KfK-88 tests; from [25].

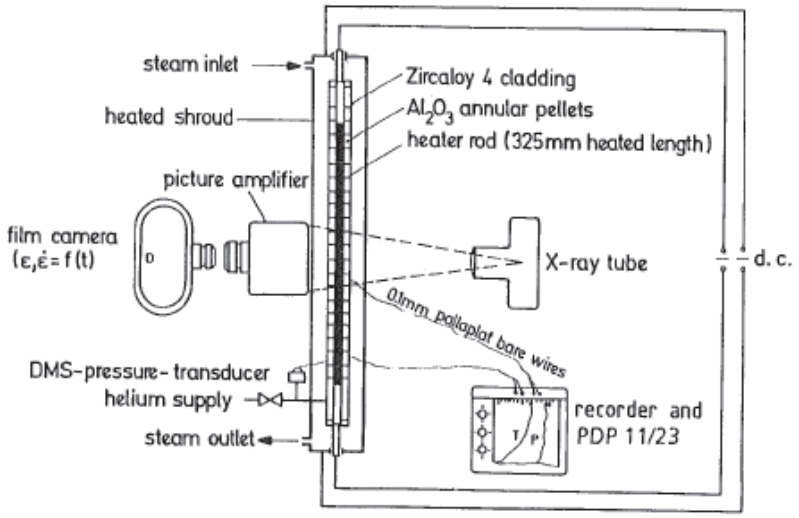

Figure 12: Single-rod test rig in KfK-88 experiments; from [25, 40].

Each test was started after the entire assemblage was equilibrated at an initial temperature of about 300 °C using the internal and shroud electrical heaters and superheated steam. Tests were run with tube internal pressures varying from 0.65 to 9.8 MPa at a nominal heating rate of 1 K/s [25]. The amount of circumferential expansion, the extent of wall thinning, axial length change, burst temperature and physical appearance of the tubing for each test were measured and recorded [25]. The tests were limited to two controlled independent variables, namely internal pressure and heating rate. The dependent variables were burst temperature, time to burst, circumferential and radial (wall thickness) strain, and the physical appearance of the ruptured tubing.

Markiewicz and Erbacher [25] measured the hoop strain by wrapping a piece of Scotch tape around the tube at the rupture, marking the tape at the rupture edges, removing the tape, and measuring the circumference from one edge of the rupture around to the other. The hoop strain was defined as $\epsilon_\theta = (\ell_f/\ell_0 - 1)$, where ℓ_f is the final length and ℓ_0 the initial circumference. Finally, they sectioned each tube through the region of maximum expansion and measured the remaining wall thickness. The measured burst pressures were converted to burst stresses according to the formula in Eq. (5). Moreover, the cross section at the burst location was examined for tubes that were ruptured at temperatures below 1113 K (840°C). The true radial fracture strain of the cladding was determined using the following formula:

$$\varepsilon_r = \ln \frac{w_a}{2w_0}, \tag{6}$$

where ε_r is the true rupture radial strain, w_a is the thickness of the rupture tip, and w_0 is the initial cladding thickness.

The burst data in which the tubes experienced uniform cladding temperature distribution comprising burst pressure, burst temperature, burst strain, burst stress and time-to-burst are listed in Tables 12 and 13 for CONVAR and NRG tubes, respectively. In these tests the failure mode of the cladding was strongly influenced by the burst temperature. Markiewicz and Erbacher [25] observed two different failure modes in the temperature range between 973 and 1273 K. The specimens that ruptured in the α phase region, the rupture was violent and the opening area was large with nearly rectangular shape. For bursts that occurred in the $\alpha+\beta$ mixed phase and the low β phase, the burst opening was narrow with a very small area. In more detail, the size of the opening increased with increasing burst pressure, with a maximum of 21 mm^2 in the $\alpha+\beta$ phase and low β phase, and between 68 and 320 mm^2 for ruptures that occurred in the α phase. This indicates the effect of increase in stored energy on deformation during the burst.

It is anticipated that during refilling and reflooding stage of a LOCA, both axial and circumferential temperature differences are generated. To investigate the effect of temperature nonuniformity on the maximum circumferential expansion of Zircaloy cladding Markiewicz and Erbacher carried out a series of transient-heating burst tests [25]. As described in [25], the variation in the circumferential temperature measured with and without the shroud heater were within 3 K (minimum) and 58 K (maximum) respectively, for the CONVAR cladding. Table 14 lists these values and those of burst strains. All the tests were performed at the same constant internal pressure with a heating rate of 1 K/s. The temperature in the last part of each test was monitored at every 0.1 s. Choosing this interval was because of the higher azimuthal temperature differences that the cladding developed in the few seconds prior to the rupture due to the nonuniformity in the ballooning in this type of experiments. More details regarding the conduct of the tests and discussion of the results can be found in [25].

Table 12: Burst test data for CONVAR Zircaloy-4 tubes in steam [25], KfK-88 data set VII. The heating rate $\dot{T} = 1$ K/s.

Test # -	Burst pressure MPa	Burst Temperature K	Burst hoop strain -	Burst hoop stress MPa	Axial strain -	Burst time s
1	4.00	1105	0.84	39.0	0.0066	450
2	4.00	1093	0.70	39.0	0.0	442
3	4.00	1111	1.06	39.0	-0.065	450
4	5.40	1049	0.99	53.0	-0.113	399
5	5.40	1041	0.76	53.0	-0.113	398
6	5.40	1061	> 0.71	53.0	-0.06	407
7	6.70	1031	1.07	66.0	-0.145	376
8	6.70	1037	0.85	66.0	-0.102	382
9	6.70	1030	0.84	66.0	-0.055	457
10	8.00	997	0.74	78.5	-0.108	348
11	8.00	1000	0.72	78.5	-0.043	358
12	8.00	997	0.76	78.5	-0.06	351
13	9.40	983	0.70	92.0	-0.033	337
14	9.40	988	0.78	92.0	-0.073	339
15	9.40	982	0.67	92.0	-0.053	341
16	2.70	1160	0.80	26.5	0.027	587
17	2.70	1162	0.55	26.5	0.0017	496
18	2.70	1162	0.52	26.5	0.0066	497
27	9.80	976	0.74	96.0	-0.0967	330
28	4.70	1067	1.02	46.0	-0.0783	415
29	2.30	1174	0.45	22.6	0.0033	515
39	1.34	1231	0.68	13.1	0.023	545
40	1.34	1233	0.56	13.1	0.032	555
41	0.65	1285	0.26	6.4	0.052	608
42	0.65	1281	0.24	6.4	0.055	604

Table 13: Burst test data for NRG Zircaloy-4 tubes in steam [25], KfK-88 data set VII. The heating rate $\dot{T} = 1$ K/s.

Test # -	Burst pressure MPa	Burst Temperature K	Burst hoop strain -	Burst hoop stress MPa	Axial strain -	Burst time s
1	4	1084	0.73	39.0	-0.013	420
2	4	1071	0.82	39.0	-0.005	416
3	4	1089	0.88	39.0	-0.048	431
4	5.4	1051	0.93	53.0	-0.038	401
5	5.4	...	...	53.0	-0.035	...
6	5.4	1045	0.69	53.0	-0.0033	404
7	6.4	1013	0.67	63.0	-0.0033	366
8	6.7	1028	0.72	66.0	-0.075	372
9	6.7	1017	0.76	66.0	-0.03	377
10	6.7	1007	0.77	66.0	-0.0067	370
11	8	1004†	0.79	78.5	-0.02	354
12	8	1000	0.76	78.5	-0.0267	348
13	8	1000	0.89	78.5	-0.08	336
14	9.4	980	0.77	92.0	-0.05	332
15	9.4	982	0.86	92.0	-0.085	333
16	9.4	981	0.72	92.0	-0.01	336
17	2.7	1150	0.6	26.5	0.028	490
18	2.7	1160	0.63	26.5	0.022	502
19	2.7	1162	0.6	26.5	0.023	500

† This temperature is misprinted in [25] as 7231°C; we have deemed it to be 731°C.

Table 14: Burst test data for Zircaloy-4 tubes in steam with circumferential temperature difference (CTD), KfK-88 data set VII [25]. The heating rate $\dot{T} = 1$ K/s.

Test #	Burst pressure	Burst Temperature	Burst hoop strain	CTD
-	MPa	K	-	K
CONVAR cladding				
19A	6.56	990	0.25	33
20A	6.70	990	0.353	21
21A	4.25	1056	0.287	41
22A	4.27	1057	0.357	16
23A	4.30	1086	$>$0.282	58
24A	4.27	1074	0.27	49
25A	6.40	1071	0.36	33
NRG cladding				
21G	6.66	1002	0.42	41
22G	6.68	1027	0.49	70
23G	4.25	1050	0.6	23
24G	4.23	1046	$>$0.40	14
25G	4.25	1057	0.52	22
26G	4.25	1047	0.7	11
27G	4.28	1067	0.475	28
29G	4.28	1050	0.55	34

2.3 CEGB creep rupture tests: Zircaloy-4 cladding

The creep rupture of Westinghouse Zircaloy-4 fuel cladding tubes of the 17×17 PWR design at temperatures between 973 and 1223 K, using constant pressure biaxial creep tests, has been reported by Donaldson and coworkers [26, 27]. They have presented data on creep rates, cladding rupture strain and times to rupture as a function of stress and temperature. Here, we only consider their creep rupture data. In an earlier report, the creep rate behavior of these tubes were assessed [41]. We do not have access to their creep rupture data made in the pure β phase, that is, at temperatures between 1323 K and 1473 K as alluded in [42]. Sample cladding tubes with nominal dimensions of 9.5 mm outside diameter and 0.56 mm wall thickness were studied. Test samples, 760 mm long, were cut from as-fabricated tubing that was in stress relieved condition. A Pt-Pt/13 percent Rh thermocouple was spot welded to the inner surface of each tube sample at the mid-length plane, where diametral changes were measured during creep deformation. Donaldson et al. tested all the tube samples under isothermal conditions at constant internal pressure using purified argon gas. They evacuated the tube containment vessel to 5×10^{-3} Pa pressure. Tests were continued until rupture of the specimen.

In the two-phase coexistence domain, samples were heated electrically to the test temperature within the $(\alpha + \beta)$ domain at a rate of 10 K/s and then kept at that temperature for 10 minutes (annealing time) before pressurizing the tubes and performing the creep testing. Additional annealing times at temperatures were used to examine the influence of this parameter on creep rate.

The estimated axial temperature variations were ± 2 K over the central 350 mm of the test sample while the internal gas pressure was controlled to $\pm 7 \times 10^{-3}$ MPa for pressures in the range 0.1 to 8 MPa. They measured the increase in tube diameter during the test at a single position mid-way along the tube using a laser gauge. They report that the tube "distension" was uniform up to large strains before local ballooning and rupture occurred at a random position along the tube. The method for determining the creep strain rate and the strain rupture is detailed in [42].

The data on rupture time versus rod pressure for temperatures between 973 K and 1073 K (α phase) are shown in Fig. 13. In Fig. 14 portion of these data at 1073 K (Donaldson et al. 1985 [42]) are compared with the creep rupture data of Leistikow & Schanz (KfK-87) [24]; these data are discussed in section 2.2.5. Note that despite the difference between the test environments, i.e. argon/vacuum (CEGB-84/85) vs. steam (KfK-87), the two sets of data at 1073 K fall into the same track. The corresponding data for temperatures between 1098 K and 1223 K ($\alpha + \beta$ phase) are shown in Fig. 15. Figure 16 displays the associating data for the engineering hoop strain as a function of applied tube pressure (lower panel). We should mention that the refs. [26, 27] give the data in terms of applied hoop stress. We have transformed these data to the tube internal pressure by using the thin tube formula $p = 2w_0\sigma_\theta/d_{i,0}$. As can be seen from Fig. 16 and also noted in [26], at the highest test temperature, 1223 K, the rupture strain does not exhibit a systematic change with internal pressure or hoop stress. But between 1098 and 1198 K, a consistent decrease is observed in the value of the rupture strain with increasing tube pressure. This pressure or stress dependence is more discernible at higher temperatures. In addition, the magnitude of the rupture strain decreases with increasing temperature at all stress levels. Donaldson et al. [26] found that the largest burst strains occur at the lowest pressures and temperatures and conversely the lowest burst strains occur at the highest pressures and temperatures.

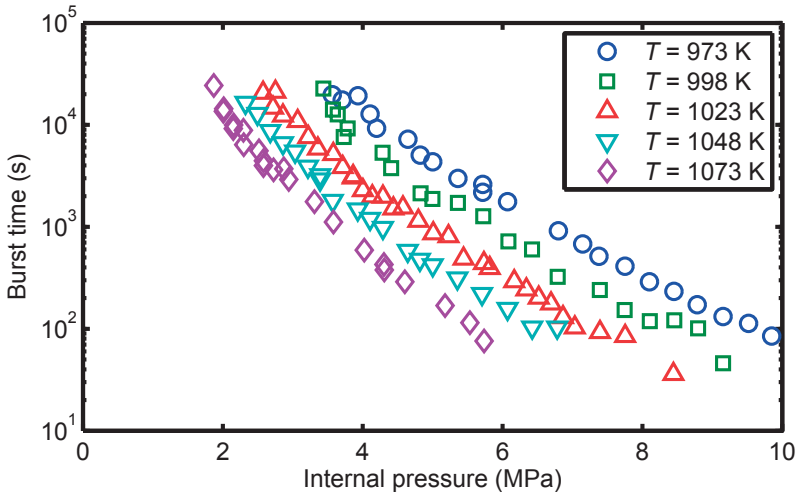

Figure 13: Variation (measured) of time-to-burst versus tube internal pressure in the Zircaloy-4 α phase temperature range; CEGB-84/5 data set VIII [27].

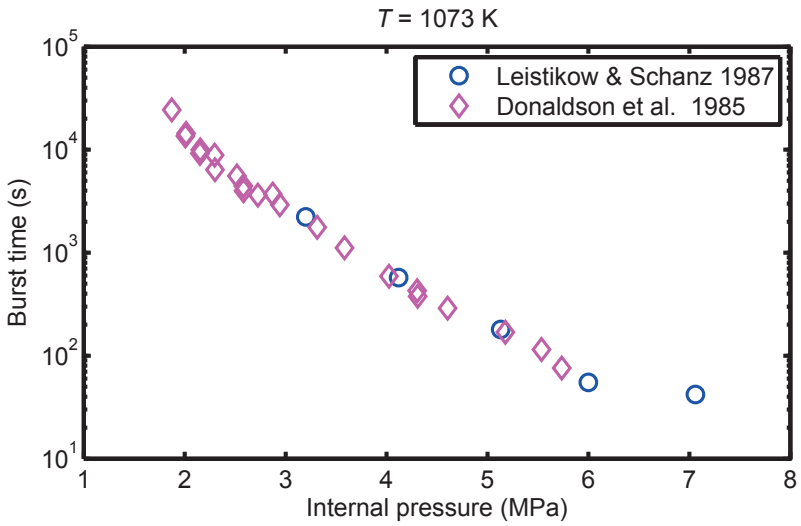

Figure 14: Variation (measured) of time-to-burst versus tube internal pressure for Zircaloy-4 at 1073 K; Leistikow & Schanz KfK-87 data [24] versus Donaldson et al. CEGB-84/5 data [27].

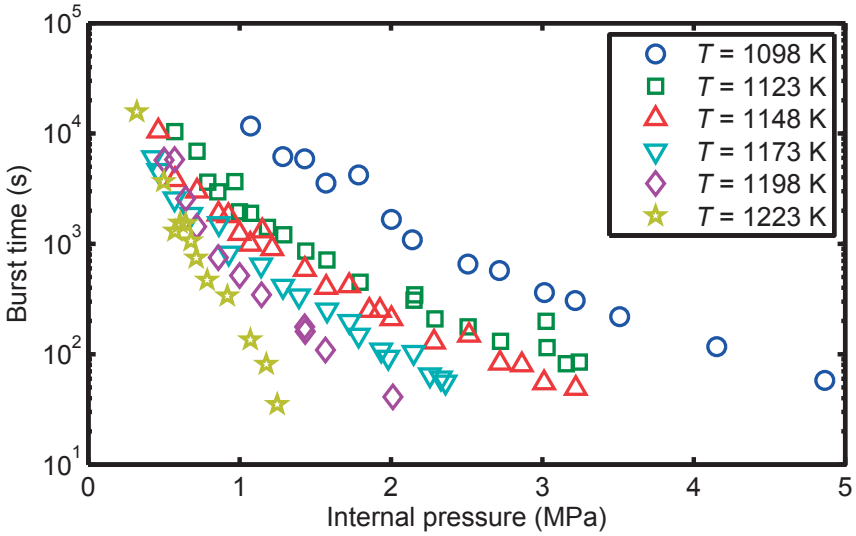

Figure 15: Time-to-burst measured data versus tube internal pressure in the Zircaloy-4 ($\alpha + \beta$) coexistent-phase temperature range; CEGB-84/5 data set VIII [26].

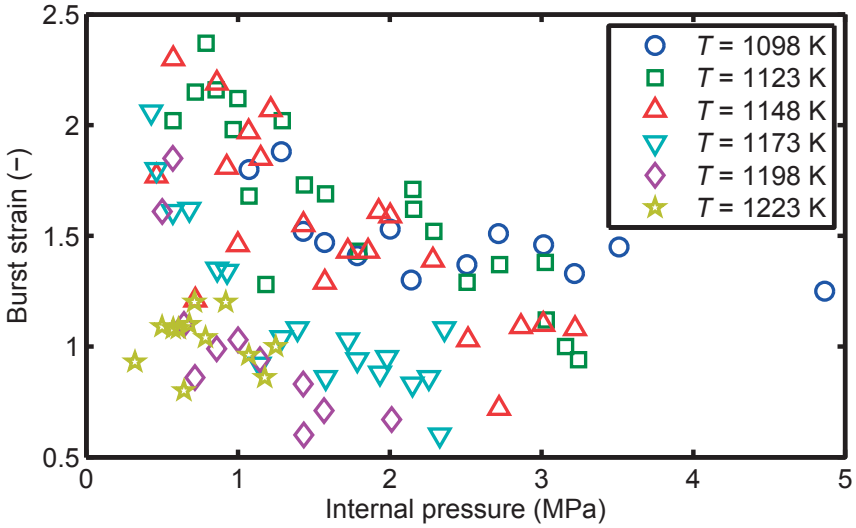

Figure 16: Variation (measured) of rupture engineering hoop strain with tube internal pressure in the Zircaloy-4 ($\alpha + \beta$) coexistent-phase temperature range; CEGB-84/5 data set VIII [26].

2.4 CEA-02 creep rupture data: Zircaloy-4 + 600 wppm hydrogen

Thermal-mechanical tests under LOCA conditions on Zircaloy-4 cladding specimens hydrogenated in a laboratory have been briefly reported by Brachet et al. [28]. The tests were performed in the EDGAR-2 test facility in CEA, France, to study separate effect behavior of fuel cladding during the initial phase of a LOCA transient [29].

The design of the Zircaloy-4 cladding used is reported to be typical of AFA-2G FRAMATOME-ANP fuel assembly with a tin content of 1.3wt% [28]. The dimensions of the cladding are not given in [28], however according to [43], for this design, the cladding tube outer diameter and wall thickness are 9.5 mm and 0.57 mm, respectively; which are that of standard 17×17 assembly design dimensions. The length of the cladding specimen tested was 490 mm and the specimens were pressurized in the EDGAR-2 facility with argon gas.

Results of two types of EDGAR-2 cladding rupture tests have been reported in [28], namely those from creep tests and those from thermal ramp tests. The creep tests were conducted in isothermal and isobaric conditions in steam environments. The test temperatures were between 873 K and 1123 K and were performed in steps of 50 K mainly on Zircaloy-4 hydrogenated to 600 wppm; a few tests were also made on Zircaloy-4 with 1000 wppm. The tests were conducted at different levels of internal pressure to examine the effect of stress on the creep strain rate. For each test temperature, the values of the internal pressure were selected such that the time-to-rupture (TTR) would range from 10 to 1000 s [28].

Time-to-rupture versus internal pressure data indicate that the hydrided samples exhibit lower creep resistance, i.e. shorter TTR than the as-fabricated samples, and the effect is most prominent for samples containing the highest concentration of hydrogen, which was 1000 wppm [28]. Burst stress versus burst temperature data obtained from these tests are depicted in Fig. 17. Unfortunately, the corresponding data on as-fabricated, i.e. unhydrogenated Zircaloy-4 samples are not provided in [28].

The thermal ramp tests in the EDGAR-2 facility were carried out under constant internal pressure with a constant heating rate from 623 K to the burst temperature in steam. Post-test measurements (uniform and total elongation) were made on Zircaloy hydrogenated to 650 and 1200 wppm tested at a rate of 10 K/s for three levels of internal pressure, namely 1, 2.5 and 7.5 MPa [28]. Brachet and coworkers [28], by recording the variation of specimen hoop strain with temperature during the transient for as-received versus hydrogenated Zircaloy-4, showed that the hydrogen content level reduces the creep resistance and also the post-test ductility of the material. The results of their measurements regarding burst stress versus burst temperature of Zircaloy-4 with 600 wppm hydrogen, three thermal ramp data, are shown in Fig. 17. We should note that the burst stress data in Fig. 17 were determined from burst strain through a formula similar to Eq. (4) without the p_B/p_0 prefactor, namely

$$\sigma_B = \sigma_0(1 + \epsilon_B)^2, \tag{7}$$

in which ϵ_B is called the local circumferential elongation measured 20 mm away from the position of rupture, cf. figure 4 in [29].

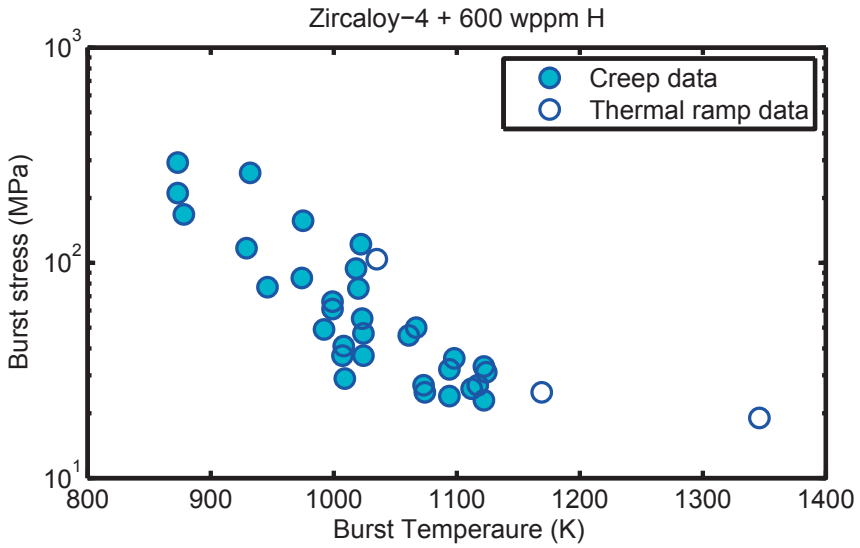

Figure 17: Measured burst data for as-received but hydrogenated Zircaloy-4 (600 wppm H); CEA-02 data set IX, Brachet et al. [28].

Brachet and coworkers [28] noted that the effect of hydrogen on the mechanical behavior of Zircaloy-4 during creep and thermal ramp tests is primarily affected by the decrease of creep resistance and loss of ductility. The results can be due to both the effect of the $\alpha \rightarrow \beta$ phase transformation temperature shifts, where hydrogen acts as β stabilizer, i.e. it expands the β domain of the phase diagram in solid solution and also by an intrinsic effect of hydrogen on the creep rate, especially in the α phase and the lower $\alpha + \beta$ temperatures.

2.5 CEA-00 creep rupture data: Zr1%Nb (M5 cladding)

Thermal-mechanical tests under LOCA conditions on as-received Zr1%Nb cladding (M5 alloy) specimens have been briefly reported by Forgeron et al. [29]. The tests were performed in the EDGAR-2 test facility in CEA, France, to study separate effect behavior of fuel cladding during the initial phase of a LOCA transient per procedure described in the previous subsection. More information regarding the EDGAR-2 test facility and testing procedure can be found in [29].

The cladding material M5, also called ZrNbO alloy, is specified to have a nominal chemical composition: Zr-base 1Nb-0.125O by wt% [29]. The dimensions of the cladding tube specimens, except their length, which was 490 mm, are not specified in [29]. We posit that they had standard 17×17 assembly design dimensions with the outer diameter and wall thickness of 9.5 mm and 0.57 mm, respectively. The tube specimens were pressurized in the EDGAR-2 facility with argon gas.

Cladding burst data, i.e. burst stress versus burst temperature, obtained by creep rupture tests and thermal ramp tests, have been reported by Forgeron and coworkers [29]. The creep tests were performed under isobaric and isothermal conditions in a steam environment. They covered temperatures between 873 and 1273 K and were performed in steps of 50 K in the single-phase α and β domains. In the coexisting ($\alpha + \beta$) domain, the temperature step was reduced to 25 K. In order to examine the effect of stress on the creep strain rate, tests were performed at several levels of internal pressure (not specified in [29]). At each test temperature, the values of the internal pressure were chosen so that time-to-rupture was between 10 and 1000 s.

The thermal ramp tests in the EDGAR-2 facility were carried out under constant internal pressure with a constant heating rate from 623 K to the burst temperature in steam. The tests performed on M5 covered sufficient data to obtain NUREG-630-type ductility correlations [19], i.e. burst hoop strain (total elongation) versus burst temperature. The heating rates in these tests ranged from 2 to 100 K/s and the internal gas pressures varied from 1 to 13 MPa. Burst temperatures in such conditions were from 923 K to 1448 K.

The results of Forgeron et al.'s [29] creep and thermal ramp measurements on burst stress versus burst temperature are shown in Fig. 18. These data are digitalized from figure 15 of [29] and replotted here. The burst stress data in Fig. 18 were determined from burst strain through Eq. (7). Based on these data, Forgeron et al. [29] developed burst criterion correlations (curves), creep burst and thermal ramp, for M5 cladding.

2.6 AEKI-00 BALL tests: E110 cladding

Single rod burst tests on E110 (Zr1%Nb) cladding have been performed under both anisothermal/isobaric and isothermal/anisobaric conditions in laboratory at the AEKI Research Institute of Hungary [30, 31]. The aim of these tests (labeled as BALL series) was to investigate the effects of internal gas pressure and heating rate on the burst pressure of the E110 cladding. Here, we only consider a portion (first group) of these data concerning the anisothermal/isobaric tests (AEKI-00 data set XI).

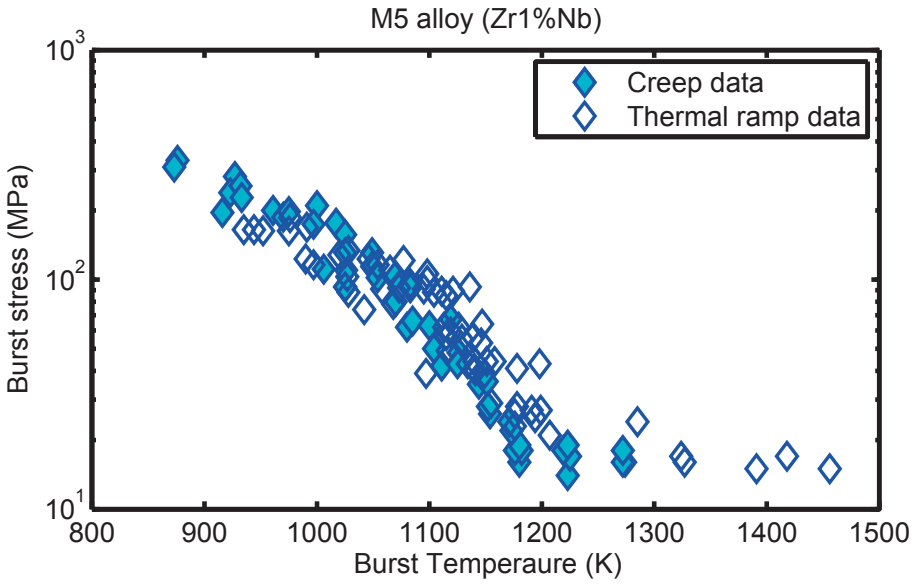

Figure 18: Measured burst data for as-received M5 alloy; CEA-00 data set X, Forgeron et al. [29].

In the first of group of the BALL tests, pressurized E110 cladding samples were subjected to various linear heatup rates up to the cladding burst. The initial pressure of the samples and the applied heating rate were varied from 1.0 to 4.0 MPa and 6.4 to 13.5 K/s, respectively. The specimens were 150 mm long of original VVER (Russian pressurized water reactor) unirradiated cladding tubes with an outer-diameter/wall-thickness of 9.1/0.65 mm. Table 15 gives a summary results of the first group of the BALL tests, AEKI-00 data set XI. Detailed thermal and pressure histories for these test rods have been made available through the NEA database [44].

Table 15: Single rod ballooning test data for E110 cladding; from [30, 31].

Test	$\dot{T}$	p_0	T_B	p_B	ϵ_B	Atmosphere
#	K/s	MPa	K	MPa	-	-
1	6.4	1.0	913	1.59	0.862	steam
2	8.2	1.0	1173	1.4	0.663	steam
3	8.9	4.0	1118	6.08	0.239	Ar
4	8.5	4.0	1136	4.87	0.254	Ar
5	6.7	2.0	1149	3.2	0.268	Ar
6	11.4	2.0	1171	3.29	0.225	Ar
7	12.8	2.0	1162	3.01	0.245	steam
8	6.5	1.0	1113	1.77	0.491	Ar
9	13	1.0	1215	1.41	0.587	Ar
10	9.9	1.0	1194	1.54	0.944	Ar
11	12.3	4.0	1103	6.81	0.378	steam
12	13.5	4.0	1141	5.61	0.129	Ar

2.7 W-EDF-09 burst data: ZIRLO cladding

Single rod burst test data on Westinghouse ZIRLO claddings have been reported by Chapin et al. [32]. Data on both Standard and Optimized ZIRLO are included in a burst temperature versus hoop stress diagram, Fig. 19, which exhibit expected behavior. Chemical composition of these alloys are given by Foster et al. [45]; in brief Standard ZIRLO is Zr-base,1.0Nb,1.02Sn,0.10Fe,0.1O, whereas Optimized ZIRLO is Zr-base,1.0Nb,0.7Sn,0.12Fe, 0.1O in wt% (cf. Table 1).

The test procedure is not described in [32]; however it is indicated that the data span hoop stresses from about 10 to 110 MPa, burst temperatures from 973 to 1473 K, and heating rates between 2.8 and 28 K/s. These data are reproduced here in Fig. 19.

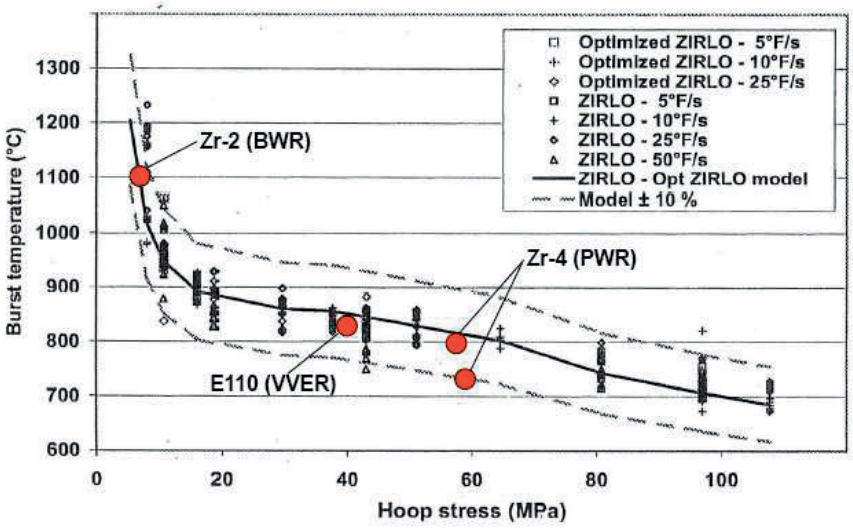

Figure 19: As-received Standard ZIRLO and Optimized ZIRLO cladding burst data presented by Chapin et al. [32]. The red circles are irradiated Zr-base cladding tubes tested in the Halden reactor under LOCA conditions [46], shown for comparison.

2.8 ANL-10 burst data: ZIRLO cladding

Argonne National Laboratory (ANL) workers have performed a number of burst tests on as-fabricated, i.e. unirradiated, ZIRLO [sic] cladding tubes [33]. These tests are within a larger test program, which includes cladding oxidation, quenching and post-LOCA rod bending tests [33, 34, 47]. They were precursors to the integral LOCA tests conducted at Studsvik on irradiated cladding tubes discussed in the succeeding subsection.

The description of the burst test procedure given in [33, 34, 47] is cursory. Table 16 summarizes the ANL test conditions for ballooning, rupture, oxidation, and quench of pressurized, as-fabricated 17×17 ZIRLO cladding LOCA integral samples as given in [47]. Two further sample burst tests on as-fabricated ZIRLO cladding tubes using the ANL procedure have been reported in [35]. For example, during test #175 the cladding was first heated from room temperature to 573 K with a heating rate of 5 K/s, then steam was added for about

960 s, after which temperature was further increased (5 K/s) up to 1473 K. The cladding burst occurred around 1023 K at the pressure of 8.77 MPa.

Results of the ANL burst tests are shown in Table 17. The burst strain values listed in this table are the engineering hoop strains. In more detail, as noted in [33], the rupture strain is defined here as the increase in cladding mid-wall circumference normalized to the initial mid-wall circumference ($\ell_{mi} = 28.05$ mm for 17×17 ZIRLO cladding). For burst strains of the tests #7, #11, and #19, mid-wall circumference was measured from 25X composite images of the cross section through the midspan of the rupture opening. All other burst strains in Table 17 were calculated from an empirical relationship for the final mid-wall circumference (ℓ_{mf}) as a function of measured diameters at two orientations and rupture-opening width, see [33]. This empirical relationship was used to determine ℓ_{mf} as a function of the average of the maximum (rupture tips to back of cladding, d_{max}) and minimum (90° from rupture opening, d_{min}) outer diameters, $d_{av} = (d_{max} + d_{min})/2$, and the rupture width δ_R via $\ell_{mf} = \pi(d_{av} - 0.333\delta_R)$, where the empirical factor 0.333 gave the best fit to the 6 measured ℓ_{mf} values according to Yan et al. [33].

Table 16: Characteristic data for ANL-10 tests on as-fabricated 17×17 ZIRLO cladding specimens [47].

Cladding outer diameter (mm)	9.5
Wall thickness (mm)	0.57
Sample length, minus end caps (mm)	295
Cladding hydrogen content (wppm)	≈ 10
Pellet material	zirconia
Pellet stack length (mm)	280
Gas volume (cm^3)	10
Fill pressure (gauge) at 573 K (MPa)	$4.1 - 11$
Heating rate (K/s)	5

Table 17: Burst test data for as-received ZIRLO cladding tubes in steam, ANL-10 data set XIII [33, 34, 47]. ΔT_B denotes the uncertainty in burst temperature.

Test ID	Fill pressure	Burst temperature	ΔT_B	Burst strain	Burst time†
#	MPa	K	$\pm$ K	-	s
6	8.3	1023	30	0.41	90
7	5.5	1083	30	0.22	102
8	4.1	1118	25	0.19	109
9	2.8	1148	15	0.33	115
10	11.0	988	10	0.68	83
11	9.7	1023	...	0.4	90
12	6.9	1078	20	0.31	101
13	8.3	1014	15	0.41	88.2
14	8.3	1008	6	0.46	87
15	8.3	1028	23	0.5	91
17	8.3	1023	17	0.47	90
18	8.3	1021	4	0.43	89.6
19	4.1	1113	12	0.23	108
21	4.1	1123	10	0.25	110
22	4.1	1110	12	0.2	107.4
25	8.3	1030	21	0.42	91.4
26	8.3	1038	39	0.31	93
27	8.3	1033	23	0.38	92
29	8.3	1019	19	0.49	89.2
30	8.3	1019	19	0.42	89.2
32	8.3	1021	8	0.49	89.6
Studsvik qualification tests [35]					
130	7.9	1028	...	...	91
175	8.5	1023	...	...	90

† Burst time is calculated from burst temperature minus 573 K divided by the constant heating rate of 5 K/s.

2.9 Studsvik-12 burst data: ZIRLO cladding

Six single-rod integral LOCA tests were conducted at the hot cell laboratory of Studsvik Nuclear, Sweden to examine the mechanical performance of ballooned and ruptured high-burnup fuel rods [35, 36]. The program was commissioned by the U.S. Nuclear Regulatory Commission. In each of these tests, a pressurized irradiated (high-burnup) fuel rod segment was subjected to a temperature transient in steam (atmospheric pressure) to induce ballooning, rupture, and high-temperature steam oxidation.

The LOCA equipment utilized was designed to externally heat a 300 mm long, pressurized, irradiated fuel rod up to 1473 K by infrared (IR) radiation [35, 36]. The fuel rodlets were heated in a flowing steam environment from 573 K to a target temperature of about 1473 K at a rate of 5 K/s. The rod temperature was measured with a thermocouple attached by a metal clamp 50 mm above the axial mid plane. The test segment was pressurized with helium. Internal pressures were consistent with a typical end-of-life rod internal pressure, although likely on the high-end, and were selected to induce ballooning and rupture with rupture strains in the range of 30 - 50 %. Rod temperatures were held at 1473 K for either

0, 5, 25, or 85 s to obtain various levels of cladding oxidation [36].

Basic design data and pretest characteristic data for the test rods are listed in Table 18. The cladding material was ZIRLO, but its nominal chemical composition is not given in [35, 36]. The total void volume of the rod was about 10.4 cm^3. More information regarding the LOCA apparatus and test design can be found in [35, 36].

Table 18: Characteristic data for Studsvik-12 ballooning and rupture tests on as-fabricated 17 × 17 ZIRLO cladding; dimensions and initial conditions of the samples [36, 48].

Test ID #	Fuel type	Clad OD mm	Wall thick. mm	Fill pressure MPa	Rod burnup MWd/kgU	H conc. wppm
189	UO_2	9.5	0.57	11	68	176
191	UO_2	9.5	0.57	11	69	187, 271
192	UO_2	9.5	0.57	8.2	68	176, 288
193	UO_2	9.5	0.57	8.2	69	187
196	UO_2/ZrB_2	9.14	0.57	8.2	55	149
198	UO_2/ZrB_2	9.14	0.57	8.2	55	225

Fill pressure is measured at 573 K. UO_2/ZrB_2 is Integral Fuel Burnable Absorber (IFBA). Rod burnup refers to the fuel rod average burnup of the original full length as-discharged rod.

Table 19 lists the values of peak cladding temperature, burst temperature, burst pressure and maximum hoop engineering strain for each test. Specific results of each test are given in [36]. These include cladding temperature and rod internal pressure as a function of time during the transient. Also, post-transient examinations such as profilometry of the cladding, which offers data on the cladding outer diameter as a function of distance from bottom of fuel stack, the burst width and the burst center, etc. are provided in [36]. For two of the tests, 192 and 198, detailed results were made available to us through our participation in the IAEA coordinated research project Fuel Modeling in Accident Conditions (FUMAC) [49]. Cladding temperature and rod internal pressure histories for these rods are depicted in Fig. 20.

Table 19: Burst test data for irradiated ZIRLO cladding in steam, Studsvik-12 data set XIV [36]. Burst strain is the engineering hoop strain.

Test ID #	Peak temperature K	Burst temperature K	Burst pressure MPa	Burst strain -	Burst time† s
189	1223	973	10.90	0.48	80
191	1458	953	10.40	0.50	76
192	1458	973	8.10	0.56	80
193	1458	1001	8.10	0.50	86
196	1223	959	8.10	0.25	77
198	1458	966	8.10	0.25	79

† Burst time is calculated from burst temperature minus 573 K divided by the constant heating rate of 5 K/s.

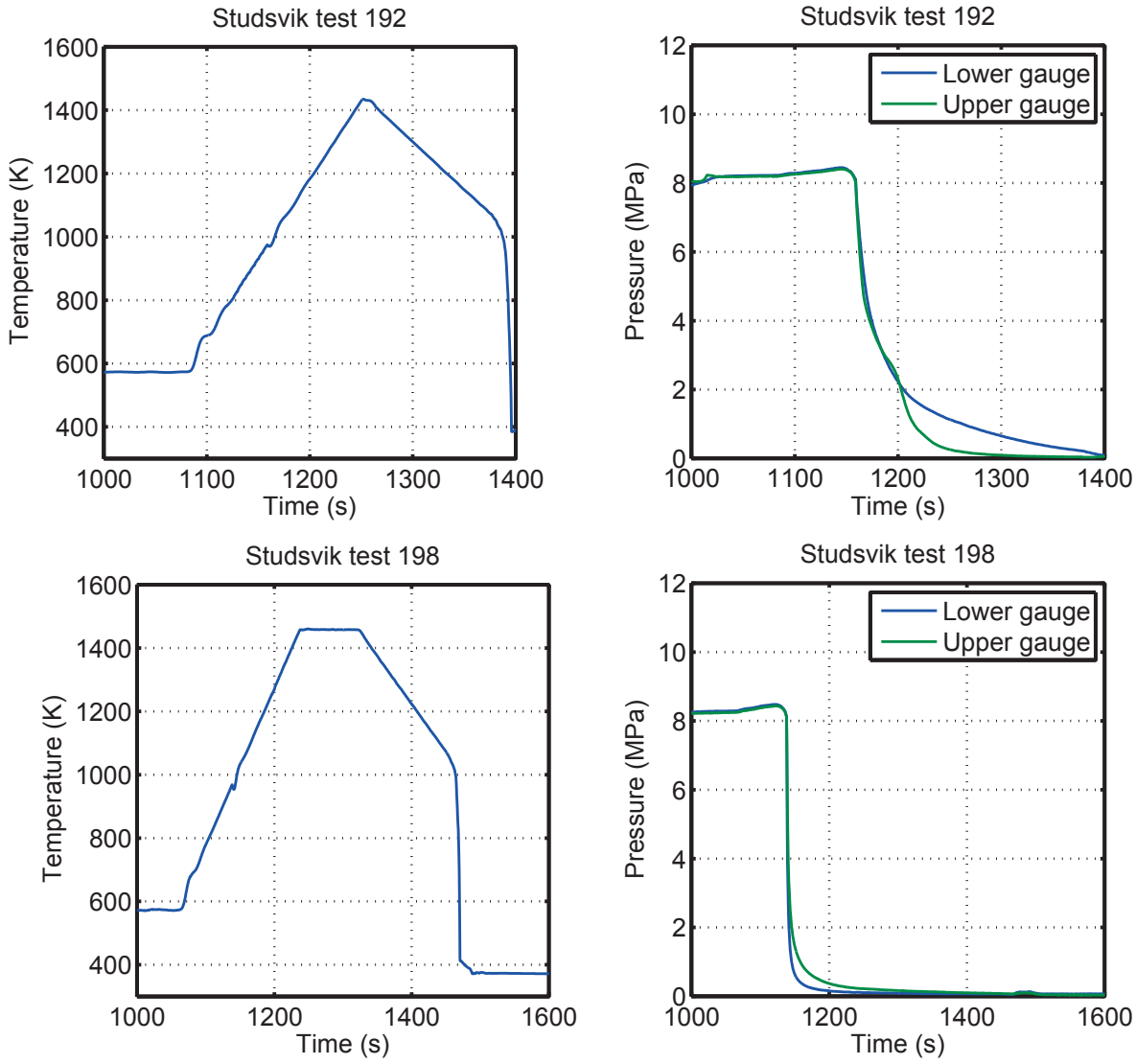

Figure 20: Cladding temperature/internal pressure histories during transient for Studsvik tests 192 (upper panel) and 198 (lower panel).

2.10 Halden IFA-650 test series

The Halden IFA-650 series of tests refer to fuel rod experiments performed in the Halden boiling heavy-water reactor (HBWR) under simulated LOCA conditions. A comprehensive summary of these test series (12 tests) carried out in the Halden reactor between 2003 and 2012 is provided in [50]. Here, we consider six of the tests, namely 2-7, which were assessed earlier [37]. A schematic drawing of the IFA-650 test rig is shown in Fig. 21. In a typical experiment, the test rod is placed in the center of the axisymmetric rig and surrounded by an electrical heater inside a pressure flask. The heater is part of a flow separator, which divides the space into a central channel adjacent to the fuel rod and an outer annulus. The heater is used to simulate the thermal boundary conditions, i.e. the heat dissipated from neighboring fuel rods during a LOCA. Cladding temperature is affected by both the fission power of the test fuel rod and the heater power. The rod power is controlled by varying the reactor power [37].

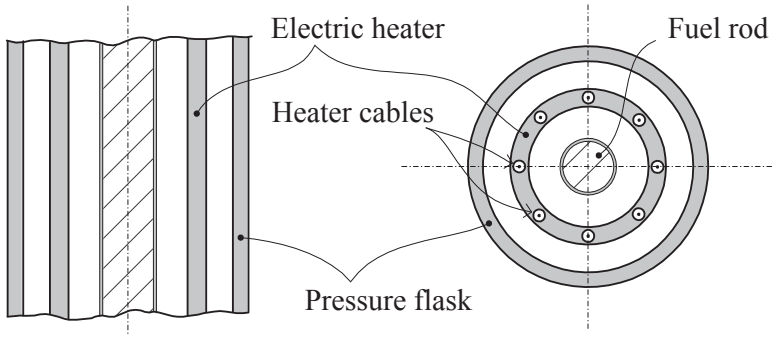

Figure 21: Schematic drawing of the IFA-650 test rig cross sections; from [37].

The test fuel rods 3, 4, 5, 6 and 7 were refabricated from full-length rods preirradiated in different commercial nuclear power reactors. Test 2, however, was made on a fresh fuel rod. The refabricated test rods were filled with a gas mixture typically of 95 vol.% argon and 5 vol.% helium to a prescribed pressure at room temperature. Argon was selected to mimic the behavior of fission product gases, while a small amount of helium was added to leak test the rod. The rod for test 2 was filled with helium gas only. The rod plenum volume (free gas volume) in each test rod was made sufficiently large to maintain stable pressure conditions during the test until cladding burst [37]. The active length of the test rods was about 480 mm, except for the test 2 rod, which had an active length of 500 mm.

The general IFA-650 test procedure is as follows [51, 52]. Prior to the LOCA test, the reactor power is tuned so that the predefined power level in the fuel rod is obtained. The heater is then switched on to its predefined constant power value. At this preparatory phase, the reactor is operating under forced circulation (using an outer flow loop). After reaching the desired fuel power, the test rig is disconnected from the outer loop and the temperatures are left to stabilize under natural circulation for a few minutes before initiation of the LOCA transient (blowdown).The magnitudes of the heat generation rates in the heater and fuel rod are selected to reach a desired (target) peak cladding temperature during the test.

The blowdown phase is initiated by opening the valves to a dump tank, whereby the rig is rapidly emptied of water (coolant). During the blowdown, the coolant pressure falls quickly. The coolant pressure (p_c) transient resulting from the blowdown operation is illustrated in Fig. 22. The associated responses of cladding temperature (T, dashed line) and rod internal gas pressure (p_g) are also depicted in the figure. The cladding temperature starts to rise rapidly due to insufficient cooling of the rod. In addition, the linear heat generation rates for fuel rod (Q_f) and heater (Q_h) are schematically shown by the dash-dot lines in Fig. 22. Upon fuel rod failure (cladding burst), the rod pressure drops to the pressure of the surrounding medium. Typically, as shown in figure 22, the heater is switched off shortly before test termination (reactor scram) [52].

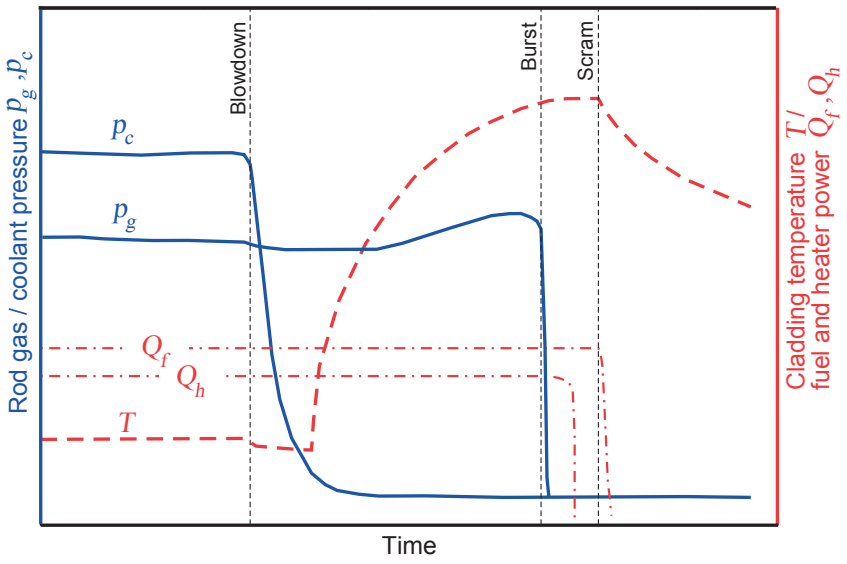

Figure 22: Schematic description of typical time responses of some selected parameters during a Halden IFA-650 LOCA experiment. The LOCA transient (test) is initiated by the blowdown and terminated by reactor scram; from [52].

An outline of the rod designs and conditions of the UO_2 rod segments used in the IFA-650 tests 2-7 is provided in the top part of Table 20. The test rod data are given as nominal as-fabricated (unirradiated condition) values. In the bottom part of Table 20, selected results from the tests are summarized. Here, the time to cladding burst after initiation of the blowdown is denoted by t_B and the associated measured cladding temperature at this time by T_B. The average cladding heating rate from the temperature T_S at start of heat-up phase until burst (at T_B) is given by $\dot{T}_{av}$. The rod pressure just prior to burst is denoted by p_B. The maximum measured cladding diameter increase after burst, ϵ_B, relative to the initial cladding outer diameter d_0 is given by the ratio $\Delta d/d_0$. More details on these data can be found in [37, 50–52] and the source references cited therein.

Table 20: Outline of test rod data and experimental outcome of the IFA-650 tests 2-7.

Test number	2	3	4	5	6	7
Rod design/	PWR	PWR	PWR	PWR	VVER	BWR
UO_2 fuel	17×17	16×16	16×16	16×16	...	10×10
Pellet diameter, mm	8.29	9.13	9.13	9.13	7.55	8.19
Fuel length, mm	500	480	480	480	480	480
Burnup, MWd/kgU	0	81.9	92.3	83.4	55.5	44.3
Fill pressure,§ MPa	4.0	4.0	4.0	4.0	3.0	0.6
Cladding*	Zry-4	Zry-4	Zry-4	Zry-4	E110	Zry-2
Outer diameter, mm	9.5	10.75	10.75	10.75	9.13	9.62
Wall thickness, mm	0.57	0.721	0.725	0.721	0.679	0.63
T_s, K	493	473	463	483	483	473
T_B, K	1073	1053	1058	1023	1103	1373
$\dot{T}_{av}$, K/s	8.5	2.5	2.0	5.0-5.5	1.7-1.9	9.0
p_B, MPa	5.6	7.1	7.1	7.2	6.4	1.05
ϵ_B, -	0.9	< 0.1	0.65	0.17	0.36	0.22
t_B, s	99	267	336	178	525	247

§ Pressure at room temperature; *Zry = Zircaloy and E110 is a Zr1wt%Nb alloy variety.

Additional IFA-650 test series data, tests 9-14, have been made available recently, see [50] and references therein. Information on post-irradiation examination of test 12 can be found in a 2103 presentation by Oberländer [53]. Test and PIE data for IFA-650 tests 13 and 14 can be found in [54–57]. Characteristic data for these tests (9-14) are outlined in Table 21.

Table 21: Characteristic data for the test rods in the IFA-650 tests 9-14.

Test number	9	10	11	12	13	14
Rod design/	PWR	PWR	VVER	BWR	BWR	BWR
UO_2 fuel	16×16	17×17	...	10×10	10×10	10×10
Pellet diameter, mm	9.13	8.21	7.55	8.19	8.19	8.19
Fuel length, mm	480	440	480	380	380	360
Burnup, MWd/kgU	90	60	56	72.3	74.1	70.8
Fill pressure,§ MPa	4.0	4.0	3.0	2.0	2.0	2.0
Cladding*	Zry-4	Zry-4	E110	Zry-2	Zry-2	Zry-2
Outer diameter, mm	10.75	9.5	9.13	9.62	9.62	9.62
Wall thickness, mm	0.725	0.57	0.679	0.63	0.63	0.63
T_s, K	493	463	461	448	453	473
T_B, K	1063	1022	1073	1070	1084	No burst
$\dot{T}_{av}$, K/s	6.7-8.7	4.4-5.3	6.5-7.5	3.4	5.5	4.2
p_B, MPa	7.7	7.1	5.57	7.6	4.23	$p_{max} = 7.7$
ϵ_B, -	0.6	0.32	0.16	0.4	0.4	$\epsilon_{max} = 0.56$
t_B, s	133	249	207	360	300	No burst

§ Pressure at room temperature; *Zry = Zircaloy and E110 is a Zr1wt%Nb alloy variety.

3 Computer model

Cladding behavior under LOCA conditions involve several coupled phenomena comprising Zr-H_2O reaction (oxidation), Zr-alloy $\alpha \Leftrightarrow (\alpha + \beta) \Leftrightarrow \beta$ transformations, creep deformation leading to ballooning, and rupture (burst). A set of models that treat these phenomena in a unified fashion has been been implemented in the `FRAPTRAN` computer program [58], and used to evaluate Halden-650 LOCA tests [37, 51, 52].

The cladding material properties model applicable to LOCA conditions comprise several submodels; namely, the Zr-alloy steam oxidation, structural phase transformation (solid-solid $\alpha \Leftrightarrow \beta$), high-temperature creep deformation, and eventually rupture. The main quantities calculated by the method are (i) the oxygen parameters generically denoted by χ, which can be either the total amount of oxygen picked up by the cladding during the oxidation process, the oxide layer thickness or the oxygen concentration in the cladding metal layer; (ii) the volume fractions of the β-Zr φ and α-Zr $(1 - \varphi)$; (iii) the cladding effective strain due to creep ε_e; (iv) and the cladding burst (hoop) stress σ_B. All these quantities are coupled through a set of kinetic equations and a burst criterion. They may be expressed generically in the form

$$\frac{\mathrm{d}\chi}{\mathrm{d}t} = f_1(\chi, T, \varepsilon_e), \tag{8}$$

$$\frac{\mathrm{d}\varphi}{\mathrm{d}t} = f_2(\varphi, \chi, T), \tag{9}$$

$$\frac{\mathrm{d}\varepsilon_e}{\mathrm{d}t} = f_3(T, \sigma_e, \varphi, \chi), \tag{10}$$

$$\text{and} \quad \sigma_B = f_4(\chi, T), \tag{11}$$

where f_i, $i = \{1, 2, 3\}$ are the respective functions for the time evolution of the variables during the transient, σ_e is the cladding von Mises effective stress, and $T = T(\mathbf{x}, t)$ is the cladding temperature, which in general, is a function of space $\mathbf{x}$ and time t, controlled by power and/or coolant boundary conditions during the transient. Moreover, f_4 is purely an empirical function of cladding temperature and oxygen concentration. The burst criterion can also be the burst strain, which is taken to be a function of temperature, i.e. $\varepsilon_B = f_5(T)$. This set of three first order differential equations (8)-(10) are solved numerically to obtain the time evolution of the respective variables during the transient. The explicit forms of f_i, $i = \{1, 2, 3\}$ are described in [58], and the relationships for various options of cladding burst (f_4, f_5) are provided in Appendix A. Our related publications are refs. [4, 59–61].

The aforementioned cladding high-temperature properties models have been implemented in a stand-alone MATLAB program. This program is called `ftmat` and uses a thin-shell mechanical model for an internally pressurized cladding tube [58]. This eliminates the space dependence and renders the computed parameters only functions of time. It has been verified that `ftmat` and `FRAPTRAN` give very similar results when the same high-temperature cladding material properties models are used. `ftmat` assumes as input cladding material options, various modeling options, cladding dimensions, initial cladding temperature and its heating rate, if any, pressure in the cladding and its rate of change, if any. It outputs cladding burst time, cladding burst temperature, cladding true burst hoop strain/stress, and the volume fraction of β-phase at burst. A more detailed input/output description is provided in [62].

4 Computations

In this section, we present the results of our evaluations of several cladding burst test programs surveyed in section 2 using the MATLAB program `ftmat`, which we glanced over in the foregoing section. For most of the tests, described in section 2, the required input data for `ftmat` could be found or could discretely be generated. Exceptions were the tests KfK-82 (data set III, Zircaloy-4), KfK-85 (V, Zircaloy-4), CEA-2 (IX, Zircaloy-4 with 600 wppm H), CEA-00 (X, M5 alloy), and W-EDF-09 (XII, ZIRLO), cf. Table 2. For these data sets, only partial information could be traced in the open literature, although disconnected comparisons with applicable burst models would be possible, which were done in certain cases. Our results for the tests KfK-83 (set IV, Zircaloy-4), ANL-10 (XIII, ZIRLO), Studsvik-12 (XIV, ZIRLO) and Halden-650 (XV, tests 2-7, Zircaloy-2/4, E110) are presented in this section. Additional comparisons, i.e. between measurements and computations, on these tests and others, are given in the supplementary material [62].

Two kinds of comparisons are displayed here: (i) Calculated versus measured cladding time-to-burst (burst time), burst temperature, burst stress, and burst strain, (ii) these quantities as a function of the test rod pressure. Among the four measured burst quantities, perhaps the most accurate is the burst time, followed by burst temperature, burst stress (pressure) and burst strain in the order of accuracy.

In the comparisons, the measured engineering hoop burst stress (calculated from measured burst pressure) is converted to the true (Cauchy) hoop burst stress by the formula

$$\sigma_\theta = \frac{R_0}{w_0}(1+\epsilon_\theta)^2 \Delta P. \tag{12}$$

Here, σ_θ is the true hoop stress, $R_0 = (R_{coo} + R_{cio})/2$, R_{coo} the cladding tube outer radius, R_{cio} the inner radius, w_0 the tube wall thickness, all as-fabricated values, ϵ_θ the engineering hoop strain, and ΔP the inner/outer pressure difference. Hence, to determine the true burst stress component, we need to know the values for the engineering hoop strain and the burst pressure, besides the tube dimensions and the outside pressure. Similarly, the measured engineering hoop burst strain ϵ_θ is converted to the true strain ε_θ via the relationship

$$\varepsilon_\theta = \ln(1+\epsilon_\theta). \tag{13}$$

The true (logarithmic) burst strain is shown in all the figures.

4.1 KfK-83 data: Zircaloy-4 cladding

We show the results of our evaluation of the measured burst data on Zircaloy-4 cladding listed in Table 8 (cf. Sec. 2.2.3) using the `ftmat` program. Input data comprise cladding inner and outer diameters, initial cladding temperature (623 K), heatup rate, among others, and a number of model options. We show our results for the stress-based cladding burst criterion, namely, the Rosinger best-estimate burst [20], together with Rosinger's high-temperature creep model [20], which exhibits a best all-round performance among the burst criteria implemented in `ftmat`. Moreover, the Ashby-Verrall model [61] for creep in the mixed phase domain of zirconium alloys is utilized. For cladding oxidation, the Cathcart-Pawel relation is chosen [63].

The computed results versus measurements on cladding burst time, burst temperature, burst stress and strain are shown in Fig. 23. It is seen that the retrodictions of burst time and burst temperature are fair, while for burst strain, the scatter is too large. The data on cladding burst hoop stress, which is proportional to rod burst pressure, are mostly underestimated, meaning that the measured burst stress is larger than the calculated stress in most cases. Likewise, computations were carried out with `ftmat` using the stress-based Erbacher burst criterion [14]. The results were very similar to the ones presented in Fig. 23. Tables 23-24 summarize these results with statistics.

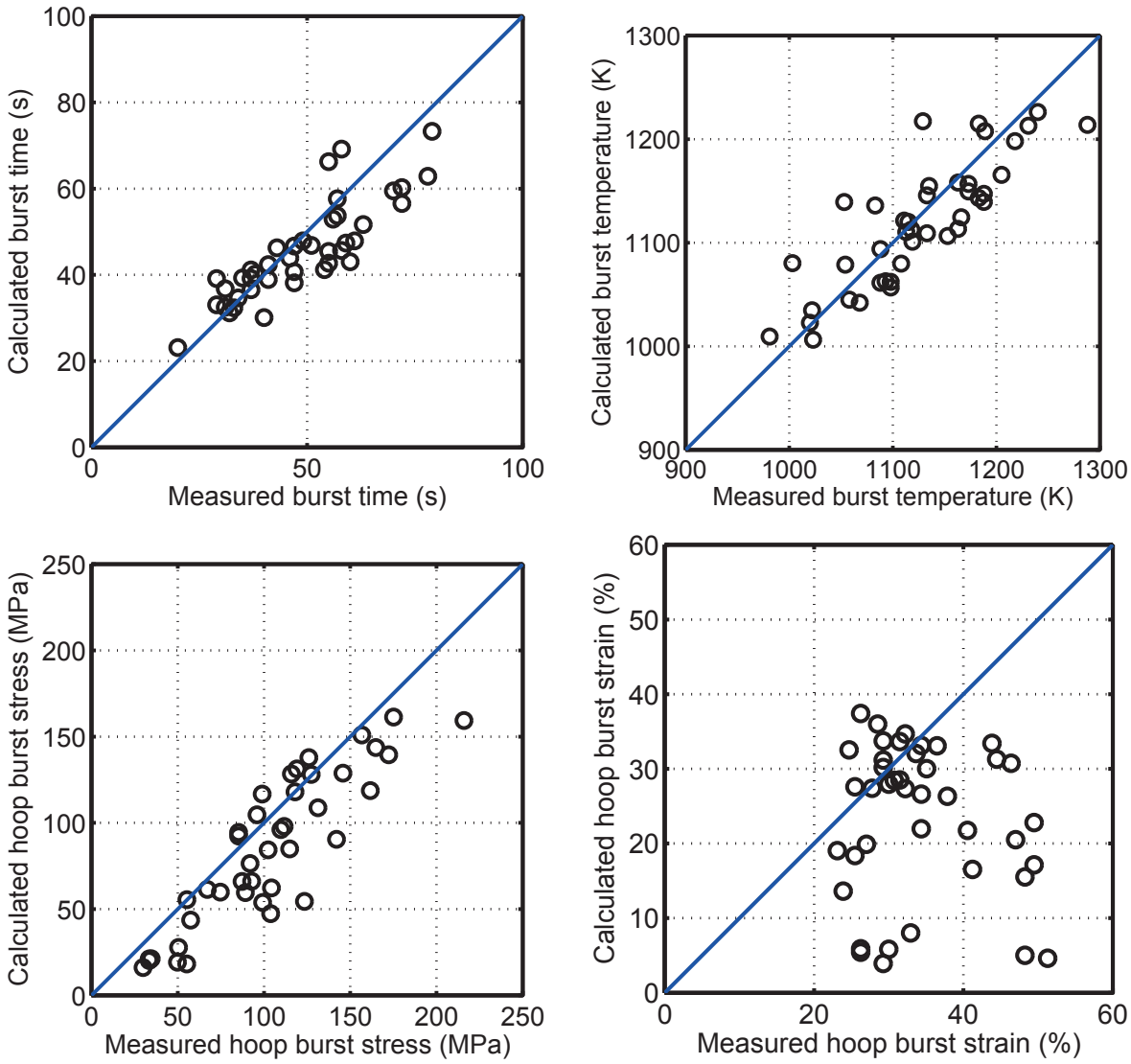

Figure 23: KfK-83 Zircaloy-4 cladding burst data: Measured per table 8, calculated per Rosinger BE burst criterion [20].

The results of our computations for the considered cladding burst quantities as a function of the test rod pressure are depicted in Fig. 24, where besides the Rosinger BE criterion, the strain-based burst criterion in `FRAPTRAN-1.5` [64] was also invoked for comparison. It should be remarked that this burst criterion is usually used together with a localized ballooning model (`BALON2`) in `FRAPTRAN-1.5`. We have used it here without that model.

In the computations, we have used as input an initial temperature of 623 K, a heatup rate of 11.5 K/s, and varied the rod pressure from 0.5 to 20 MPa. In regard to burst time and burst temperature, both criteria give very similar results in the range of the measured quantities (Fig. 24), but the strain-based `FRAPTRAN-1.5` criterion deviates sharply relative to that of Rosinger BE at low pressures. As regards burst stress, results obtained using the strain-based criterion of `FRAPTRAN-1.5` get out-of-bound at pressures larger than 5 MPa, which is inappropriate. Similarly, computation of burst strain is not meaningful with this criterion. As can be seen in Fig. 24, both burst time and burst temperature are declining functions of rod pressure, whereas the increase in rod pressure raises the burst hoop stress. The situation for burst strain is more complex.

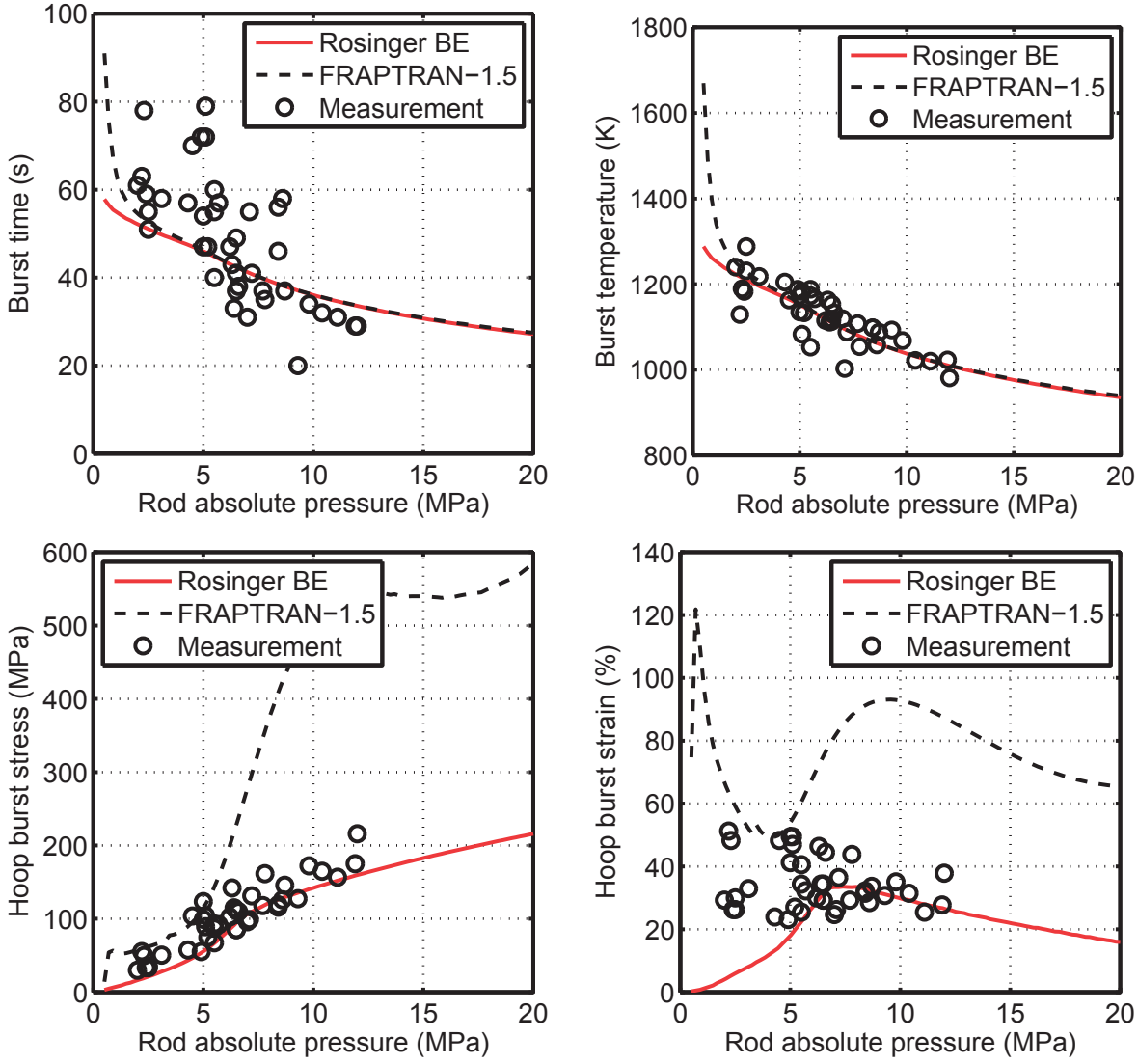

Figure 24: KfK-83 Zircaloy-4 cladding burst data: Measured per table 8, calculated per Rosinger BE and `FRAPTRAN-1.5` burst criteria in `ftmat`. Computations assume a heatup rate of 11.5 K/s for all the test rods, contrary to measurements.

4.2 ANL-10 data: ZIRLO cladding

We show the results of our evaluation of the measured burst data on unirradiated ZIRLO cladding listed in Table 17 (cf. Sec. 2.8) using the `ftmat` program. Input data comprise cladding inner and outer diameters, initial cladding temperature (573 K), heatup rate (5 K/s), among others, and a number of model options. We show our results for the Rosinger best-estimate burst criterion [20] together with Rosinger's high-temperature creep model [20], which were originally developed for Zircaloy but exhibit a best behavior among the burst models implemented in `ftmat`. Moreover, the Ashby-Verrall model [61] for creep in the mixed phase domain of zirconium alloys is utilized. For cladding oxidation, the Cathcart-Pawel relation is chosen [63].

The results of our computations versus measurements on cladding burst time, burst temperature, burst stress and strain are shown in Fig. 25. It is seen that the burst time and burst temperature are somewhat overestimated, while for burst strain the scatter is large. The data on cladding burst hoop stress are fairly reproduced. The uncertainty in cladding burst temperature was reported to be up to ± 40 K, cf. Table 17. This corresponds to a burst time uncertainty of ± 8 s. Tables 23-24 summarize the mean and standard deviations between the calculated and measured burst variables.

The upshots of our computations for the considered cladding burst quantities as a function of the test rod pressure are depicted in Fig. 26, where besides the Rosinger BE burst criterion, the strain-based burst criterion in `FRAPTRAN-1.5` [64] was also invoked for comparison. In these computations, we have used as input an initial temperature of 573 K, a heatup rate of 5 K/s, and varied the rod pressure from 2 to 14 MPa.

In regard to burst time and burst temperature, both criteria yield very similar results in the range of the measured quantities (Fig. 26), but the `FRAPTRAN-1.5` criterion deviates sharply relative to that of Rosinger BE at low pressures. Vis-à-vis the burst stress, results obtained with the strain-based criterion of `FRAPTRAN-1.5` get out-of-bound at pressures larger than 4 MPa, which is inappropriate. Similarly, burst strains are much overestimated with this criterion. As can be seen in Fig. 26, both burst time and burst temperature are declining functions of rod pressure, whereas the increase in rod pressure raises the burst hoop stress. The situation for burst strain is more subtle.

4.3 Studsvik-12 data: ZIRLO cladding

We show the outcome of our evaluation of the measured burst data on irradiated ZIRLO cladding (six data points) listed in Table 19 (cf. Sec. 2.9) using the `ftmat` program. Input data to the computations are as in the previous subsection 4.2, see Table 18. Among the six test rods, 4 have standard (normal) 17×17 cladding dimensions and two have IFBA dimensions.

The computed results versus measurements on cladding burst time, burst temperature, burst stress and strain are shown in Fig. 27. It is seen that for burst time and burst temperature, all the data are overestimated, while for burst strain, the scatter is moderate. The data on cladding burst hoop stress are fairly reproduced. Tables 23-24 summarize the mean and standard deviations between the calculated and measured burst variables.

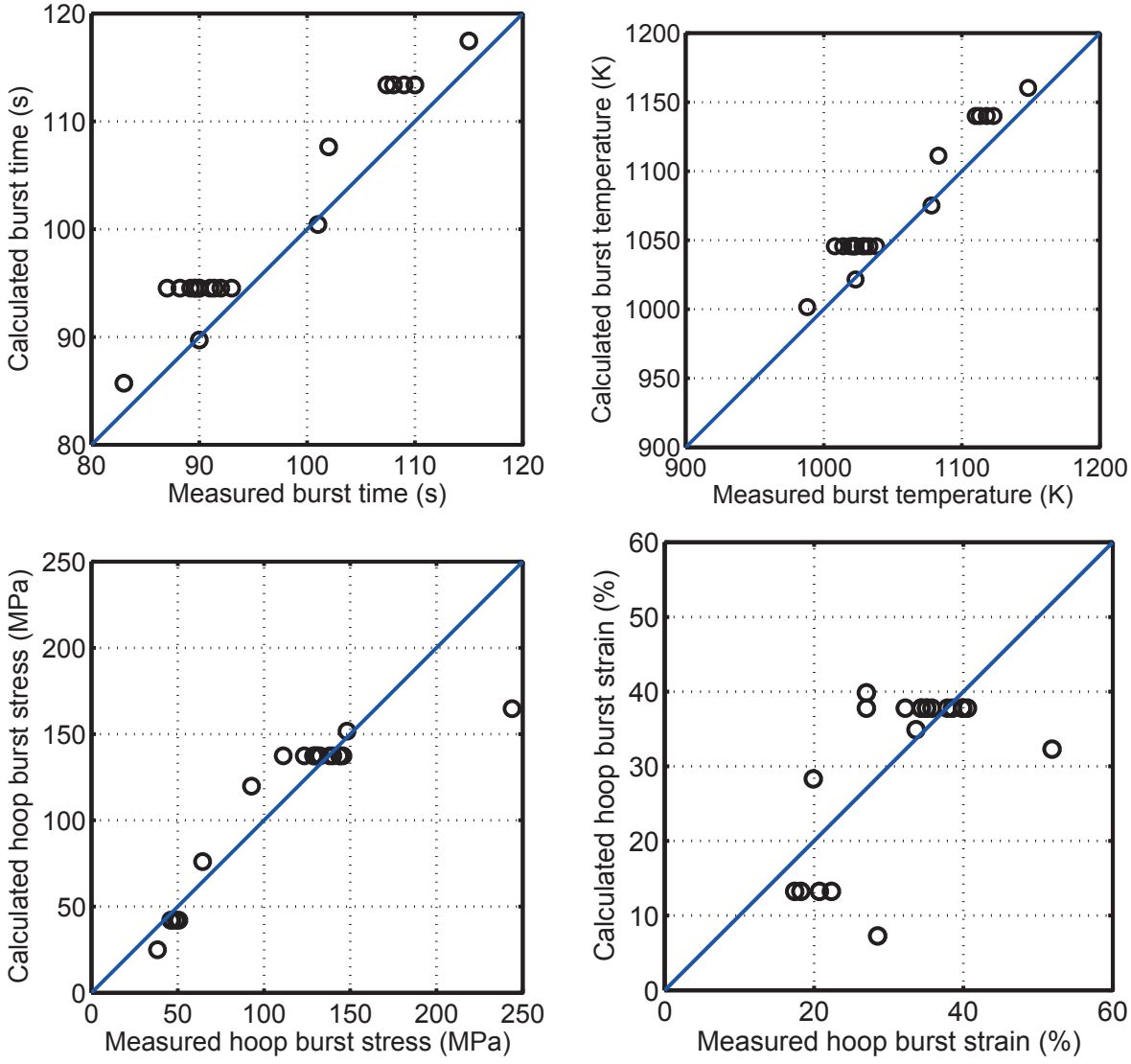

Figure 25: ANL-10 ZIRLO cladding burst data: Measured per table 17, calculated per Rosinger BE burst criterion [20].

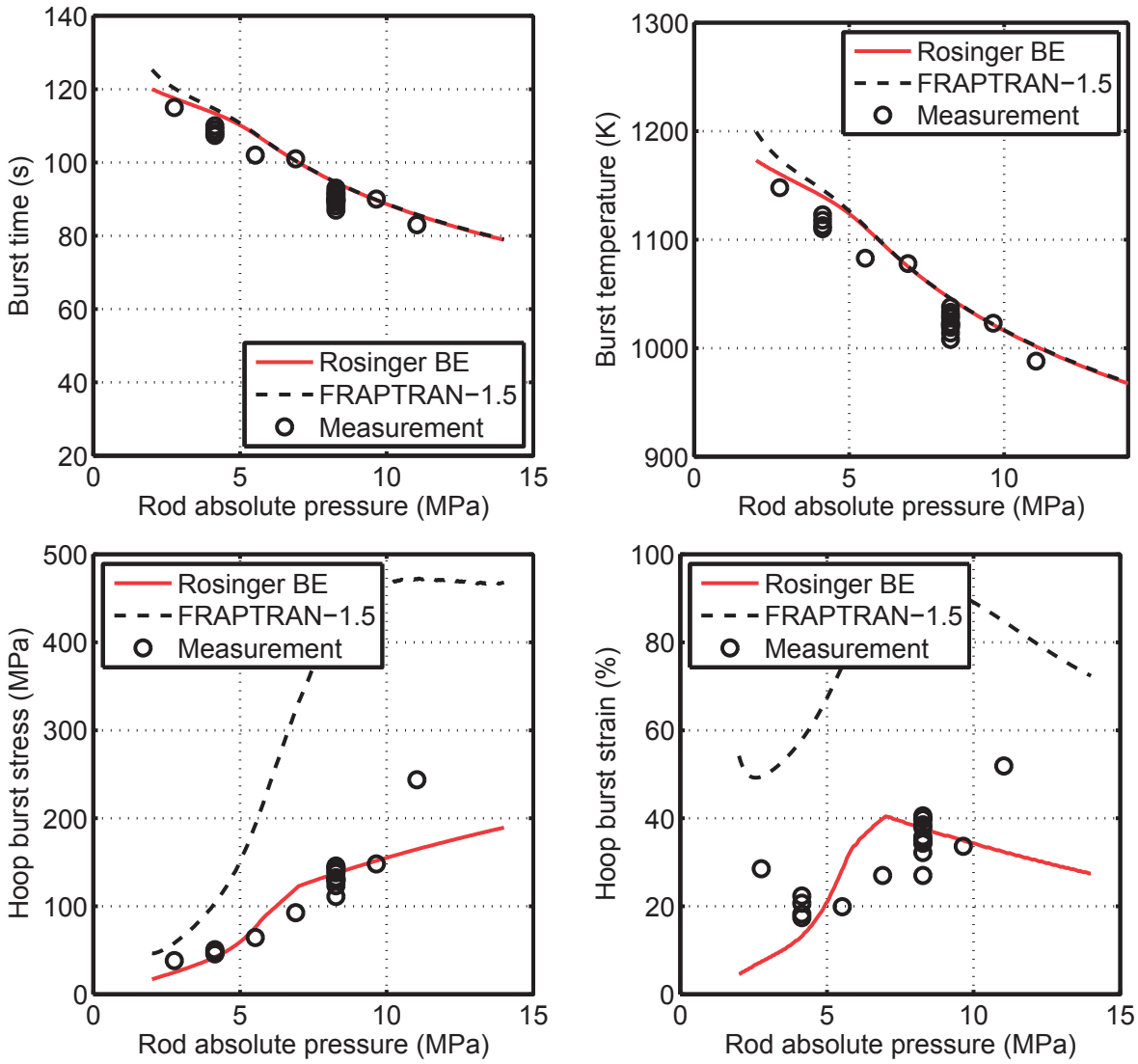

Figure 26: ANL-10 ZIRLO cladding burst data: Measured per table 17, calculated per Rosinger BE and `FRAPTRAN-1.5` burst criteria in `ftmat`. Computations assume a heatup rate of 5 K/s for all the test rods as in the tests.

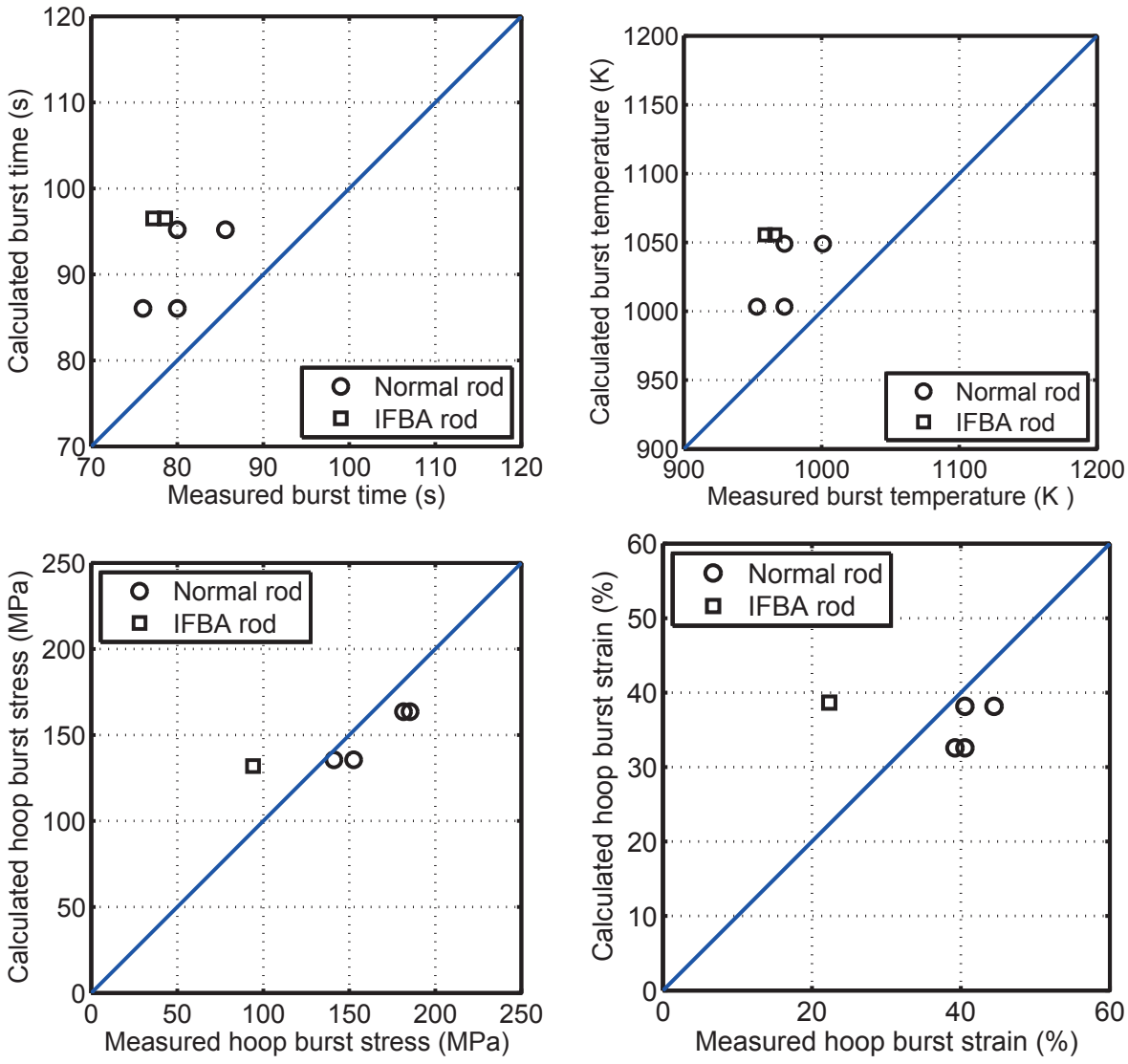

Figure 27: Studsvik-12 ZIRLO cladding burst data: Measured per table 19, calculated per Rosinger BE burst criterion [20].

The results of computations for the considered cladding burst quantities as a function of the test rod pressure are depicted in Fig. 28 where besides the Rosinger BE burst criterion, the strain-based burst criterion in FRAPTRAN-1.5 [64] was also invoked for comparison. In these computations, we have used as input, cladding dimensions of standard rod, an initial temperature of 573 K, a heatup rate of 5 K/s, and varied the rod pressure from 2 to 14 MPa.

In regard to burst time and burst temperature, both criteria yield very similar results in the range of the measured quantities (Fig. 28), but the FRAPTRAN-1.5 criterion deviates sharply relative to that of Rosinger BE at low pressures. Vis-à-vis the burst stress, results calculated with the strain-based FRAPTRAN-1.5 get out-of-bound at pressures larger than 4 MPa, which is improper. Similarly, burst strains are much overestimated with this criterion. As can be seen in Fig. 28, both burst time and burst temperature are declining functions of rod pressure, whereas the increase in rod pressure elevates the burst hoop stress. For burst strain, the data points are too few to see a trend.

We should recall that the Studsvik test samples were from high burnup fuel rods with moderate levels of hydrogen concentration in the ZIRLO cladding samples (176 - 290 wppm), cf. Table 18. Currently in the considered models, the effect of hydrogen concentration is ignored. Thus the systematic underestimation of the burst time and burst temperature may be related (or partly be due) to the level of the hydrogen concentration in the cladding. Moreover, it may just as well be an effect of the cladding initial oxide layer thickness, which was 20-30 μm for the Studsvik/NRC test rods.

Both the ANL-10 and Studsvik-12 test programs utilized a nominal heatup rate of 5 K/s in all the tests. In postulated LOCAs one expects a spectrum of heating rates. We have here examined the response of the ftmat program to variations in heating rate, from 5 to 30 K/s, for the standard Studsvik-12 rod in regards to cladding burst temperature, burst stress and burst strain versus rod pressure. We have chosen the Rosinger BE burst criterion and kept all the other model options and input data as in the preceding computations. The results of our computations are shown in Fig. 29. As can be seen, increasing the heatup rate elevates the burst temperature, while it lowers the cladding burst stress and strain, the latter in a complicated fashion.

As mentioned in section 2.9, for two of the Studsvik-12 tests, 192 and 198, detailed data were made available to us through our participation in the IAEA FUMAC project. Cladding temperature and rod internal pressure histories for these rods are depicted in Fig. 20. The ftmat program is capable of computing the quantities of interest as a function of time during the test transient. We have made such computations for the two tests and the results on cladding temperature, rod pressure, cladding hoop stress and strain are depicted in Figs. 30 and 31 for tests 192 and 198, respectively.

We note that the start of the main temperature ramps were at 1086 s and 1064 s in tests 192 and 198, respectively. The corresponding burst times after the ramp starts were 80 and 79 s, perhaps with a few seconds of uncertainty. From the figures (30 and 31) it can be seen that ftmat overestimates the burst temperature while it underestimates the burst pressure (or equivalently engineering stress) and burst strain. The uncertainty in time-to-burst (order of seconds) contributes to this deviation.

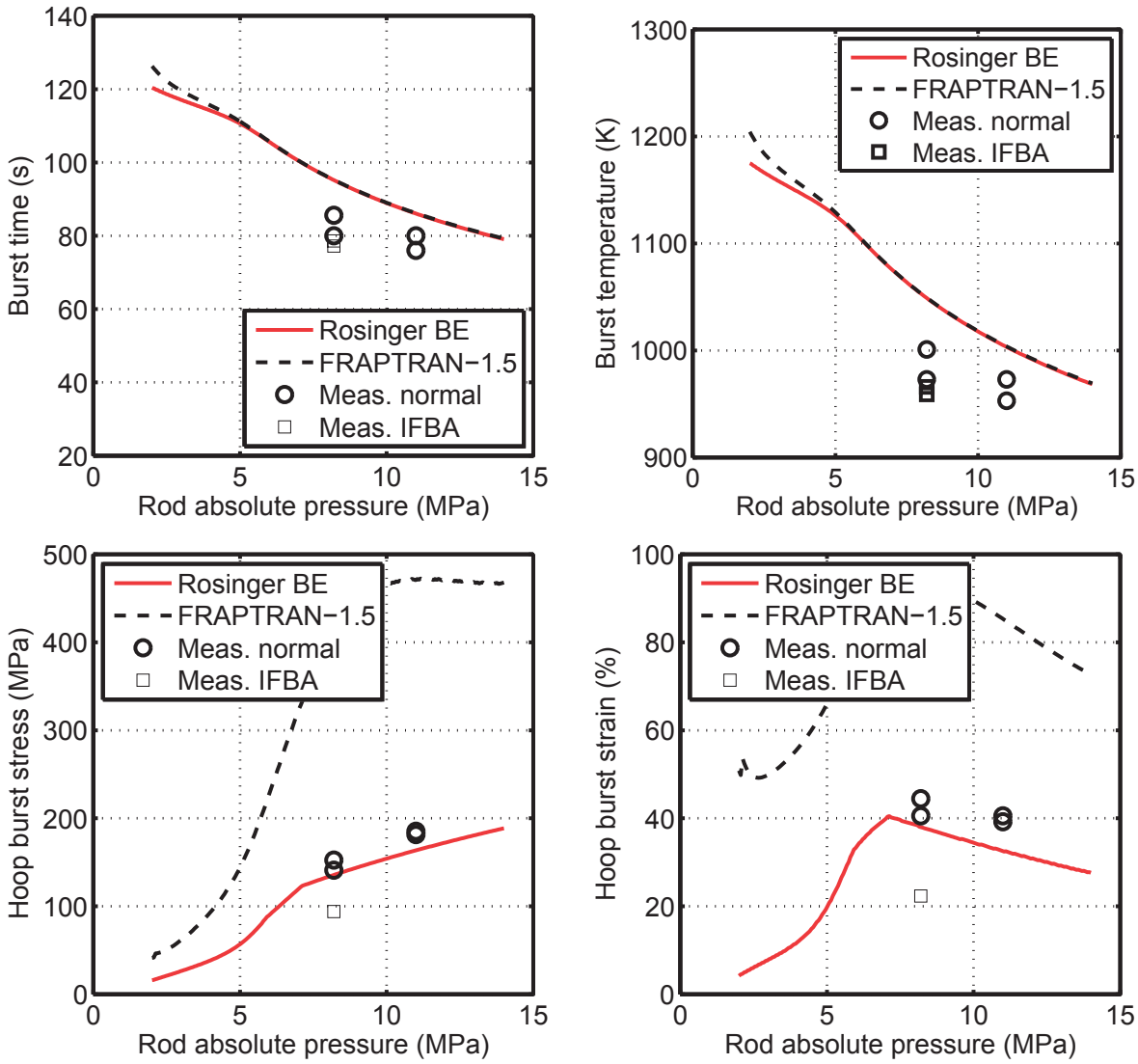

Figure 28: Studsvik-12 ZIRLO cladding burst data: Measured per table 19, calculated per Rosinger BE and `FRAPTRAN-1.5` burst criteria in `ftmat`. Computations assume a heatup rate of 5 K/s for all the test rods as in the tests.

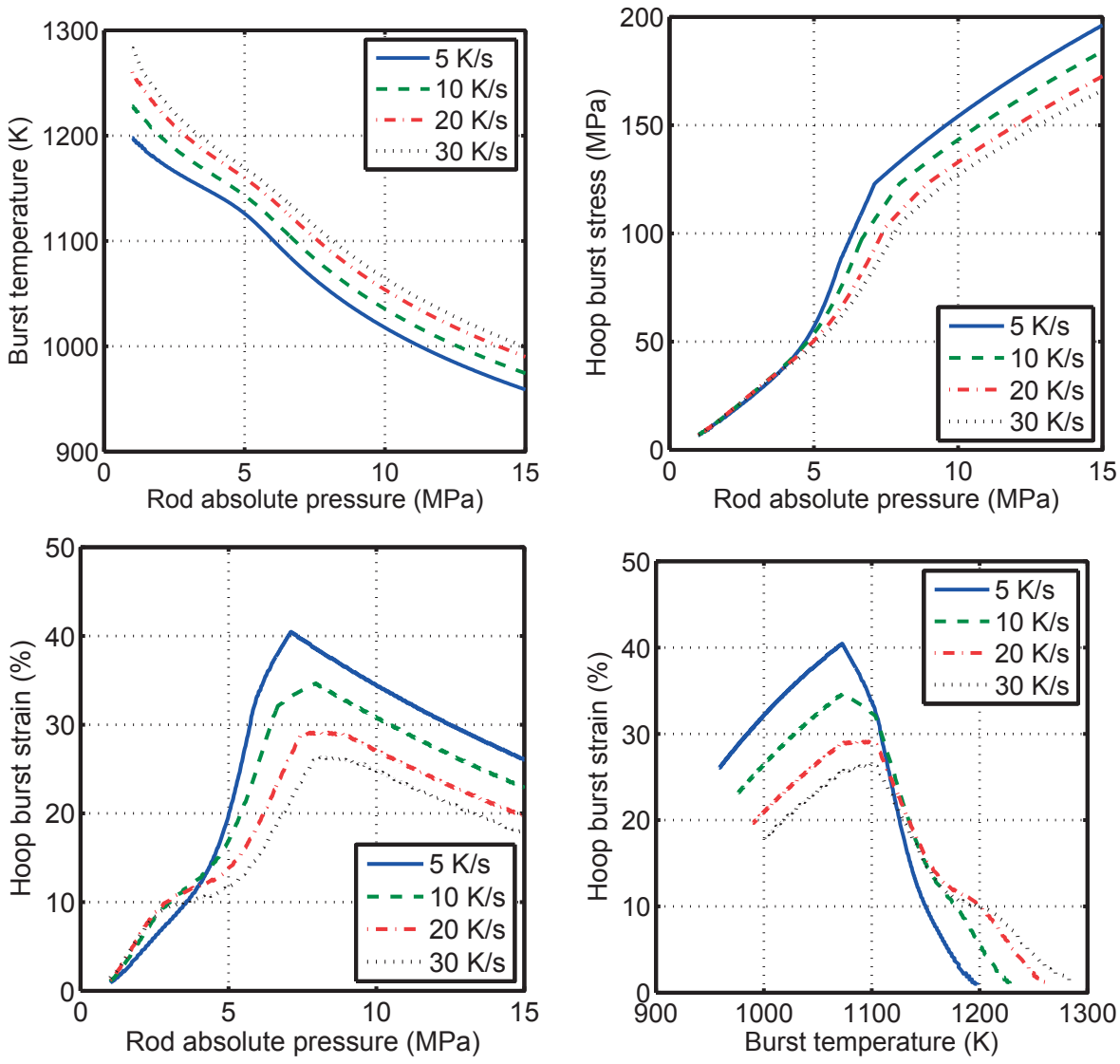

Figure 29: Studsvik-12 ZIRLO cladding burst: `ftmat` computations using the Rosinger BE burst criterion at various heatup rates.

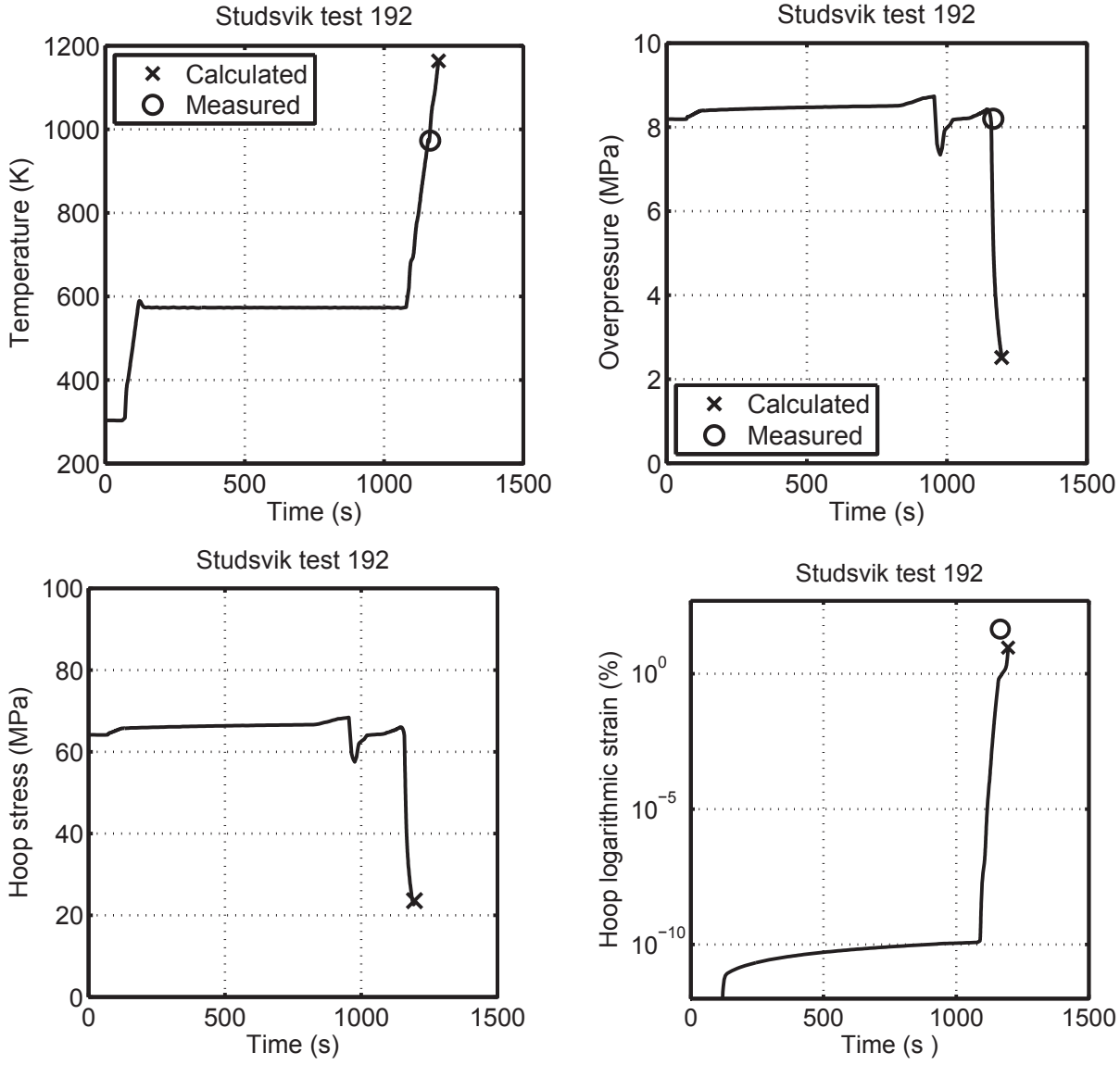

Figure 30: Computer simulation of Studsvik test 192 on ZIRLO cladding. The circle indicates the measured time of burst, while the cross the calculated burst.

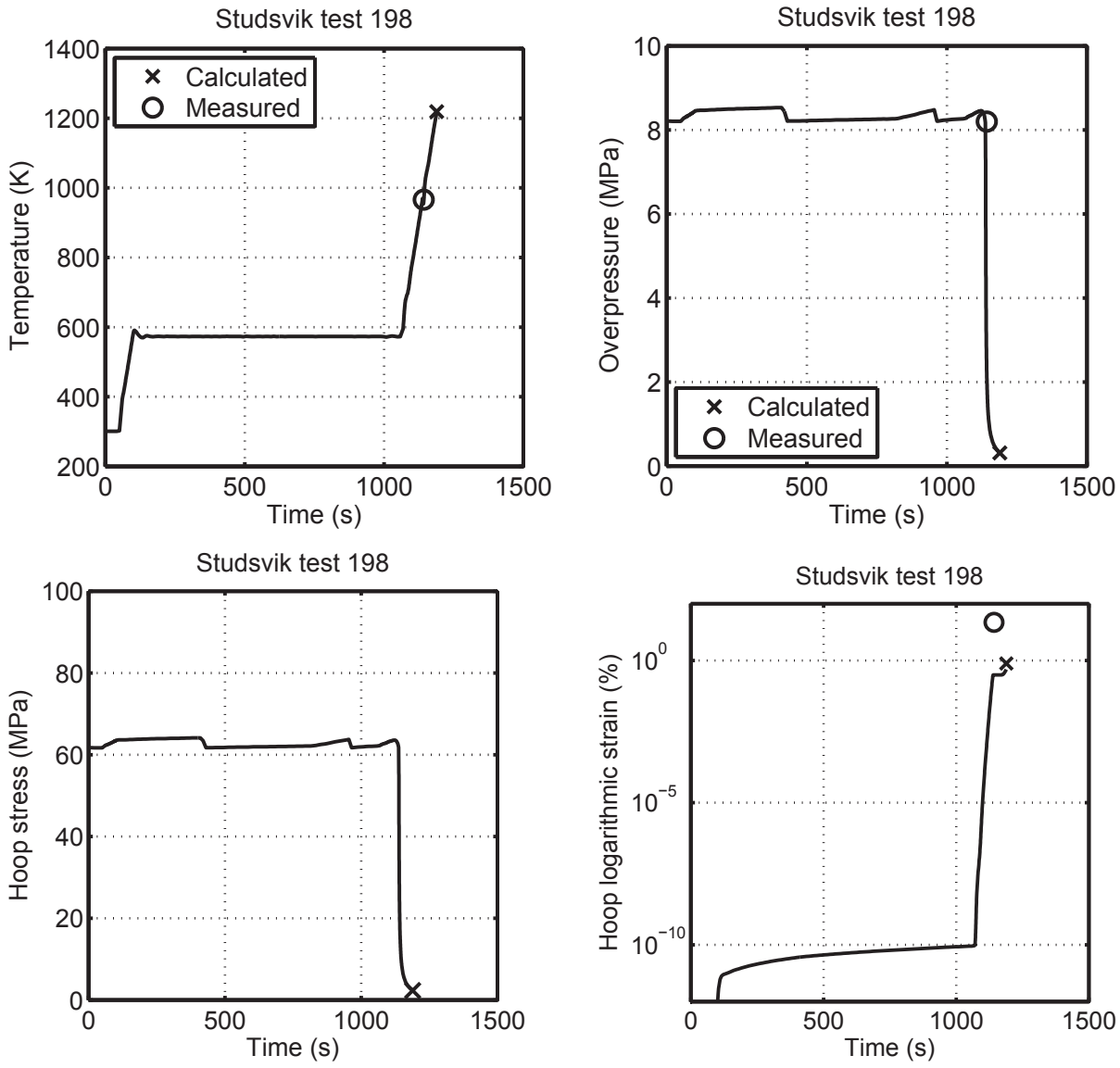

Figure 31: Computer simulation of Studsvik test 198 on ZIRLO cladding. The circle indicates the measured time of burst, while the cross the calculated burst.

4.4 Halden IFA-650 test data

The results of computations for 6 of the Halden IFA-650 tests (2 to 7) are summarized here. A brief description of this program and test rod characteristics are given in section 2.10. The computations of these tests were made with `FRAPTRAN-QT1.4c` [37], which has identical cladding burst models and options as `ftmat`, and with the same modeling options as in the aforementioned cases in this section.

Table 22: Calculated vs. measured clad burst quantities for the IFA-650 tests [37].

Burst quantity	Calculated	Measured	Calculated	Measured
	Test 2		Test 3	
Time, s	108	99	259	266
Temperature, K	1079	1073	1066	1053
True hoop strain, %	58	64	64	9.5
Pressure, MPa	5.6	5.6	5.9	7.1
	Test 4		Test 5	
Time, s	331	336	157	178
Temperature, K	1058	1058	1074	1023
True hoop strain, %	65	50	61	15
Pressure, MPa	5.6	7.1	5.9	7.2
	Test 6		Test 7	
Time, s	518	525	213	247
Temperature, K	1095	1103	1365	1373
True hoop strain, %	64	31	26	22
Pressure, MPa	4.2	6.4	0.86	1.1

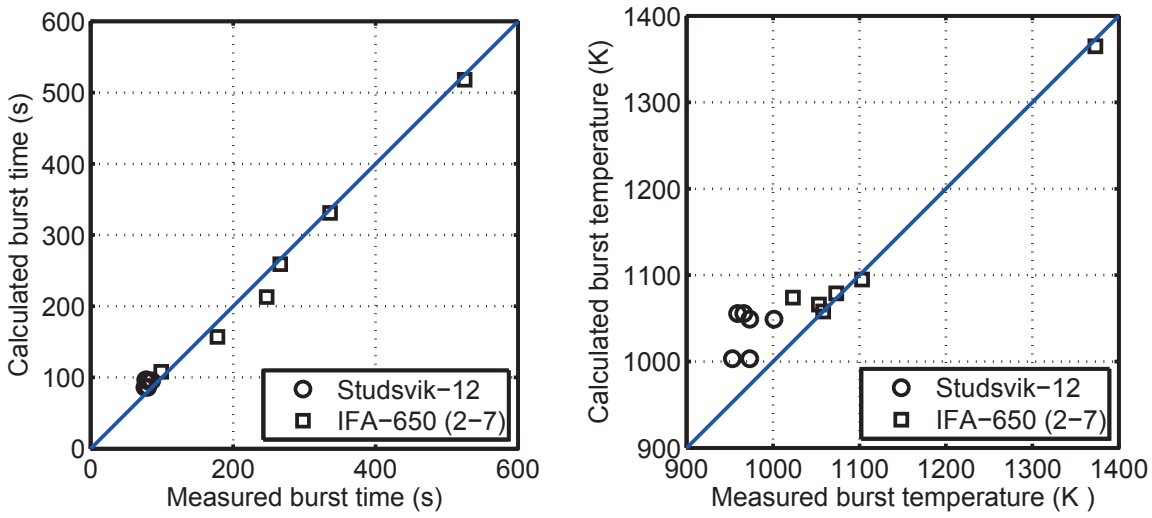

Figure 32: Comparison between measured and calculated burst data of Studsvik-12 tests and Halden IFA-650 tests (2-7).

As mentioned at the end of Sec. 2.10, additional IFA-650 test series data, tests 9-14, have been made available recently, see [50] and references therein. Characteristic data for these tests are outlined in Table 21. An evaluation of IFA-650 tests 9-14, with an extended version of `FRAPTRAN-QT`, is left out to a separate project.

4.5 Deviations and uncertainties

In this subsection, we attempt to quantify the deviations between the calculated and measured burst variables detailed in the foregoing subsections and partly in [62]. In particular, the relative differences between model calculations and measurements on burst time, burst temperature and burst stress are quantified. To this end, we have evaluated two attributes of the deviation or the uncertainty, namely the mean of the relative deviation and the root-mean square deviation (RMSD), between the calculated and measured values.

The mean relative deviation, between the calculated and measured quantity, in a data set is

$$\langle \mathrm{R}_n \rangle = \frac{1}{n} \sum_{i=1}^{n} \left| \frac{y_i - \hat{y}_i}{y_i} \right|, \tag{14}$$

where y_i and $\hat{y}_i$ are the i-th measured and calculated quantity, respectively, and n is the number of measurements in the data set. The root-mean square deviation is defined by

$$\langle \mathrm{S}_n \rangle = \sqrt{\frac{1}{n} \sum_{i=1}^{n} \left(\frac{y_i - \hat{y}_i}{y_i} \right)^2}, \tag{15}$$

The RMSD formula (15) can be considered as an uncertainty (1σ-level) in the computed quantity relative to the measured value, if sufficient number of data points are taken into account. Tables 23 and 24 summarize the results of evaluations of the cladding burst data, presented in tabular form in Sec. 2, by using Eqs. (14) and (15), respectively. Model A, etc. refers to the burst criterion and the associating models. The upper portions of the tables are for Zircaloy-4 cladding, AEKI-00 data are on E110 cladding, while ANL-10 and Studsvik-12 data are on ZIRLO cladding. The IFA-650 data include tests made on Zircaloy-2/4 and E110 claddings. Furthermore, we have computed the overall deviations in models A and B relative to measurements, i.e. by combining the individual uncertainty obtained from each data set listed in Tables 23 and 24. These results are presented in Table 25.

As noted earlier, there exist also uncertainties in measurements which need to be considered. However, not all the test programs assessed have provided such information in their publications, exceptions are the KfK-83 (Table 9) and ANL-10 (Table 17) programs. In the KfK-83 test program, the uncertainties in the measurements for burst temperature, burst pressure ($\equiv$ engineering hoop stress) and burst strain are given. The uncertainty (1σ-level) in burst temperature ranged from ± 45 to ± 80 K, which is within the range of data scatter seen in Fig. 23. The uncertainty in the burst pressure measurement is given as ± 0.15 MPa, which amounts to an engineering hoop stress of $\approx \pm 1.1$ MPa. This is much less than the scatter seen in Fig. 23 for the true Cauchy stress, which includes the contribution of the deformation. As can be seen from this figure the `ftmat` model with the selected options underestimate the Cauchy burst stress level. The RMSD value for this quantity, Table 24 (model A), is $\approx 30\%$. We expect that a similar level of experimental uncertainty (as in KfK-83) is prevalent in the other KfK trials.

Table 23: Mean relative difference between calculated and measured burst variable $\langle \mathrm{R}_n \rangle$.

Burst variable ⇒			Time	Temperature	Hoop stress
Data	Model	No. of Trials, n	$\langle \mathrm{R}_n \rangle$	$\langle \mathrm{R}_n \rangle$	$\langle \mathrm{R}_n \rangle$
ORNL-79	A	34	0.071	0.036	0.263
	B	34	0.050	0.025	0.720
KfK-83	A	41	0.128	0.027	0.246
	B	41	0.123	0.026	0.649
KfK-88	A	45	0.116	0.036	0.333
	B	45	0.119	0.034	0.447
KfK-87†	A	5	0.716	...	0.587
	B	5	0.672	...	0.443
KfK-87t‡	A	6	0.539	0.110	0.522
	B	6	0.505	0.103	0.540
AEKI-00	C	12	0.149	0.096	0.654
ANL-10	A	21	0.0429	0.0193	0.117
	B	21	0.0459	0.0208	0.972
Studsvik-12	A	6	0.165	0.0672	0.196
	B	6	0.166	0.0676	1.238
IFA-650 (2-7)*	A	6	0.067	0.0135	0.181

$\langle \mathrm{R}_n \rangle$ is given by Eq. (14); Model A is Rosinger BE [20], B is Erbacher et al. [14] and C is per ref. [65]. †Isothermal-isobaric creep-rupture tests. ‡Transient-temperature-isobaric creep-rupture tests. *Burst pressure (instead of hoop stress) is evaluated.

Table 24: RMSD between calculated and measured burst variable $\langle \mathrm{S}_n \rangle$.

Burst variable ⇒			Time	Temperature	Hoop stress
Data	Model	No. of Trials, n	$\langle \mathrm{S}_n \rangle$	$\langle \mathrm{S}_n \rangle$	$\langle \mathrm{S}_n \rangle$
ORNL-79	A	34	0.082	0.043	0.319
	B	34	0.062	0.032	0.820
KfK-83	A	41	0.154	0.033	0.298
	B	41	0.149	0.034	0.788
KfK-88	A	45	0.123	0.043	0.368
	B	45	0.125	0.040	0.520
KfK-87†	A	5	0.737	...	0.595
	B	5	0.693	...	0.490
KfK-87t‡	A	6	0.550	0.134	0.559
	B	6	0.520	0.126	0.547
AEKI-00	C	12	0.244	0.151	0.664
ANL-10	A	21	0.0475	0.0213	0.155
	B	21	0.0504	0.0228	1.088
Studsvik-12	A	6	0.176	0.0718	0.246
	B	6	0.177	0.0721	1.379
IFA-650 (2-7)*	A	6	0.0839	0.0214	0.207

$\langle \mathrm{S}_n \rangle$ is given by Eq. (15); Model A is Rosinger BE [20], B is Erbacher et al. [14] and C is per ref. [65]. †Isothermal-isobaric creep-rupture tests. ‡Transient-temperature-isobaric creep-rupture tests. *Burst pressure (instead of hoop stress) is evaluated.

The ANL-10 workers have provided the burst temperature uncertainties in their measurements, which range from ± 4 to $\approx$ 40 K. Because a constant heating rate of 5 K/s was utilized in these tests, e.g. the 40 K temperature uncertainty corresponds to a burst time uncertainty of 8 s. These values are within the spread of data scatter seen in Fig. 25. The RMSD values shown in Table 24 (model A) are 4.7% and 2.13% for burst time and burst temperature, respectively. The level of uncertainty in the Studsvik-12 tests is expected not to be lower than that of the ANL-10 tests, however, to our knowledge, so far only six rods have been published on these tests, therefore a meaningful statistical treatment cannot be made on these data.

Table 25: Overall or combined deviations of data in tables 23-24.

Burst variable $\Rightarrow$		Time	Temperature	Hoop stress
Model	Total No. of Trials	$\langle \mathrm{R}_n \rangle$	$\langle \mathrm{R}_n \rangle$	$\langle \mathrm{R}_n \rangle$
A	164	0.134	0.033	0.273
B	158	0.129	0.031	0.661
C	12	0.149	0.096	0.654
		$\langle \mathrm{S}_n \rangle$	$\langle \mathrm{S}_n \rangle$	$\langle \mathrm{S}_n \rangle$
A	164	0.202	0.046	0.331
B	158	0.195	0.043	0.795
C	12	0.244	0.151	0.664

$\langle \mathrm{R}_n \rangle$ is given by Eq. (14) and $\langle \mathrm{S}_n \rangle$ by Eq. (15); Model A is Rosinger BE [20], B is Erbacher et al. [14] and C is for E110 cladding [65].

As can be seen from Table 25, the difference between the overall level of uncertainty between models A and B is very small as regard to the burst time and burst temperature, but model A, i.e. the Rosinger BE burst criterion, gives less deviation from measurements regarding the burst stress, viz. roughly by a factor 2. We should recall that these burst-stress criteria were originally developed from Zircaloy-4 data; here we have also used them for ZIRLO cladding. Our data analysis guides us to use the Rosinger BE burst criterion for Zircaloy and ZIRLO clads until additional data on modern cladding materials become accessible for analysis.

In our statistical treatment of data in this subsection, we have not considered the strain-based burst criterion `FRAPTRAN-1.5` mentioned in the forgoing subsections. The reason for this is that this criterion should, strictly speaking, always be used together with the localized ballooning model (`BALON2`) in `FRAPTRAN-1.5`. This model assumes that clad ballooning occurs by plastic instability, which is activated when the calculated cladding plastic strain exceeds an empirically determined instability strain [64]. This approach is much different from the one used in `QT/SSM-FRAPTRAN`, where creep rather time-independent plasticity governs cladding ballooning and burst. Therefore, the `BALON2` model and its associated burst criterion is not used here.

5 Discussion on burst criteria

In this report, we have used the set of cladding material correlations in QT/SSM-FRAPTRAN, applicable to LOCA conditions, to retrodict cladding burst data, which were obtained from various experimental programs. The computer model consists of submodels for the zirconium alloy solid-solid phase transformation, creep deformation, oxidation and burst. Therefore, the cladding burst is a combined effect of various phenomena reflected in the model.

As has been noted in the foregoing two sections, the model contains a number of cladding burst options. There are two types of cladding burst criteria: strain-based versus stress-based correlations, see Appendix A. The former type includes the widely used NUREG-0630 correlations [19] from 1980 and the recent FRAPTRAN-1.5 correlation [64]. These correlations were obtained by curve-fitting of the available experimental data on cladding burst strain versus temperature (see Fig. A1 in Appendix A). The NUREG-0630 correlations are in tabular forms for high and low heating rates, namely $\leq$ 10 K/s and $\geq$ 25 K/s. They also include tables for the channel flow blockage (in %) as a function of burst temperature, which have not been considered in the present report. So, strictly speaking, there is a gap in the NUREG-0630 correlations for heating rates between 10 to 25 K/s. The FRAPTRAN-1.5 burst strain correlation is in the form of a 4-degree polynomial function of temperature.

All the stress-based burst criteria in the model (available in QT/SSM-FRAPTRAN) are in the form of an exponential declining function of temperature, which may include the effect of oxygen concentration in the cladding. These correlations are also empirical, meaning that they were obtained by fitting the measured data, i.e. cladding hoop stress (or pressure) versus temperature, to an exponential function. Despite this, they follow the trend of such data. Five correlations of this kind, three for Zircaloy cladding, one for M5 cladding and another for E110 cladding have been implemented (Appendix A). In particular, the correlations for Zircaloys are compared in Fig. A2, while those for M5 and E110 with their supporting data are depicted in Fig. A3 of Appendix A.

There are a number of review reports and articles on cladding burst data and behavior published over the years, prominent among them is the aforementioned 1980 compendium of Powers and Meyer [19], which reviews data up to 1979. The more recent reviews include [21, 66, 67]. Reference [66], issued by the European Commission (EC) in 2000, merits some comments. It compares the methods that have been adopted in several countries to estimate the radiological consequences of design basis faults (accidents). The collaborators of the study were from several west European organizations and countries, namely Belgium, France, the Netherlands, Spain, Switzerland and the United Kingdom. In more detail, the objectives of the study were three-fold: (i) review the existing (i.e. up to 1999) cladding failure criteria and licensing practices in each participant's country, (ii) form a consensus on cladding failure criteria, (iii) determine the effect of cladding failure criteria on the calculated extent of cladding failure (i.e. the number of fuel rod failures in the core during a postulated LOCA) for a reference design in the participating countries.

Although the EC report [66] summarizes the existing (1999) cladding burst criteria practiced in the aforementioned countries, the details of some important correlations are not revealed, thereby could not be compared e.g. with the ones used in QT/SSM-FRAPTRAN.

These include the French EDGAR criterion and the German (Siemens) cladding ballooning and burst model. The authors of [66] divide the models for cladding ballooning and burst to two categories: non-mechanistic and mechanistic. The NUREG-0630 correlations [19] fall into the former category while the stress-based criteria as implemented in `QT/SSM-FRAPTRAN` seem to belong to the latter category.

In the literature, there exist sketchily reported burst criteria for modern and widely utilized PWR fuel claddings such as M5 and ZIRLO. In Fig. 18, we showed burst stress versus burst temperature data on M5, for which a burst criterion has been depicted in [29] without providing sufficient details on the background data. Based on these data, we have developed a specific correlation for M5 cladding that has been implemented in `QT/SSM-FRAPTRAN`; see Appendix A and Fig. A3. Likewise in Fig. 19, we displayed data and lines, burst temperature versus hoop stress, for ZIRLO cladding, which are reproduced from [32]. The relations for the lines, which are the burst criterion plus its uncertainty, have not been described in [32].

Powers and Meyer [19] also display an empirical formula (burst criterion), attributed to R. H. Chapman, which relates the cladding burst temperature to the engineering hoop stress and the heating rate. This correlation has not been implemented in `QT/SSM-FRAPTRAN`, hence it could not be used to retrodict the cladding burst time and other burst quantities. However, we have compared the output of this correlation with the burst temperature versus engineering hoop stress transient data for Zircaloy-4 cladding shown in Sec. 2 and the results were in good agreement [62]. A similar conclusion has also been reached in [66]. In fact, it is stated in [66] that most of the EC-project participants use Chapman's correlation as the sole criterion, others for comparisons to their own criteria. In addition, an improvement of this correlation for use in codes has been suggested in [66]. Despite all this, we have found that the original Chapman correlation has limited applicabilities for implementation in a transient analysis computer program such as `FRAPTRAN`.

As mentioned in Sec. 1, the cladding burst criterion is not an item of the LOCA acceptance criteria [5], however, a LOCA safety evaluation method must include a model for cladding ballooning and burst by considering the temperature of the cladding and the difference in pressure between the inside and outside of the cladding, both as functions of time.

There are other kinds of cladding burst or failure criteria that we have not considered in our study. Noted among them is given in a neat 1987 paper by Arai et al. [68], appraised in [67], which employs the Larson-Miller parameter (LMP) approach to retrodict successfully thermal transient and isothermal tests conducted on unirradiated Zircaloy-2 cladding specimens. The LMP method is deliberately formulated to treat creep rupture data and predict time-to-rupture of the material. It is based on the assertion that the time at temperature and stress determines the rupture of the material. For isothermal conditions, the LPM formula is

$$f(\sigma) = aT[\log_{10}(t_B) + C], \tag{16}$$

where $f(\sigma)$ is the LMP, a dimensionless parameter and a function of the tensile hoop stress σ, $a \equiv 1$ /K is a constant, T the absolute temperature, t_B the burst time (h), and C is a material constant put as $C = 20$ for Zircaloys. Arai et al. [68] determined $f(\sigma)$ from their test data. For transient burst data a *life-fraction rule* (LFR) in connection with the LMP

formula was used [68]

$$L(\sigma) = \frac{b}{\dot{T}} \int_{T_0}^{T_B} e^{-cf(\sigma)/T} dT = 1, \tag{17}$$

where b and c are positive constants, T_0 the initial temperature, T_B the burst temperature and $\dot{T}$ is the heating rate. The numerical constants and experimental data supporting the model are all provided in [68]. The LMP life-fraction method was also successfully applied to thermal transient tests on unirradiated and irradiated Zircaloy-4 cladding [68]. Arai et al. conclude that the LMP life-fraction approach could be used to satisfactorily predict failure of fuel cladding under various high-temperature (LOCA) conditions in BWRs.

Figure 33a shows the Larson-Miller parameter developed in [68] based on thermal transient and isothermal burst data for internally pressurized Zircaloy-2 tubes. The test data cover isothermal temperatures 923-1023 K, heating rates 5 to 200 K/s, pressures 6.5 to 100 MPa, and burst temperatures up to 1400 K. The burst time t_B calculated according to Eq. (17), at several temperatures, and measured data [68] are shown in Fig. 33b. We have not examined Arai et al's transient test data and computations.

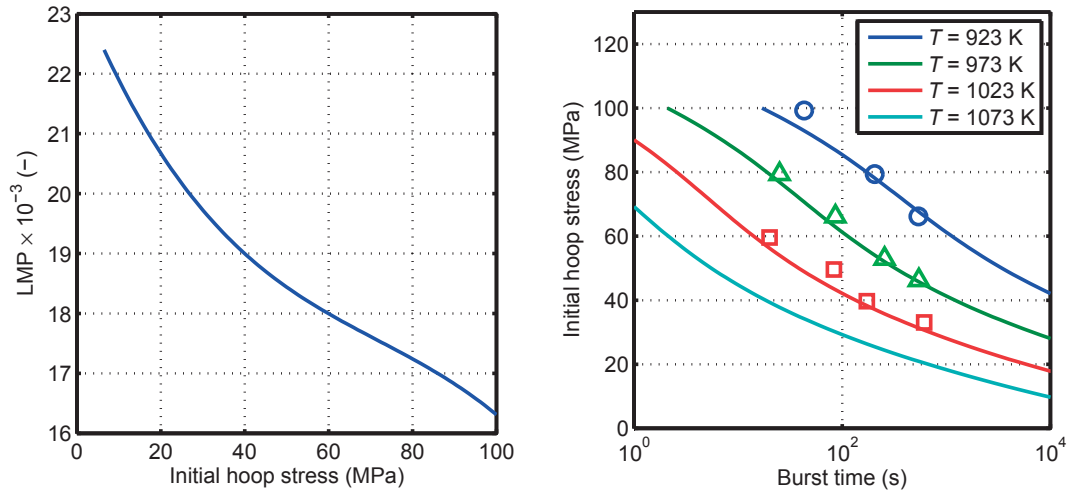

(a) (b)

Figure 33: (a) Larson-Miller parameter (LMP) developed based on thermal transient and isothermal burst data for internally pressurized Zircaloy-2 tubes according to [68]. (b) Burst time computations (lines) using Eq. (16) for isothermal tests; measurements: ◯ 923 K, △ 973 K, □ 1023 K.

The LMP method has also been utilized to evaluate the creep rupture behavior of cladding tubes under off-normal dry storage conditions; e.g. Mayuzumi and Onchi [69] evaluated isothermal tests in the temperature and pressure ranges of 727 to 857 K and 8.5 to 19.5 MPa. The LMP functional form $f(\sigma)$ used by these authors is quite different from that formulated by Arai et al. Moreover, it gives different results if applied to the same conditions, but it fit their measured data quite well [69].

The LMP approach is widely used to characterize the high-temperature creep rupture behavior of engineering materials. Because ballooning of cladding is primarily caused by creep deformation, LMP could be a suitable parameter for characterizing cladding burst data under LOCA conditions.

A similar approach, i.e. a life-fraction rule based method, but not an LMP formulation, was proposed by Rashid in a 1987 paper [70], which has also been implemented in the FALCON code [71]. Rashid's life-fraction rule burst criterion is expressed in the form

$$L = \int_0^{t_B} \frac{\dot{\varepsilon}}{\varepsilon_B} dt + \int_0^{t_B} \frac{\dot{T}}{T_B} dt = 1. \tag{18}$$

Here, $\dot{\varepsilon}$ is the true creep strain rate, ε_B is the hoop burst strain at constant temperature and T_B is the burst temperature at constant stress and constant heating rate. Both ε_B and T_B are empirically based parameters taken from the literature [70]. This burst criterion is compelling, since it combines the cladding deformation ($\propto$ stress) and temperature as the basis of cladding rupture. However, its underlying experimental base is not as solid as that of the LMP-LFR criterion by Arai et al. [68]. Note that the LMP-LFR also combines the cladding stress, the temperature and the heating rate to compute the cladding life, but in another fashion.

There are other cladding burst data reported in the literature which we have not addressed here. For example, the recent transient burst tests conducted in argon gas on Zircaloy-4 cladding tubes [72]. These tests cover heating rates from 17.6 to 81 K/s and internal rod pressures from 2 to 8 MPa. Burst temperature, burst time and burst strain were determined and correlations similar to Erbacher et al.'s [14], but suitable for argon environment, were constructed. Khan et al.'s strain data [72] are more uniform and exhibit less scatter than Erbacher et al.'s [14]. Furthermore, the authors have deduced a suitable burst criterion, similar to [14], for Zircaloy-4 cladding burst in inert gas environment [73].

Finally, we should comment that all the material correlations and burst criteria discussed and reviewed in this report are engineering test-based and non-mechanistic, meaning that they do not rest on the physics or the mechanisms of high-temperature rupture in metals [74], less in zirconium alloy. With the existing test data, however, one may be able to formulate a burst criterion based on the combined mechanical (strain) and thermal energy (temperature) which gets conveyed to the material, and thereby dissipated through rupture, during the transient.

6 Summary, conclusions and outlook

6.1 Summary and conclusions

In this report, we have endeavored to systematize and assess LWR fuel cladding burst test data obtained under LOCA conditions from various past and current test programs. After an introductory section (Sec. 1) regarding the LOCA conditions in LWRs and Zr-base cladding materials (Table 1), in Sec. 2 we have summarized the considered cladding burst data base. A synopses of the data base is shown in Table 2, in which the basic characteristics of the tests are outlined. These comprise the method of heating the test rods, the applied heating rates and the circumferential temperature difference around cladding tube during the test. The primary cladding burst quantities, obtained from the tests, are time-to-burst, burst temperature, hoop burst stress (or burst pressure) and hoop burst strain.

The tests in the data base (Sec. 2) comprise the ORNL (1979) program, the KFK-series (1979-1988), the CEGB (1984-1985) creep rupture tests, and the CEA (2002) creep rupture tests on hydrided cladding tubes. These tests were made on Zircaloy-4 cladding tubes in steam environments except the CEGB tests, which were carried out in vacuum. Most of the tests were on unirradiated Zircaloy-4, except the KfK-83 tests (Sec. 2.2.3) which were performed in the FR2 test reactor with rods irradiated up to 35 MWd/kgU. The data base also contains some tests on Zr-Nb-base alloy fuel clads, which includes the AEKI (2000) tests on E110 cladding, the ANL-2010 tests on ZIRLO and the Studsvik-2012 tests on preirradiated ZIRLO cladding tubes (up to 69 MWd/kgU). All these tests were conducted in laboratories, i.e. out-of-reactor. The tests were made in steam environments, except some AEKI tests which were conducted in argon gas. The data base also includes burst data obtained from the Halden reactor through the IFA-650 integral LOCA tests (tests 2-7) on rods irradiated up to 74 MWd/kgU. The cladding materials on these tests were Zircaloy-4 (tests 2-5), E110 (test 6) and Zircaloy-2 (test 7). The measured data are reproduced in tables and graphs in Sec. 2.

The extent of the background information and the quality of the data vary between the tests in the data base. For some tests, such as CEA-2000 (M5 cladding) and CEA-2002 (hydrided Zircaloy-4 cladding) and W-EDF (ZIRLO cladding), sufficient information were not available in the publications to make one-to-one comparisons between the model computations and measurements.

In Sec. 3, we outlined the ingredients of the computer model used to retrodict the measured burst quantities of the interest, i.e. time-to-burst, burst temperature, hoop burst stress and strain of the cladding. The utilized unified model computes in tandem cladding oxidation, the Zr-alloy phase transformation (i.e., $\alpha \rightleftharpoons (\alpha + \beta) \rightleftharpoons \beta$) and cladding creep deformation during a LOCA. It includes a criterion for cladding rupture, either a stress-based or a strain-based, as a function of temperature. The detailed expressions for several burst criteria (options in the model) are outlined in the appendix. The unified cladding model has been implemented in a stand-alone MATLAB program (`ftmat`) and it corresponds to the mechanical analysis module of the `QT/SSM-FRAPTRAN` program used for LOCA analysis.

In Sec. 4, we showed the results of `ftmat` computations (i.e. its retrodictions) against test

data on burst quantities obtained from the aforementioned programs. We have examined the performance of different burst criteria available in the QT/SSM-FRAPTRAN program. Only the highlights of our assessment are presented in Sec. 4 and summarized in Tables 23-25. Additional results and details are documented in the supplementary report [62]. To be more specific, for each data set in our data base, Table 23 lists the mean relative difference between calculated and measured burst quantities while Table 24 shows the associating data regarding the root mean square deviation, which can be considered as a 1σ-level of uncertainty in the specific model. The outcome of two stress-based burst criteria, Rosinger BE (also called model A) and Erbacher et el. (model B), used for Zircaloy and ZIRLO claddings, are tabulated. For E110 cladding (AEKI-00 tests), we have used the custom-made burst criterion of van Uffelen et al. (model C). Furthermore, we have computed the overall deviations of our computations relative to measurements, i.e. by combining the individual uncertainty obtained for each data set; see Table 25. We found that, tentatively, the stress-based Rosinger BE criterion [20] is suitable for applications to Zircaloy and ZIRLO claddings.

In Sec. 5, we discussed the characteristics of the cladding burst criteria utilized in our assessment. We compared our utilized criteria with some other criteria used in the industry. The details of some of those criteria or data, in particular for M5 and ZIRLO cladding tubes, have not been revealed or published. Therefore, quantitative comparisons between measurements and computations, using the specific burst criterion, could not be made for these alloys. We also discussed other formulations of cladding burst criteria reported in the literature, namely the so-called life-fraction rule criterion, where the cladding strain and stress are combined in certain manner to predict cladding burst-time versus hoop stress at different temperatures.

Predicting cladding burst is an important component of LOCA safety analysis. Indeed, as stated in [5], a LOCA safety evaluation method must include a model for cladding ballooning and burst by considering the temperature distribution of the cladding and the difference in pressure between the inside and outside of the cladding, both as functions of time. For the LOCA analysis model to be acceptable, the ballooning and rupture computations must be based on pertinent data in such a way that the degree of ballooning and occurrence of burst are not underestimated. The degree of ballooning and burst shall be taken into account in computations of pellet-cladding gap conductance, cladding oxidation and embrittlement, and hydrogen generation. Hence, an accurate model for burst is paramount to LOCA analysis.

6.2 An outlook

Additional improvements regarding cladding burst criteria are needed. These may be as follows:

- Further optimize the Rosinger BE burst criterion for Zircaloy-4 and ZIRLO, as-well-as the associating creep correlations to reduce the uncertainty in the calculated burst quantities relative to measurements.
- Reformulate the aforesaid criterion, so that it relies on the excess oxygen concentration in the cladding metal rather than the total oxygen uptake; see Appendix A.

- Extend the burst criterion to hydrided cladding if such data are accessible, because it is known that excessive hydrogen concentration in the cladding may reduce the burst threshold.
- Examine a burst criterion based on the life-fraction concept discussed in Sec. 5, which accounts for burst strain (or stress) and temperature simultaneously.
- Examine an energy controlled burst criterion, which combines mechanical and thermal energy during the transient.
- Evaluate the burst properties of recent Halden IFA-650 tests 9-13, which include Zircaloy-2 and Zr1%Nb (E110) cladding materials.

Acknowledgements

The work was supported by the Swedish Radiation Safety Authority (SSM) under the contract number SSM2014-2355. We thank Tero Manngård for his contributions during the initial phase of this project and Anna Alvestav for helpful comments.

References

[1] P. D. Parsons, E. D. Hindle, and C. A. Mann. The deformation, oxidation and embrittlement of PWR fuel cladding in a loss-of-coolant accident. Technical Report CSNI 129, OECD Nuclear Energy Agency, Paris, France, 1986.

[2] A. R. Massih. Review of experimental data for modelling LWR fuel cladding behaviour under loss of coolant accident conditions. Technical Report 2007:14, Swedish Nuclear Power Inspectorate, Stockholm, Sweden, 2007.

[3] K. Pettersson. Nuclear fuel behaviour in loss-of-coolant (LOCA) conditions. Technical Report NEA No. 6846, OECD Nuclear Energy Agency, Issy-les-Moulineaux, France, 2009.

[4] T. Manngård and A. R. Massih. Modelling and simulation of reactor fuel cladding under loss-of-coolant conditions. *J. Nucl. Sci. Techn.*, 48:39–49, 2011.

[5] U.S. Code of Federal Regulations 10 Part 50. http://www.nrc.gov/reading-rm/doc-collections/cfr/part050/, Updated 23 February 2015. See Appendix K: ECCS Evaluation Models.

[6] H. M. Chung. Fuel behavior under loss-of-coolant accident situations. *Nucl. Eng. Techn.*, 37:327–362, 2005.

[7] K. J. Geelhood, W. G. Luscher, and C. E. Beyer. FRAPTRAN 1.4: A computer code for transient analysis of oxide fuel rods. Technical Report NUREG/CR-7023, United States Nuclear Regulatory Commission, 2011. Volume 1.

[8] C. Lemaignan and A. T. Motta. Zirconium alloys in nuclear applications. In R. W. Cahn, P. Haasen, and E. J. Kramer, editors, *Nuclear Materials*, volume 10B of *Materials Science and Technology*, chapter 7, pages 1–51. VCH, Weinheim, Germany, 1994. Volume editor B.R.T. Frost.

[9] A. Miquet, D. Charquet, and C. H. Allibert. Solid state phase equilibria of Zircaloy-4 in the temperature range 750-1050°C. *J. Nucl. Mater.*, 105:132–141, 1982.

[10] N. V. Bangaru, R. A. Busch, and J. H. Schemel. Effects of beta quenching on the microstructure and corrosion of Zircaloys. In R.B. Adamson and L.F.P. van Swam, editors, *Zirconium in the Nuclear Industry: Seventh International Symposium*, volume ASTM STP 939, pages 341–363, Philadelphia, USA, 1987. American Society for Testing and Materials.

[11] R. Jerlerud Peréz and A. R. Massih. Thermodynamic evaluation of the Nb-O-Zr system. *J. Nucl. Mater.*, 360:242–254, 2007.

[12] D. Kaddour, S. Frechinet, A. F. Gourgues, J. C. Brachet, L. Portier, and A. Pineau. Experimental determination of creep properties of zirconium alloys together with phase transformation. *Scripta Mater.*, 51:515–519, 2004.

[13] H. M. Chung and T. F. Kassner. Pseudobinary Zircaloy-oxygen phase diagram. *J. Nucl. Mater.*, 84:327–339, 1979.

[14] F. J. Erbacher, H. J. Neitzel, H. Rosinger, H. Schmidt, and K. Wiehr. Burst criterion of Zircaloy fuel claddings in a loss-of-coolant accident. In D. G. Franklin, editor, *Zirconium in the Nuclear Industry: Fifth Conference*, volume ASTM STP 754, pages 271–283, Philadelphia, USA, 1982. American Society for Testing and Materials.

[15] E. H. Karb, M. Prüßmann, L. Sepold, P. Hofmann, and G. Schanz. LWR fuel rod behavior in the FR2 in-pile tests simulating the heatup phase of a LOCA. Technical Report KfK 3346, Kernforschungszentrum Karlsruhe, Germany, March 1983.

[16] F. J. Erbacher and S. Leistikow. Zircaloy fuel cladding behavior in a loss-of-coolant accident: A review. In R. B. Adamson and L. F. P. van Swam, editors, *Zirconium in the Nuclear Industry: Seventh International Symposium*, volume ASTM STP 939, pages 451–488, Philadelphia, USA, 1987. American Society for Testing and Materials.

[17] R. H. Chapman, J. L. Crowley, A. W. Longest, and G. Hofmann. Zirconium cladding deformation in a steam environment with transient heating. In *Zirconium in the Nuclear Industry: Fourth Conference*, volume ASTM STP 681, pages 393–408. American Society for Testing and Materials, 1979.

[18] R. H. Chapman, J. L. Crowley, A. W. Longest, and E. G. Sewell. Effect of creep time and heating rate on deformation of Zircaloy-4 tubes tested in steam with internal heaters. Technical Report NUREG/CR-0343, ORNL/NUREG/TM-245, US NRC, October 1978.

[19] D. A. Powers and R. O. Meyer. Cladding swelling and rupture models for LOCA analysis. Technical Report NUREG-0630, US NRC, April 1980.

[20] H. E. Rosinger. A model to predict the failure of Zircaloy-4 fuel sheathing during postulated LOCA conditions. *J. Nucl. Mater.*, 120:41–54, 1984.

[21] C. Grandjean. A state of art review of past programs devoted to fuel behavior under LOCA conditions: Part I. Technical Report NT SEMCA 2005-313, IRSN, Cadarache, France, December 2005.

[22] E. H. Karb, L. Sepold, P. Hofmann, C. Petersen, G. Schanz, and H. Zimmermann. LWR fuel rod behavior during reactor tests under loss-of-coolant conditions: Results of the FR2 in-pile tests. *J. Nucl. Mater.*, 107:55–77, 1982.

[23] F. J. Erbacher and S. Leistikow. A review of Zircaloy fuel cladding behavior in a loss-of-coolant accident. Technical Report KfK 3973, Kernforschungszentrum Karlsruhe, Germany, September 1985.

[24] S. Leistikow and G. Schanz. Oxidation kinetics and related phenomena of Zircaloy-4 fuel cladding exposed to high temperature steam and hydrogen-steam mixtures under PWR accident conditions. *Nucl. Eng. Des.*, 103:65–84, 1987.

[25] M. E. Markiewicz and F. J. Erbacher. Experiments on ballooning in pressurized and transiently heated Zircaloy-4 tubes. Technical Report KfK 4343, Kernforschungszentrum Karlsruhe, Germany, February 1988.

[26] A. T. Donaldson and T. Healey. Creep deformation of Westinghouse Zircaloy-4 fuel cladding tubes in alpha plus beta phase temperature range. Technical Report TRPD/B/0564/N85, Central Electricity Generating Board, Berkeley, Gloucestershire, UK, 1984.

[27] A. T. Donaldson, T. Healey, and R. A. L. Horwood. Creep behaviour of Westinghouse Zr-4 fuel between 973 and 1073 K. Technical Report TRPD/B/0008/N82, Central Electricity Generating Board, Berkeley, Gloucestershire, UK, 1985.

[28] J. C. Brachet, L. Portier, and T. Forgeron. Influence of hydrogen content on the α/β phase transformation temperatures and on the thermal-mechanical behavior of Zy-4, M4 (ZrSnFeV), and M5$^{\mathrm{TM}}$ (ZrNbO) alloys during the first phase of LOCA transient. In G. D. Moan and P. Rudling, editors, *Zirconium in the Nuclear Industry: Thirteenth International Symposium*, volume ASTM STP 1423, pages 673–701, West Conshohocken, PA, USA, 2002. American Society for Testing and Materials.

[29] T. Forgeron, J. C. Brachet, F. Barcelo, A. Castaing, J. Hivroz, J. P. Mardon, and C. Bernaudat. Experiment and modeling of advanced fuel rod cladding behavior under LOCA conditions: alpha-beta phase transformation kinetics and EDGAR methodology. In G. P. Sabol and G. D. Moan, editors, *Zirconium in the Nuclear Industry: Twelfth International Symposium*, volume ASTM STP 1354, pages 256–278, West Conshohocken, PA, USA, 2000. American Society for Testing and Materials.

[30] Z. Hózer, C. Győri, M. Horvath, I. Nagy, L. Maroti, L. Matus, and P. Windberg. Balooning experiments with VVER cladding. *Nucl. Techn.*, 152:273–285, 2005.

[31] E. Perez-Fero et al. Experimental database of E110 claddings under accident conditions. Technical Report AEKI-FRL-2007-123-01/01, AEKI, Research Institute of the Hungarian Academy of Sciences, Budapest, November 2007.

[32] D. L. Chapin, G. Wikmark, C. Maury, B. Therache, M. Claeys, M. Q. Gutierrez, and C. M-R. Ruiz. Optimized ZIRLO qualification program for EDF reactors. In *Proceedings of Top Fuel 2009*, number Paper 2040, pages 60–65, Paris, France, September 6-10 2009.

[33] Y. Yan, T.A. Burtseva, R.O. Meyer, and M.C. Billone. Update of LOCA-integral and post-LOCA-bend test results for fresh ZIRLO cladding. Argonne National Laboratory letter report to U.S. Nuclear Regulatory Commission, July 2010. USNRC ADAMS Accession No. ML111380437.

[34] Y. Yan, T.A. Burtseva, R.O. Meyer, and M.C. Billone. Argonne results for ANL-Studsvik benchmark tests. Argonne National Laboratory letter report to U.S. Nuclear Regulatory Commission, August 2010. USNRC ADAMS Accession No. ML111380445.

[35] M. Helin and J. Flygare. NRC LOCA tests at Studsvik: Design and construction of test train device and tests with unirradiated cladding material. Technical Report N-11/130, Studsvik Nuclear AB, 2012.

[36] M. E. Flanagan, P. Askeljung, and A. Puranen. Post-test examination results from integral, high-burnup, fueled LOCA tests at Studsvik nuclear laboratory. Technical Report NUREG-2160, U.S. Nuclear Regulatory Commission, 2013.

[37] T. Manngård, J. O. Stengård, and L. O. Jernkvist. Evaluation of the Halden IFA-650 loss-of-coolant accident experiments 2, 3, 4, 5, 6 and 7. In *Proceedings of Enlarged Halden Programme Group meeting 2013*, Gol, Norway, March 10-15 2013. Paper F1.2.

[38] R. L. Varty and H. E. Rosinger. Comparison of sheath failure model with published experimental data. Technical Report AECL-6806, Atomic Energy of Canada Limited, Pinawa, Manitoba, Canada, 1982.

[39] F. J. Erbacher, H. J. Neitzel, and K. Wiehr. Studies on Zircaloy fuel clad ballooning in a loss-of-coolant accident - results of burst tests with indirectly heated fuel simulators. In *Zirconium in the Nuclear Industry: Fourth Conference*, volume ASTM STP 681, pages 429–446, Philadelphia, USA, 1979. American Society for Testing and Materials.

[40] F. J. Erbacher, H. J. Neitzel, and K. Wiehr. Cladding deformation and emergency core cooling of a pressurized water reactor in a LOCA: Summary description of the REBEKA program. Technical Report KfK 4781, Kernforschungszentrum Karlsruhe, Germany, August 1990.

[41] A. R. Massih. An evaluation of high-temperature creep of zirconum alloys: data versus models. Technical Report 2014:20, Swedish Radiation Safety Authority (SSM), Stockholm, Sweden, 2014.

[42] A. T. Donaldson, T. Healey, and R. A. L. Horwood. Biaxial creep deformation of Zircaloy-4 PWR fuel cladding in the alpha, (alpha+beta) and beta phase temperature range. In *Proceedings of Nuclear Fuel Performance Conference*, pages 83–89, UK, 1985. British Nuclear Energy Society (BNES).

[43] NEI staff. Fuel review: design data. Nuclear Engineering International magazine, September 2004. pp. 26-32.

[44] International Fuel Performance Experiments (IFPE) database of the OECD Nuclear Energy Agency (NEA), Reviewed 18 January 2012. https://www.oecd-nea.org/science/wprs/fuel/ifpelst.html.

[45] J. P. Foster, H. K. Yueh, and R. J. Comstock. ZIRLO cladding improvement. *J. ASTM International*, 5:457–469, 2008.

[46] E. Kolstad, W. Wiesenack, B. Oberländer, and T. Tverberg. High burnup fuel behaviour under LOCA conditions as observed in Halden reactor experiments. In *Fuel Behaviour and Modelling Under Severe Transient and Loss of Coolant Accident (LOCA) Conditions*, IAEA-TECDOC-CD-1709, pages 207–218, Vienna, Austria, 2013. International Atomic Energy Agency. Presented in Mito, Japan, 18-21 October 2011.

[47] M. E. Flanagan. Mechanical behavior of ballooned and ruptured cladding. Technical Report NUREG-2119, U.S. Nuclear Regulatory Commission, 2012.

[48] M. E. Flanagan and P. Askeljung. Observations of fuel fragmentation, mobility and release in integral, high-burnup, fueled LOCA tests. Presented at the LOCA workshop of the May 2012 Halden Program Group Meeting in Lyon, France., May 2012.

[49] Personal communication, Patrick Raynaud, November, 2014.

[50] W. Wiesenack. Summary of the Halden Reactor Project LOCA Test Series IFA-650. Technical Report HPR-380, Institutt for Energiteknikk, Halden, Norway, May 2013.

[51] T. Manngård, A. Massih, and J. O. Stengård. Evaluation of the Halden IFA-650 loss-of-coolant accident experiments 2, 3 and 4. Technical Report 2014:18, Swedish Radiation Safety Authority (SSM), Stockholm, Sweden, 2014.

[52] T. Manngård and J. O. Stengård. Evaluation of the Halden IFA-650 loss-of-coolant accident experiments 5, 6 and 7. Technical Report 2014:19, Swedish Radiation Safety Authority (SSM), Stockholm, Sweden, 2014.

[53] B. C. Oberländer, H. K. Jenssen, and N. O. Solum. Update on PIE on the test rod from LOCA test IFA-650.12. In *Proceedings of Enlarged Halden Programme Group meeting 2013*, Gol, Norway, March 10-15 2013. Paper F1.8.

[54] F. Khattout. The BWR LOCA test IFA-650.13: in-pile measurements. Technical Report HWR-1042, Institutt for Energiteknikk, Halden, Norway, January 2013.

[55] R. Tradotti. LOCA testing at Halden, the BWR fuel experiment IFA-650.14. Technical Report HWR-1084, Institutt for Energiteknikk, Halden, Norway, January 2014.

[56] B. C. Oberländer and H. K. Jenssen. PIE on the rod from the LOCA test IFA-650.13 on high burn-up BWR fuel. Technical Report HWR-1095, Institutt for Energiteknikk, Halden, Norway, August 2014.

[57] B. C. Oberländer and H. K. Jenssen. PIE on the rod from the LOCA test IFA-650.14 on high burn-up BWR fuel. Technical Report HWR-1096, Institutt for Energiteknikk, Halden, Norway, August 2014.

[58] L. O. Jernkvist. Implementation of models for cladding high temperature metal-water reactions, phase transformation, creep and failure in the FRAPTRAN-1.4 computer program. Technical Report TR10-005V2, Quantum Technologies AB, Uppsala, Sweden, May 2012.

[59] A. R. Massih. Transformation kinetics of zirconium alloys under non-isothermal conditions. *J. Nucl. Mater.*, 384:330–335, 2009.

[60] A. R. Massih and L. O. Jernkvist. Transformation kinetics of alloys under non-isothermal conditions. *Modelling Simul. Mater. Sci. Eng.*, 17:055002, 2009.

[61] A. R. Massih. High-temperature creep and superplasticity in zirconium alloys. *J. Nucl. Sci. Techn.*, 50:21–34, 2013.

[62] L. O. Jernkvist and A. R. Massih. Supplementary material to present report: Additional plots. Technical Report TR15-001v1, Quantum Technologies AB, Uppsala, Sweden, 2015.

[63] J. V. Cathcart, R.E. Pawel, R. A. McKee, R. E. Druschel, G. J. Yurek, J. J. Campbell, and S. H. Jury. Zirconium metal-water oxidation kinetics IV: Reaction rate studies. Technical Report ORNL/NUREG-17, Oak Ridge National Labrotory, TN, USA, 1977.

[64] K. J. Geelhood, W.G. Luscher, and J. M. Cuta. FRAPTRAN-1.5: A computer code for the transient analysis of oxide fuel rods. Technical Report PNNL-19400, Pacific Northwest National Laboratory, Richland, Washington, May 2014.

[65] P. Van Uffelen, C. Győri, A. Schubert, J. van de Laar, Z. Hózer, and G. Spykman. Extending the application range of a fuel performance code from normal operating to design basis accident conditions. *J. Nucl. Mater.*, 383:137–143, 2008.

[66] European Commission. Fuel cladding failure criteria. Technical Report EUR 19256 EN, European Commission Directorate-General Environment, 2000.

[67] T. Alam, M. K. Khan, M. Pathak, K. Ravi, R. Singh, and S. K. Gupta. A review on the clad failure studies. *Nucl. Eng. Des.*, 241:3658–3677, 2011.

[68] S. Arai, H. Murabayashi, A. Tanabe, K. Yoshida, and S. Sumida. Failure correlation for Zircaloy-2 fuel cladding under high temperature transient conditions. *J. Nucl. Sci. Techn.*, 24:214–219, 1987.

[69] M. Mayuzumi and T. Onchi. Creep deformation and rupture properties of unirradiated Zircaloy-4 nuclear fuel cladding tube at temperatures of 727 to 857 K. *J. Nucl. Mater.*, 175:135–142, 1990.

[70] Y. R. Rashid. Transient failure of zircaloy cladding. *Nucl. Eng. Des.*, 101:305–313, 1987.

[71] W. F. Lyon, N. Jahingir, R. O. Montgomery, and S. Yagnik. Capabilities of the FALCON steady state and transient fuel performance code. In *Proceedings of the 2004 International Meeting on LWR Fuel Performance, Orlando, Florida, September 19-22*. American Nuclear Society, 2004.

[72] M. K. Khan, M. Pathak, S. Suman, A. Deo, and R. Singh. Burst investigation for Zircaloy-4 fuel cladding in inert environment. *Ann. Nucl. Energy*, 69:292–300, 2014.

[73] M. K. Khan, M. Pathak, S. Suman, A. Deo, and R. Singh. Burst criterion for Zircaloy-4 fuel cladding in an inert environment. *Nucl. Eng. Des.*, 265:886–894, 2013.

[74] H. Riedel. *Fracture at high temperatures*. Springer-Verlag, Berlin, 1987.

Appendix A Cladding burst criteria

Correlations for calculating the occurance of cladding rupture (burst) are available in the set of high temperature cladding models, developed for QT/SSM-FRAPTRAN [58]. More precisely, cladding high temperature rupture can be predicted by use of eight different burst criteria. The user selects the desired criterion through the input switch irupt, according to the logic in Table A1. Two types of burst criteria are used, a strain-based or a stress-based. These criteria are purely empirical, meaning that they are derived by fitting correlations to different set of measured data on cladding burst. In paragraphs below, as in [58], we describe these correlations.

Table A1: Cladding high temperature burst criteria, available in QT/SSM-FRAPTRAN.

Value set to irupt	Cladding burst criterion	Cladding material
1	Threshold hoop total strain, NUREG-0630 (fast heating) [19]	Zircaloys
2	Threshold hoop total strain, NUREG-0630 (slow heating) [19]	Zircaloys
3	Threshold for hoop total strain, FRAPTRAN-1.5 [64]	Zircaloys
4	Threshold for hoop stress, Rosinger (upper bound) [20]	Zircaloys
5	Threshold for hoop stress, Rosinger (best estimate) [20]	Zircaloys
6	Threshold for hoop stress, Erbacher et al. [14]	Zircaloys
7	Threshold for hoop stress, Forgeron et al. [29]	M5
8	Threshold for hoop stress, Van Uffelen et al. [65]	E110

Strain-based burst criteria When the strain-based burst criteria are used in FRAPTRAN, it is assumed that the cladding fails when the total hoop strain $\varepsilon_{\theta\theta}^{Tot}$ (-) exceeds the burst strain ε_B (-), which is a function of temperature, determined empirically from isothermal burst tests on Zircaloy-4 cladding tubes. The burst strain used, when option irupt is either 1 or 2, is taken from the 1980 US NRC report NUREG-0630 [19]. In that report, the cladding total hoop strain at failure is tabulated with respect to temperature for two different ranges of heating rates: <10 Ks^{-1} (slow heating) and >25 Ks^{-1} (fast heating). The tabulated values for ε_B are shown in Fig. A1. With irupt=3, ε_B is calculated from a fourth-order polynomial [64]

$$\varepsilon_B = C_0 + C_1 T + C_2 T^2 + C_3 T^3 + C_4 T^4, \tag{A.1}$$

where T (K) is temperature and the coefficients C_0-C_4 are defined in Table A2. The correlation in Eq. (A.1) is plotted in Fig. A1.

A drawback with these strain-based and temperature dependent failure criteria is that cladding failure may be falsely predicted at negligible mechanical load, merely due to changes in temperature. To avoid this problem in FRAPTRAN-1.5, the strain-based failure criterion $\varepsilon_{\theta\theta}^{Tot} > \varepsilon_B$ is supplemented with the condition $\Delta\tilde{\varepsilon}_{c+p} > 10^{-6}$, where $\Delta\tilde{\varepsilon}_{c+p}$ is the increment of effective creep and plastic strain during the considered time step. The supplemental condition ensures that failure occurs only if the cladding undergoes non-elastic deformation as a consequence of non-negligible mechanical load.

Table A2: Coefficients used for the cladding hoop burst strain in FRAPTRAN-1.5 [64], per equation (A.1).

T	$\Longrightarrow$	940-1200 K	1200-1700 K	$>$ 1700 K
C_0	-	1.90622×10^{3}	2.81199×10^{1}	5.44589×10^{-1}
C_1	K^{-1}	-7.33105	-7.36049×10^{-2}	0
C_2	K^{-2}	1.05305×10^{-2}	6.23050×10^{-5}	0
C_3	K^{-3}	-6.69280×10^{-6}	-1.67939×10^{-8}	0
C_4	K^{-4}	1.58798×10^{-9}	0	0

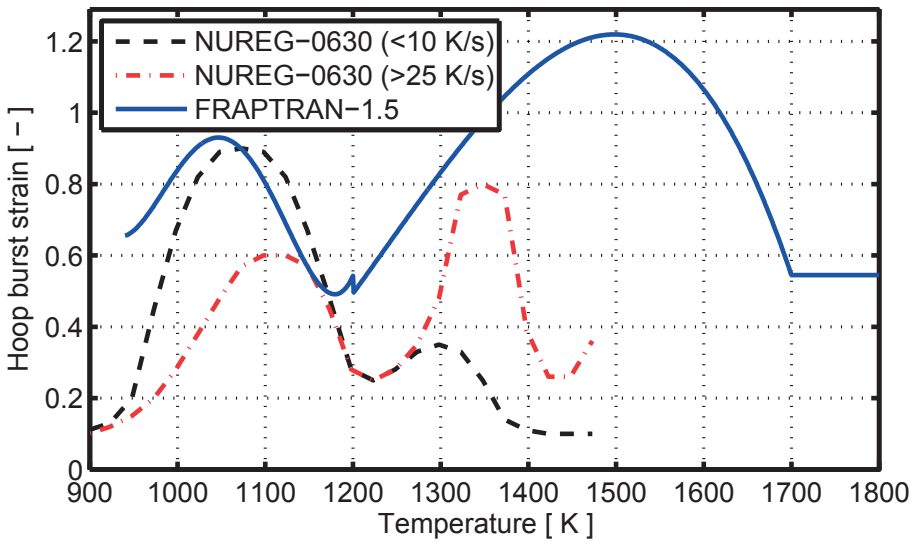

Figure A1: Cladding hoop burst strain versus temperature, according to the different failure criteria listed in table A1. The burst strains marked NUREG-0630 are tabulated in [19], whereas the FRAPTRAN-1.5 [64] criterion is given by Eq. (A.1) and listed in table A2.

Stress-based burst criteria The stress-based criteria for cladding high temperature failure used with options `irupt`=4-8 are taken from the works by Rosinger [20], Erbacher et al. [14], Forgeron et al. [29] and Van Uffelen et al. [65]. Failure is assumed to occur, when the cladding hoop stress $\sigma_{\theta\theta}$ (Pa) exceeds the burst stress σ_B (Pa), given by the correlation

$$\sigma_B = A_b\, e^{-B_b T}\, e^{-\left(\frac{x_{Tot}}{0.00095}\right)^2}, \tag{A.2}$$

where T (K) is temperature, x_{Tot} (-) is the total weight fraction of oxygen picked up in high temperature metal-water reactions and A_b and B_b are material dependent constants.
Five different sets of constants are available in `QT/SSM-FRAPTRAN`, and any of these sets can be selected by setting option `irupt`; see Table A1. Two sets of constants, presented in Table A3, are taken from the work of Rosinger [20] on Zircaloy-4 cladding. The third set, given in Table A4, is based on an evaluation of Zircaloy-4 high temperature burst data by Erbacher and co-workers [14]. Figure A2 shows a comparison of σ_B, calculated for unoxidized cladding (x_{Tot}=0) with the three sets of constants defined in Tables A3 and A4. Evidently, the largest differences are in the α-phase region, i.e. for temperatures < 1100 K.

Table A3: Constants in equation (A.2) by Rosinger [20]. The two sets of constants define the upper bound and best estimate burst stress relations for Zircaloy-4, cf. figure A2.

	Upper bound, `irupt`=4		Best estimate, `irupt`=5	
Temperature region (K)	A_b (Pa)	B_b (K^{-1})	A_b (Pa)	B_b (K^{-1})
873 to 1104	5.04×10^{9}	2.64×10^{-3}	1.00×10^{10}	4.10×10^{-3}
1104 to 1260	7.15×10^{13}	1.13×10^{-2}	3.59×10^{12}	9.43×10^{-3}
1260 to 1873	1.52×10^{9}	2.76×10^{-3}	2.09×10^{8}	1.69×10^{-3}

Table A4: Constants in equation (A.2) by Erbacher et al. [14]. In the mixed-phase temperature region, $T_\alpha < T < T_\beta$, A_b and B_b are calculated by linear interpolation of ln(A_b) and B_b between T_α, $T_{\alpha\beta}$ and T_β.

Temperature region (K)	A_b (Pa)	B_b (K^{-1})
$< T_\alpha = 1085$	8.3×10^{8}	1.0×10^{-3}
$T_{\alpha\beta} = 1166$	3.0×10^{9}	3.0×10^{-3}
$> T_\beta = 1248$	2.3×10^{9}	3.0×10^{-3}

The fourth and fifth sets of constants for Eq. (A.2) are given in Tables A5 and A6. These constants apply to Zr-Nb type cladding, and they are based on burst stress data presented for M5 and E110 cladding by Forgeron et al. [29] and Van Uffelen et al. [65], respectively. Figure A3 is a comparison of σ_B, calculated for unoxidized cladding (x_{Tot}=0) with the two sets of constants defined in Tables A5 and A6. The burst stress data, to which the constants have been fitted, are included in the plot for comparison. Also included in Fig. A3 is the Zircaloy-4 best-estimate burst stress correlation by Rosinger. The results in Fig. A3

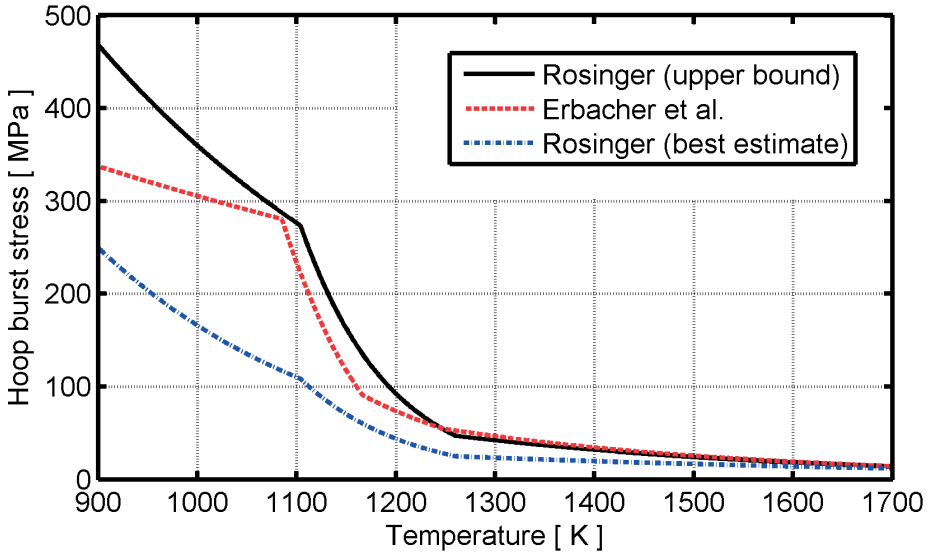

Figure A2: Hoop burst stress of Zircaloy cladding, calculated for an unoxidized material (x_{Tot}=0) through the correlation in eq. (A.2) with three different sets of constants A_b and B_b; see tables A3 and A4.

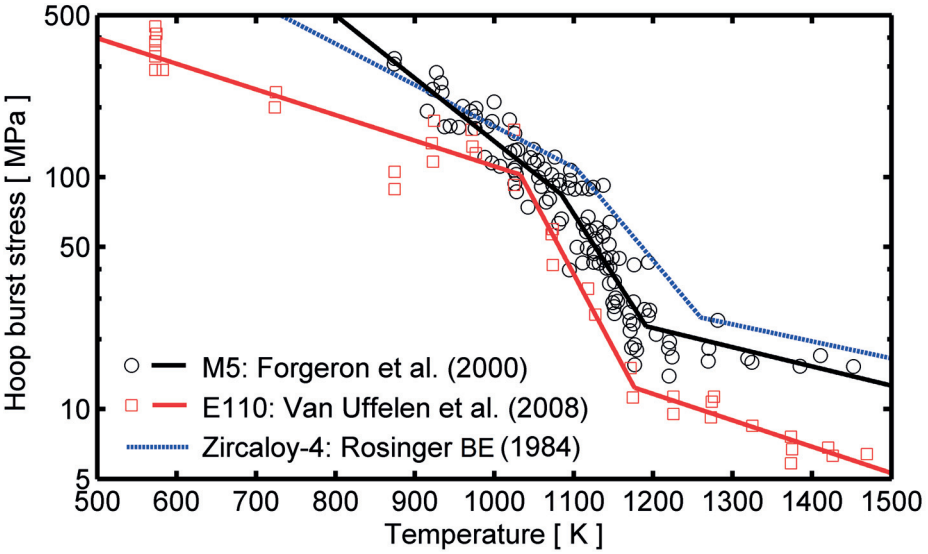

Figure A3: Hoop burst stress versus temperature: the lines show calculated results for unoxidized cladding ($x_{Tot} = 0$) through the correlation in equation (A.2) with three different sets of constants A_b and B_b; see tables A3, A5 and A6. The supporting data for M5 [29] (circles) and E110 [65] (squares) are included for comparison.

Table A5: Constants in equation (A.2), fitted to burst stress data for M5 cladding [29]. The correlation and its supporting data are plotted in figure A3.

Temperature region (K)	A_b (Pa)	B_b (K^{-1})
< 1084	7.464×10^{10}	6.260×10^{-3}
1084 to 1191	4.940×10^{13}	1.225×10^{-2}
> 1191	2.213×10^{8}	1.909×10^{-3}

Table A6: Constants in equation (A.2), fitted to burst stress data for E110 cladding [65]. The correlation and its supporting data are plotted in figure A3.

Temperature region (K)	A_b (Pa)	B_b (K^{-1})
< 1033	1.419×10^{9}	2.545×10^{-3}
1033 to 1176	4.103×10^{14}	1.472×10^{-2}
> 1176	2.703×10^{8}	2.622×10^{-3}

suggest that Zr-Nb type cladding materials have lower burst stress than Zircaloy-4, and that there are notable differences between M5 and E110 cladding.
The correlation for burst stress in Eq. (A.2) does not explicitly account for the phase composition of the cladding material. Instead, the mixed-phase region is assumed to exist in a fixed temperature span, which differs from one correlation to another; see Tables A3 - A6. An alternative method to calculate σ_B in the mixed-phase region is to use the expression

$$\sigma_{B\alpha+\beta} = (1-\varphi)\,\sigma_{B\alpha} + \varphi\,\sigma_{B\beta}, \tag{A.3}$$

where φ is the β-phase volume fraction and $\sigma_{B\alpha}$ and $\sigma_{B\beta}$ are the single-phase burst stresses, as defined through Eq. (A.2) and Tables A3 - A6. By setting the input option `icrup`=2, the burst stress in the mixed-phase region will be calculated through Eq. (A.3). Otherwise, it will be calculated through the original formulation, using only temperature as independent parameter, as in Tables A3 - A6.

The burst stress given by Eq. (A.2) drops rapidly with increasing concentration of excess oxygen in the cladding tube. We note that x_{Tot} rather than x_{Met} is used in Eq. (A.2). Since x_{Tot} includes oxygen also in the form of zirconium oxide, the question is how to treat the pre-transient oxide layer, created at low temperature under normal reactor operation. Our analyses show that if oxygen contained in the pre-transient oxide layer is included in x_{Tot}, Eq. (A.2) yields unrealistically low values for σ_B. For this reason, the contribution to x_{Tot} from the pre-transient oxide layer is neglected. A better approach would be to re-formulate Eq. (A.2) in terms of x_{Met}, i.e. the concentration of excess oxygen in the cladding metal layer. Moreover, Rosinger used the oxygen uptake correlation by Leistikow and Schanz [24] to evaluate x_{Tot} as a function of time for the cladding high temperature burst tests that form the basis for Eq. (A.2). As shown in [58], this correlation predicts a slower oxygen uptake than the standard Cathcart and Baker-Just correlations in the PNNL version of `FRAPTRAN-1.5` [64]. Hence, Eq. (A.2) will most likely overestimate the embrittling effect of oxygen, when used together with these oxygen uptake models.

2015:46

The Swedish Radiation Safety Authority has a comprehensive responsibility to ensure that society is safe from the effects of radiation. The Authority works to achieve radiation safety in a number of areas: nuclear power, medical care as well as commercial products and services. The Authority also works to achieve protection from natural radiation and to increase the level of radiation safety internationally.

The Swedish Radiation Safety Authority works proactively and preventively to protect people and the environment from the harmful effects of radiation, now and in the future. The Authority issues regulations and supervises compliance, while also supporting research, providing training and information, and issuing advice. Often, activities involving radiation require licences issued by the Authority. The Swedish Radiation Safety Authority maintains emergency preparedness around the clock with the aim of limiting the aftermath of radiation accidents and the unintentional spreading of radioactive substances. The Authority participates in international co-operation in order to promote radiation safety and finances projects aiming to raise the level of radiation safety in certain Eastern European countries.

The Authority reports to the Ministry of the Environment and has around 300 employees with competencies in the fields of engineering, natural and behavioural sciences, law, economics and communications. We have received quality, environmental and working environment certification.

Strålsäkerhetsmyndigheten
Swedish Radiation Safety Authority

SE-171 16 Stockholm
Solna strandväg 96

Tel: +46 8 799 40 00
Fax: +46 8 799 40 10

E-mail: registrator@ssm.se
Web: stralsakerhetsmyndigheten.se